Loss Minimization Control of Permanent Magnet Synchronous Machine for Electric Vehicle Applications

KANG CHANG

A Thesis

in

The Department

of

Electrical and Computer Engineering

Presented in Partial Fulfillment of the Requirements
for the Degree of Master in Applied Science
(Electrical & Computer Engineering) at
Concordia University
Montreal, Quebec, Canada

Aug 2013

CONCORDIA UNIVERSITY
SCHOOL OF GRADUATE STUDIES

This is to certify that the thesis prepared

By: Kang Chang

Entitled: "Loss Minimization Control of Permanent Magnet Synchronous Machine for Electric Vehicle Applications"

and submitted in partial fulfillment of the requirements for the degree of

Master of Applied Science

Complies with the regulations of this University and meets the accepted standards with respect to originality and quality.

Signed by the final examining committee:

_____ Chair
Dr. M. Z. Kabir

_____ Examiner, External
Dr. S. Rakheja (MIE) To the Program

_____ Examiner
Dr. P. Pillay

_____ Supervisor
Dr. S. Williamson

Approved by: _____
Dr. W. E. Lynch, Chair
Department of Electrical and Computer Engineering

_____20_____

_____
Dr. C. W. Trueman
Interim Dean, Faculty of Engineering
and Computer Science

ABSTRACT

Loss Minimization Control of Permanent Magnet Synchronous Machine for Electric Vehicle Applications

Kang Chang

With the limits of power source taken into consideration, the efficiency of the traction drive is of particular importance in the engineering of electric vehicle and plug-in hybrid electric vehicle (EV/PHEV). Thanks to its high power density, high efficiency and high torque to weight ratio, Permanent Magnet Synchronous Machine (PMSM) distinguishes itself from other traction system candidates in the EV/PHEV application market. This research sets out to explore how the control strategy of PMSM can be optimized so as to achieve a better efficiency performance of EV/PHEV.

Prior research has put forth Loss Minimization Control Strategy (LMC) and developed its algorithm by considering a certain operating point. The focus has been placed on how to approximately solve the optimal current reference from a high order expression. So far, very limited effort has been made toward a generalized form of LMC algorithm over the full machine operation region, i.e. constant torque and constant power region. In this thesis, a generalized relationship between d-q current for the LMC of PMSM is presented, and maximum torque per ampere (MTPA) and maximum torque per voltage (MTPV) can be derived as special cases of LMC. The proposed control strategy shows better response and enhancement of the machine efficiency over full speed range when compared to conventional control strategies.

In order to develop the control method, the machine operation principle is discussed first, and the machine model is built for the control purpose. Then based on the

analysis of PMSM operation performance with voltage and current constrains, the boundary of the machine operating is defined. In the light of literature review, the LMC is derived from the equivalent model of PMSM by considering the core loss. And the performance of the LMC is analyzed in detail for both constant torque and constant power region. In addition, the effects of parameters variation are investigated. Thus the control strategy is improved by considering full speed range. A Simulink model of PMSM with core loss taken into consider is developed to test the proposed control method. The experiment is performed on a lab surface-mounted PMSM. The experiment results are found to be consistent with simulation results.

ACKNOWLEDGEMENTS

I would first express my deepest gratitude to my supervisor, Dr. Sheldon S. Williamson, for his guidance, patience, trust, and financial support for me to finish this thesis. Without his firm direction and generous help, I couldn't have overcome the obstacles encountered on my way of studying. I am forever indebted to him for giving me the opportunity to explore this interesting research topic, taking effort to correct my mistakes, giving me inspiring and constructive advices, and being always available and responsive to any questions that I have had.

A heartfelt "thank you" also goes to Dr. Pragasen Pillay, who has been a constant source of knowledge and encouragement throughout my graduate studies. He has instilled in me a serious attitude towards academic research as well as a will to always pursue the best along the way in my studies and personal development.

I would also like to express my appreciation to all the friends and colleagues in the Power Electronics and Energy Research (PEER) group. I must thank Abijit Choudhury, Lesedi Masisi, Maged Ibrahim, Jemimah C. Akiror, Avrind Rmanan, Manu Jain and Chirag Desai for their kindness, expertise, and tireless help. These friends will always remain dear to me.

Last but not the least, I am grateful to my friends Yin, Yue, Lin, Jie and my wife Jun. Without their love, understanding and support, this work would not have come to fruition.

TABLE OF CONTENTS

LIST OF FIGURES

LIST OF TABLES

CHAPTER 1 INTRODUCTION

1.1 PMSM for Electric Vehicle Applications

Recent years have seen growing awareness of the risks associated with global warming, environmental pollution and nature resource crisis of the Earth. Being a major consumer of petroleum and a key contributor to carbon dioxide emissions, the transportation plays an important role in addressing those environment-related and energy-related issues. Electric vehicle (EV) and plug-in hybrid electric vehicles (PHEV) have been proposed to replace conventional fossil-fuel combustion vehicles, and progress is under way. Up to today, there have already been many commercial EV/PHEVs on the road. Among the most successful examples there are Toyota prius, Chevlet volts, and Nissan Leaf.

Speaking of electric vehicle application, the standards of choosing an appropriate traction motor for the EV/PHEV propulsion are often focused on the characteristics such as torque density, extended speed range, energy efficiency, safety and reliability, thermal cooling, and cost. As determined by vehicle dynamics and system architecture, the extended speed range ability and energy efficiency are two particularly important factors in selecting the propulsion motor [1]. In addition, the power source in EV/PHEV is the battery, whose performance is claimed by many as “Achilles Heel” of any EV/PHEV application. The traction drive system consumes the largest share of the power source, and its efficiency thus becomes vital for EV/PHEV application. Generally, the drive system includes power inverter and traction motor. In order for the whole system to achieve high efficiency, it is essential that both the power inverter and the traction motor

operate with their optimal efficiency throughout the driving schedule [2]. This thesis work will emphasize on the traction motor part.

There are many types of machine that are considered as candidates for electric vehicle traction system, which mainly include induction motor (IM), permanent magnet synchronous machine (PMSM), and switch reluctance machine (SRM). It is noteworthy that due to its high efficiency, power density and torque-inertia ratio, PMSM has now become the most common choice in the EV/PHEV. Table 1.1 shows the most important features of the principal motor types that are being considered for EV/PHEV application.

Motor Design	**Induction** (natural field weakening)	**PM**			**SR**
		SPM motor (BLDC)	SPM motor with concentrated windings	IPM motor	Non-linear solenoid type force
CPSR	4	11	Theotetically, infinity, but allow for rotational losses	Theotretically, infinity, but allow for rotational losses	Discontinuous control
Cost	$	$$	$$	$$$	$
Peak Power to Weight Ratio	Low	High	High	Highest	Low
Peak Power to Volume Ratio	Low	High	High	Highest	Low
Lifetime	Higher	High	High	High	Higher

Table 1-1: Advantage (green) and disadvantage (red) of the major motor types [3]

1.2 Motivation and Review of Technologies

In order to improve the efficiency of the machine, emphasis is often placed on the machine design. With proper topology of the machine and improvement of the material, the total efficiency can be optimized. It can also be enhanced by way of employing automatic control strategy. There has been a lot of research focused on the automatic control method, which mainly include maximum torque per ampere control (MTPA) that is meant to minimize the copper loss [4], maximum torque per voltage control (MTPV)

that works to optimize the core losses [5], and loss minimization control (LMC) conceived for both copper and core losses reduction [6,7,8]. All these strategies are implemented by finding the optimal d-q-axis current so that the objective of the control can be reached. In addition, the previous work on LMC usually considers certain steady state operating point, and there is no comprehensive analysis for the automatic control strategy over full operation region. For EV/PHEV application, the traction motor works in a wide speed range. In order to reduce the total loss of the machine, the LMC strategy should take into account the whole operating region.

In this research, based on the equivalent model of PMSM, the efficiency enhancement control strategy is generalized to an optimal d-q current relationship, from which the MTPA and MTPV can be derived. And then the performance of the LMC is analyzed in detail. Based on the traction motor operating region, an improved LMC strategy is proposed over full speed range.

1.3 Thesis Outline

The objective of this thesis is to develop a Loss Minimization Control (LMC) strategy over full speed range of permanent magnet synchronous machine (PMSM), and also the parameters variation issues will be discussed. The main body of the thesis is organized as follows:

In Chapter 2, the fundamentals of PMSM are briefly discussed. Based on the dq model equivalent circuit, the behavior of PMSM in variable speed drive application is studied. The operating areas are analytically divided in terms of current and voltage constraints.

In Chapter 3, various control strategies are discussed. The maximum torque per ampere (MTPA), maximum torque per voltage (MTPV) and flux-weakening method are derived based on the dq equivalent model. Also, their performances are analyzed from efficiency enhancement point of view.

In Chapter 4, the loss minimization control (LMC) strategies of PMSM are reviewed. With the core loss taken into consideration, the dq model with core loss resistance is used to derive the LMC. A generalized optimal current relationship is presented. And then by taking into account both constant torque and constant power region, the performance of LMC is analyzed in detail. Also, the effects of the machine parameters are examined. At the end, an improved control strategy is proposed over full speed range based on the performance of the LMC.

In Chapter 5, the simulation model is developed by using Matlab. The performance and results of the simulation are analyzed.

In Chapter 6, a lab design surface-mounted PMSM is used to test the proposed algorithm. The experimental results are compared with the simulation results and discussed in detail. In particular, the parameter variation issue is addressed in the discussion.

Chapter 7 concludes the thesis and proposes future research work.

CHAPTER 2 FUNDAMENTALS OF PERMANENT MAGNET SYNCHRONOUS MACHINE

2.1 Introduction

The permanent magnet (PM) materials with considerable energy density were firstly introduced into the designing of electrical machine during 1950s. They have experienced rapid growth and continuous improvement, especially during the past few years. Instead of field windings, the PM poles in rotor provide electromagnetic field and thus eliminate slip rings and brush assembly. Equally mentionable is that electronic commentators replace traditional mechanical ones in modern power electronics. These two factors have jointly propelled the development and growth of PM AC machine in the last two decades. It has now become possible to build high performance drive systems in a wide range of application fields including but not limited to electric vehicles.

Generally, the PM AC machine can be classified by the direction of the flux density distribution. Its two main categories are radial field PM machines and axial field ones [9]. Also, depending on their induced back-EMF shape, the radial fields PM machines are classified into PMSM with sinusoidal back-EMF and BLDC with trapezoidal back-EMF. The discussion in this research is based on the PMSM only. According to the location of the permanent magnet in the rotor, there are four topologies as shown in Figure 1.

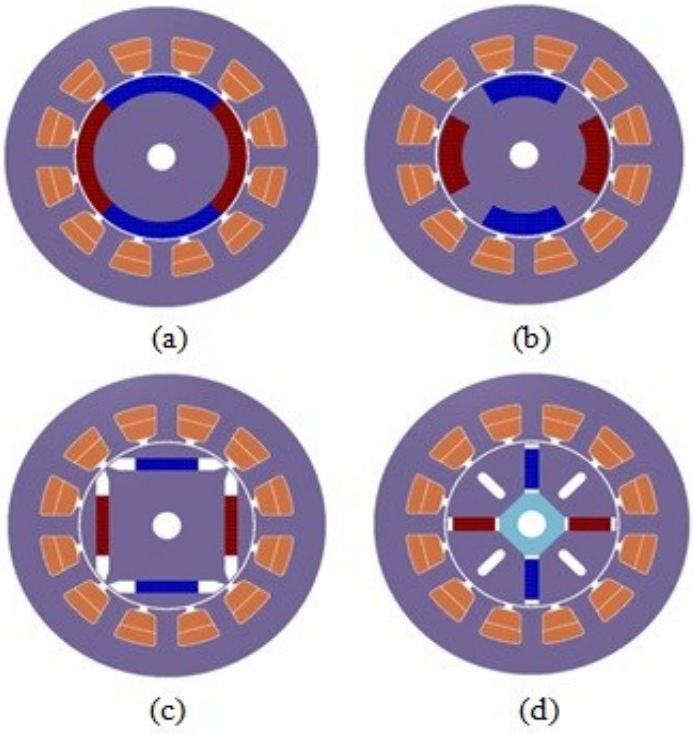

Figure 2.1: Permanent Magnet AC machine topologies: (a) Surface mounted; (b) Surface inset; (c) Interior radial; (d) Interior circumferential

In today's EV/PHEV application market and related research, the interior radial PM machine (IPM) gets increasing attention. Compared with other topologies, this kind of PMSM has less torque ripple and higher reliability because of its buried magnets. Also, the buried magnet is better protected from demagnetizing due to the armature reactance. Moreover, the IPM features a special configuration in rotor. It results in a very strong saliency, which contributes to the total load demand by additional reluctance torque. Furthermore, the strong saliency feature provides an excellent flux weakening capability, and thus enables a wide range of high speed operation suitable for EV application. As the counterpart, the surface mounted topology PMSM (SPM) can be seen as a special case of IPM. This chapter will derive the model of PMSM based on IPM.

2.2 Modeling of Permanent Magnet Synchronous Machine

In order to develop the desired algorithm, the behavior of the PMSM should be explored based on the dynamic model of the machine. In this section, the modeling of PMSM is derived from the transformation theory. And the d-q rotor reference frame model will be used for the analysis of PMSM.

2.2.1 Three phase modeling

The PMSM can be modeled in three phase stator coordinates with winding as shown in Figure 2. The two phase coordinates is also shown in Figure 2.

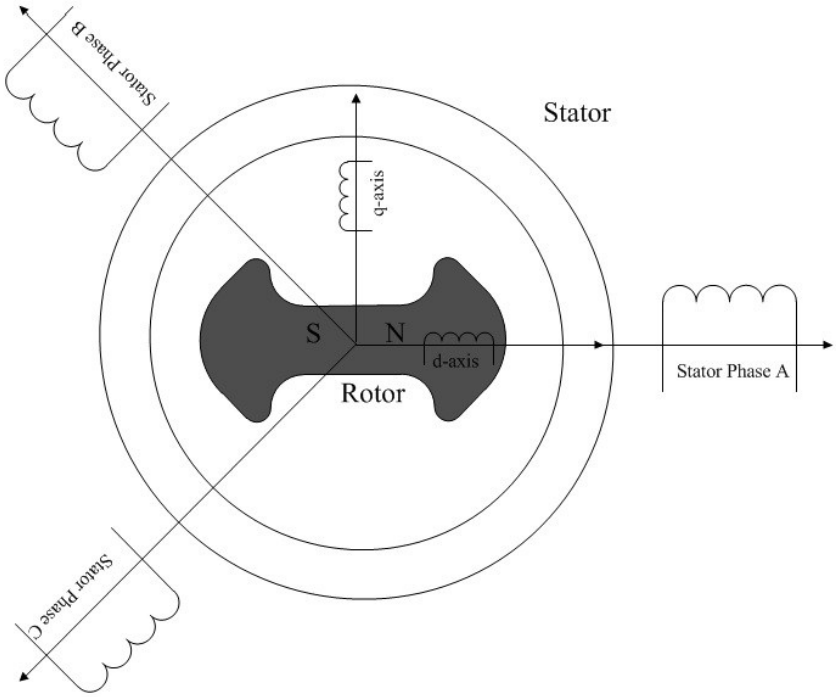

Figure 2.2: Three Phase PMSM and Two Phase PMSM

The voltage equations are

$$\begin{aligned} v_a &= R_s i_a + \frac{d\lambda_a}{dt} \\ v_b &= R_s i_b + \frac{d\lambda_b}{dt} \\ v_c &= R_s i_c + \frac{d\lambda_c}{dt} \end{aligned} \tag{2-1}$$

where v_a, v_b, v_c are stator phase voltages, i_a, i_b, i_c are stator phase currents, and $\lambda_a, \lambda_b, \lambda_c$ are the phase flux linkages. The input power for this model is

$$P_{in} = v_a i_a + v_b i_b + v_c i_c \tag{2-2}$$

Since the variables in this model are all sinusoidal or rotor position dependent, the solution of these equations will be computational complex.

2.2.2 Reference frame transformation

As one kind of observer platforms, the reference frame offers a unique view of the system. A simplified model with constant variables is desirable for the purpose of control. In PMSM, rotor frame revolves at the synchronous speed with stator sinusoidal supply frequency. As a result, sinusoidal variable can be perceived as dc signal from the rotor frame. Based on this rotor reference frame, a two-phase motor can be derived from the three-phase model in direct and quadrature axes, which is generally referred to as d-q axes model. Figure 3 shows the stator abc phase and the rotating dq phase winding.

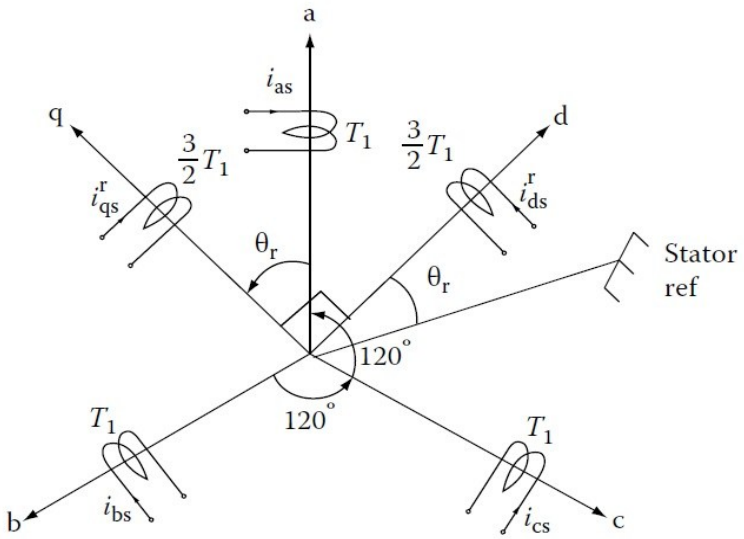

Figure 2.3. Three phase to two phase transformation [10]

By applying Park's transformation, the voltage equation in three-phase model can be transferred to the dq rotating frame as following:

$$\begin{bmatrix} v_q \\ v_d \\ v_o \end{bmatrix} = \frac{2}{3} \begin{bmatrix} \cos\theta_r & \cos(\theta_r - \frac{2\pi}{3}) & \cos(\theta_r + \frac{2\pi}{3}) \\ \sin\theta_r & \sin(\theta_r - \frac{2\pi}{3}) & \sin(\theta_r + \frac{2\pi}{3}) \\ \frac{1}{2} & \frac{1}{2} & \frac{1}{2} \end{bmatrix} \begin{bmatrix} v_{as} \\ v_{bs} \\ v_{cs} \end{bmatrix} \tag{2-2}$$

where θ_r is the rotor angle.

The Park's transformation is represented as:

$$[T_{abc}] = \frac{2}{3} \begin{bmatrix} \cos\theta_r & \cos(\theta_r - \frac{2\pi}{3}) & \cos(\theta_r + \frac{2\pi}{3}) \\ \sin\theta_r & \sin(\theta_r - \frac{2\pi}{3}) & \sin(\theta_r + \frac{2\pi}{3}) \\ \frac{1}{2} & \frac{1}{2} & \frac{1}{2} \end{bmatrix} \tag{2-3}$$

and its inverse form is

$$[T_{abc}]^{-1} = \begin{bmatrix} \cos\theta_r & \sin\theta_r & 1 \\ \cos(\theta_r - \frac{2\pi}{3}) & \sin(\theta_r - \frac{2\pi}{3}) & 1 \\ \cos(\theta_r + \frac{2\pi}{3}) & \sin(\theta_r + \frac{2\pi}{3}) & 1 \end{bmatrix} \tag{2-4}$$

This transformation is also applicable to the current and flux linkage.

2.2.3 Basic mathematic model

After applying Park's transformation, the synchronous machine variables in the abc phase equation are transferred to the dq-variable in the rotor reference frame. Since the reference frames are moving at an angular speed equal to the angular frequency of the sinusoidal supply, all sinusoidally varying inductances in the abc frame become constant in the dq frame.

With the assumption of saturation being neglected and the sinusoidal back emf, the dq equation in the rotor reference frame of the PMSM are derived as

$$v_q = R_s\, i_q + L_q p i_q + \omega_r L_d i_d + \omega_r \lambda_{PM}$$
$$v_d = R_s\, i_d + L_d p i_d - \omega_r L_q i_q \tag{2-5}$$

The electromagnetic torque is expressed as

$$T_e = \frac{3}{2}\frac{P}{2}\,[\,\lambda_{PM}\, + (L_d - L_q) i_d] i_q \tag{2-6}$$

It can be seen that the developed electromagnetic torque includes two components. The first term corresponds to the magnet exciting torque, which is the reaction between q-axis current and the permanent magnet on rotor. The second term is the feature of IPM, which is the reluctance torque due to the difference in the d-q-axis inductance.

In terms of mechanical load, the torque is

$$T_e = J\frac{d\omega_m}{dt} + T_l + B\omega_m \tag{2-7}$$

In the state space form, the PMSM model can be expressed as:

$$p i_q = \frac{1}{L_q}(v_q - R_s\, i_q - \omega_r L_d i_d - \omega_r \lambda_{PM}\,)$$
$$p i_d = \frac{1}{L_d}(v_d - R_s\, i_d + \omega_r L_q i_q\,)$$
$$p\omega_m = \frac{1}{J}(T_e - B\omega_m - T_l\,) \tag{2-8}$$

where

v_q, v_d : q-axis and d-axis voltage

i_q, i_d : q-axis and d-axis current

R_s : stator phase resistance

L_q, L_d : q-axis and d-axis inductance

p : derivative operator

λ_{PM} : permanent magnet flux

T_e, T_l : electromagnetic torque and load torque

P : number of poles

J : the moment of inertia of the load and machine combined

B : the friction coefficient of the load and machine

ω_m, ω_r : the mechanical and electrical rotor speed, $\omega_r = \frac{P}{2}\omega_m$

Alternatively, the dynamic equations of the PMSM in rotor reference frame can be represented by using flux linkages as variables. The flux linkages are continuous no matter voltage and current are continuous or not. In so doing, it is possible to differentiate the variables with numerical stability. This alternative way of representing the PMSM dynamic equations also places emphasis on how the flux and torque channels are dis-coupled.

The model in flux linkage is defined as

$$\begin{aligned} v_q &= R_s i_q + p\lambda_q + \omega_r \lambda_d \\ v_d &= R_s i_d + p\lambda_d - \omega_r \lambda_q \end{aligned} \tag{2-9}$$

where

$$\begin{aligned} \lambda_q &= L_q i_q \\ \lambda_d &= L_d i_d + \lambda_{PM} \end{aligned} \tag{2-10}$$

and the electromagnetic torque is

$$T_e = \frac{3}{2}\frac{P}{2}\left[\lambda_d i_q - \lambda_q i_d\right] \tag{2-11}$$

From the power equivalence condition, the input power in terms of d-q variable, it is

$$P_{in} = \frac{3}{2}\left(v_d i_d + v_q i_q\right) \tag{2-12}$$

2.2.4 PMSM Equivalent Electric Circuit

From the dynamic equation, the equivalent circuit of PMSM can be drawn as shown in Figure 4. There are two ciruits representing dynamic q-axis circuit and d-axis equivalent circuit.

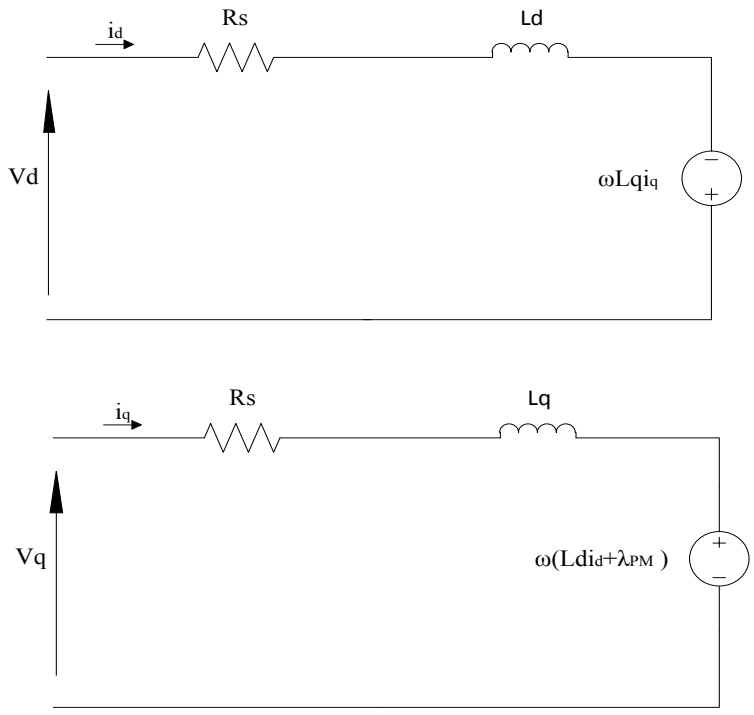

Figure 2.4: PMSM equivalent dq model circuit

The models can be used to examine both the transient and steady state behaviors of PM machine drive system.

2.3 Analysis of PMSM Operation

For EV/PHEV application, the traction motor drives are generally designed to provide a constant torque up to base speed and constant power for extended speed up to a maximum speed. The torque speed characteristic is plotted as Figure 2.5:

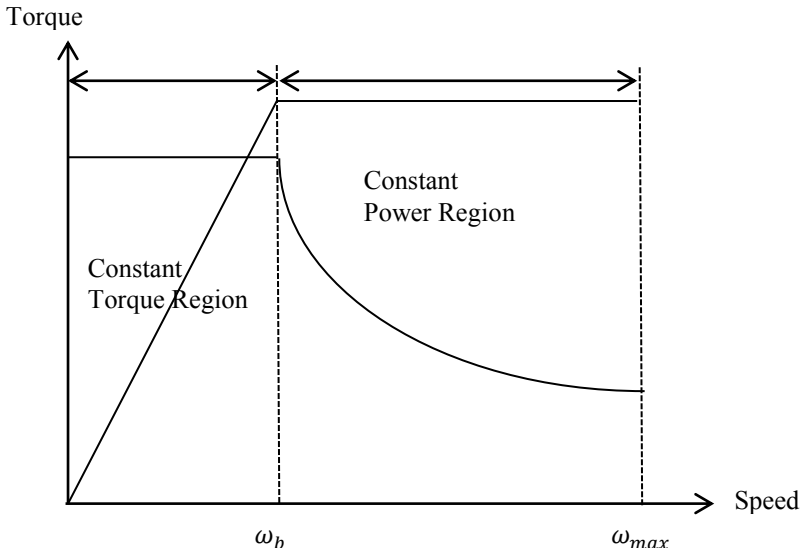

Figure 2.5. Torque-Speed characteristics

For the purpose of developing the control strategy of PMSM, the performance of PMSM is analyzed based on the d-q-axis model with the assumption ignoring the voltage drop on phase resistance and core loss. The control strategies and performance features in different regions will be discussed in detail.

2.3.1 Current and Voltage constrains

According to the equivalent circuit mentioned in section 2.2.4, the two-phase mathematic model in steady state is written as:

$$\begin{bmatrix} v_q \\ v_d \end{bmatrix} = \begin{bmatrix} R_s & \omega_r L_d \\ -\omega_r L_q & R_s \end{bmatrix} \begin{bmatrix} i_q \\ i_d \end{bmatrix} + \begin{bmatrix} \omega_r \lambda_{PM} \\ 0 \end{bmatrix} \tag{2-13}$$

And the torque produced by the machine is:

$$T_e = \frac{3}{2}\frac{P}{2} \left[\lambda_{PM} + (L_d - L_q) i_d \right] i_q \tag{2-14}$$

For the inverter-fed drive system with DC battery source, there are voltage and current constraints due to the power rating of the inverter, machine and power source. The current constraint is identified as:

$$i_d^2 + i_q^2 \leq I_{smax}^2 \tag{2-15}$$

where $I_{s,max}$ is the maximum phase current of the machine. It is a circle in the dq current plane.The voltage constraint is:

$$v_d^2 + v_q^2 \leq V_{smax}^2 \tag{2-16}$$

By ignoring the voltage drop on the phase resistance, in terms of dq current, it is:

$$\left(L_q i_q\right)^2 + (\lambda_{PM} + L_d i_d)^2 \leq \frac{{V_{smax}}^2}{\omega^2} \tag{2-17}$$

where $V_{s,max}$ is the maximum available voltage provided by the inverter. Generally,

$$V_{smax} = \frac{V_{dc}}{\sqrt{3}} \tag{2-18}$$

where V_{dc} is the dc power source voltage. For given speed, the voltage constraint is an ellipse with center $(-\frac{\lambda_{PM}}{L_d}, 0)$ in the dq current plane. With the speed increasing, the ellipse shrinks to the center. As shown in Figure 2.6, the above constraints are plotted in id-iq plane by using one example IPM.

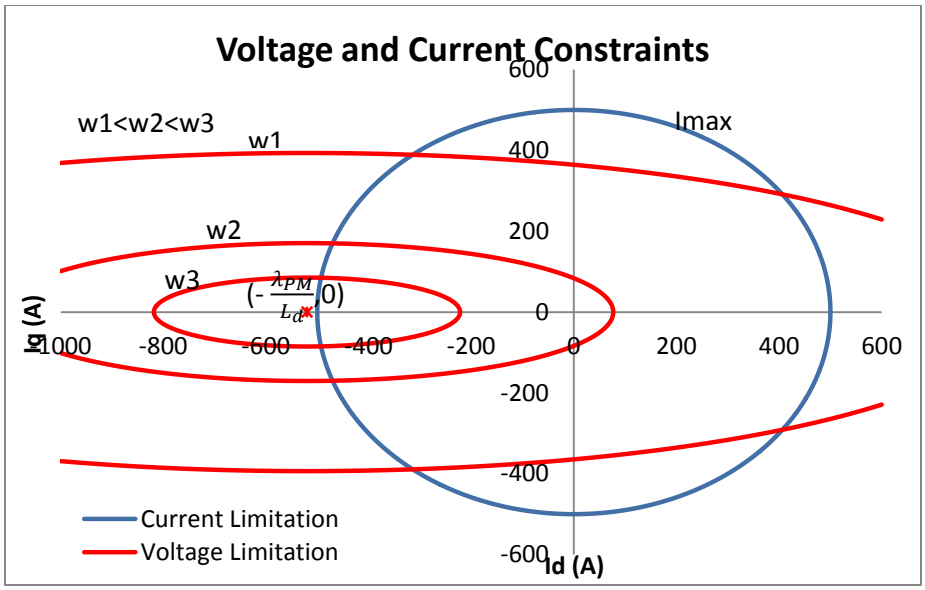

Figure 2.6. PMSM operation region with voltage and current constraint

Due to the current and voltage constraints, the operation region of the machine has to be within the overlapped area of the current and voltage constraints.

2.3.2 Constant Torque Region

In constant torque region, since the speed is lower than the base speed, the voltage constraint will not be exceeded in most cases. More concern will be placed on the current constraint. In order to fully utilize the current, maximum torque per current control strategy is widely employed, which assures the minimization of the copper loss. Under this control strategy, the highest available speed is given by

$$\omega_{mtpa} = \frac{V_{sm}}{\sqrt{\left(L_q i_q\right)^2 + \left(\lambda_{PM} + L_d i_d\right)^2}} \tag{2-19}$$

where Id, Iq are the MTPA optimal current for the peak torque, and

$$i_d^2 + i_q^2 = I_{smax}^2 \tag{2-20}$$

Below the speed ω_{mtpa}, the motor can be accelerated by this peak torque.

2.3.3 Constant Power Region

When the speed exceeds the rated speed, the voltage constraint will be reached, and the operation of machine enters into the constant power region. With appropriate stator current distribution, the stator flux linkage gets reduced, and high speed operation can be performed up to extended speed range. In this region, flux weakening control strategy such as maximum output power, MTPV or LMC is applied for the purpose of the control.

2.3.4 Power-Speed characteristic

Considering the power capacity versus speed of the PMSM, there are three cases be summarized from [11, 12]. It can be seen that from the voltage constraint equation, the eclipse center is on $(-\frac{\lambda_{PM}}{L_d}, 0)$. With different design flux linkage of the permanent magnet, d-axis inductance and the available maximum phase current, the power speed characteristic will be varied.

Case 1: $\frac{\lambda_{PM}}{L_d} > I_{max}$, which means that the permanent magnet flux is greater than the maximum d-axis flux field as caused by maximum phase current in stator. Under this circumstance, the voltage eclipse center is located outside the current constraint circle. There is a maximum available speed occurring where the two curves tangentially intersect at point $(-I_{max}, 0)$. This maximum available speed is called by many as critical speed, which is expressed as:

$$\omega_c = \frac{V_{sm}}{\lambda_{PM} - L_d I_{max}} \tag{2-20}$$

After that speed, there are no overlapped region between voltage and current constraint. The power in this case drops fast to zero when the rated speed is exceeded.

Case 2: $\frac{\lambda_{PM}}{L_d} = I_{max}$, which means that the voltage eclipse center lies on the current constraint circle. In this case, there is always an overlapped region between them at any high speed. The constant power region will be theoretical infinite.

Case 3: $\frac{\lambda_{PM}}{L_d} < I_{max}$, which means that the stator field can cancel the rotor permanent magnet field in certain phase current that is lower than the maximum phase current. In this case, the voltage constraint eclipse center goes into the current constraint circle. It can have infinite constant power region but lower output power compared with Case 2. The power versus speed characteristics are as shown in Figure 2.7:

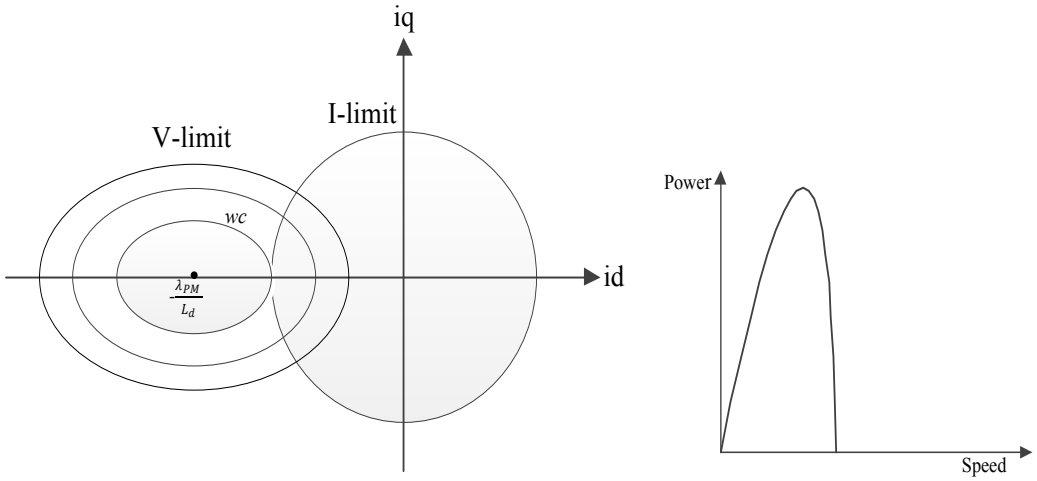

(a)

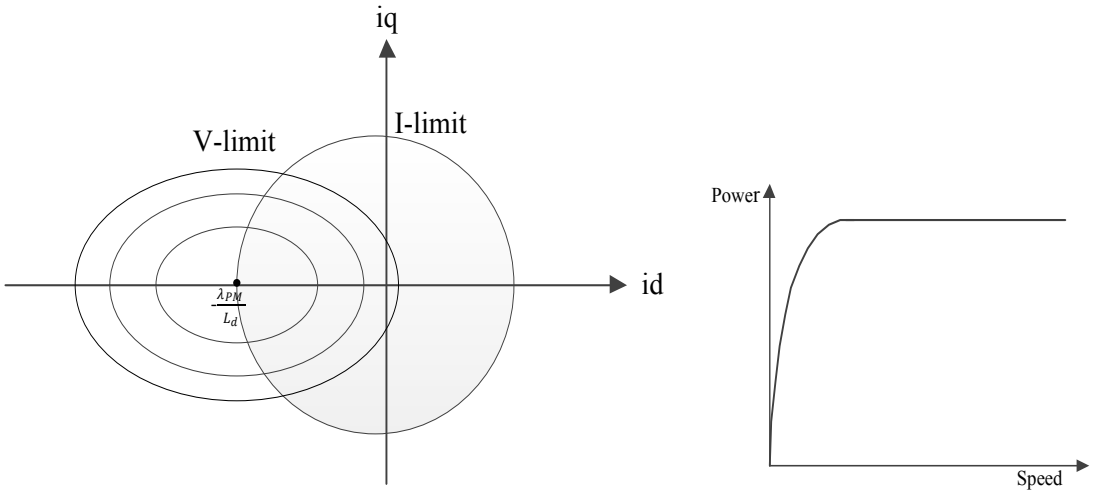

(b)

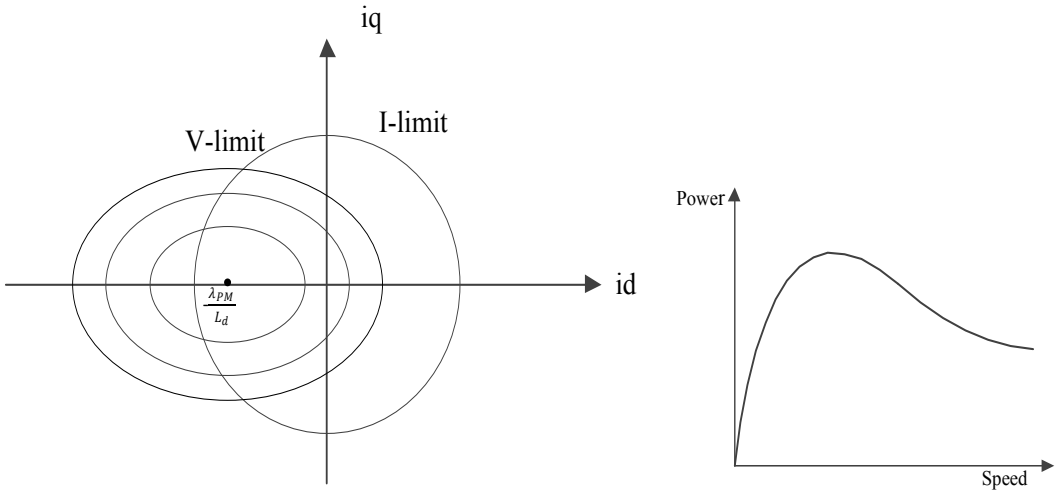

(c)

Figure 2.7 Power-speed characteristics of PMSM:
(a) Case 1, (b) Case 2, (c) Case 3

For EV/PHEV applications, Case 2 and Case 3 are the preferred designs of PMSM, due to extended constant power region. In this thesis, the LMC control strategy is developed based on this preferred design of PMSM.

2.4 Summary

In this chapter, the fundamentals of PMSM are presented. The modeling in two axes coordinate shows a convenient way to understand the behavior of PMSM. And from the

control point of view, the variable in dq-axis coordinate becomes dc value, and it is possible to make the control of PM AC machine as that of DC machine. Based on the two axes model, the dynamic mathematic equations for PMSM are derived. The equivalent electrical circuit is also presented in this chapter. Considering the operating region of PMSM, an analysis is performed at the end of this chapter. Due to voltage and current constraints, the control of inverter fed PMSM drive should be properly developed to meet with the objective within the constrained region.

CHAPTER 3 CONTROL OF PERMANENT MAGNET SYNCHRONOUS MACHINE

3.1 Introduction

With optimized design of PMSM, an appropriate control strategy will help extract full performance capability from the machine. Vector control, also known as field oriented control or decoupling control, was first proposed by Blaaske [13] and has been widely applied to the induction motor (IM). It has enabled the controlling of an AC machine like a separately excited DC machine by the orientation of the stator mmf or current vector in relation to the rotor flux to obtain the independent control of flux and torque. For PMSMs, the vector control can also be applied, and it is easier to implement thanks to the absence of slip frequency current [14]. In this chapter, the vector control for PMSM will be presented, and different control strategies will be discussed.

From the dq-axes model of PMSM, the phasor diagram of the PMSM is shown as Figure 3.1.

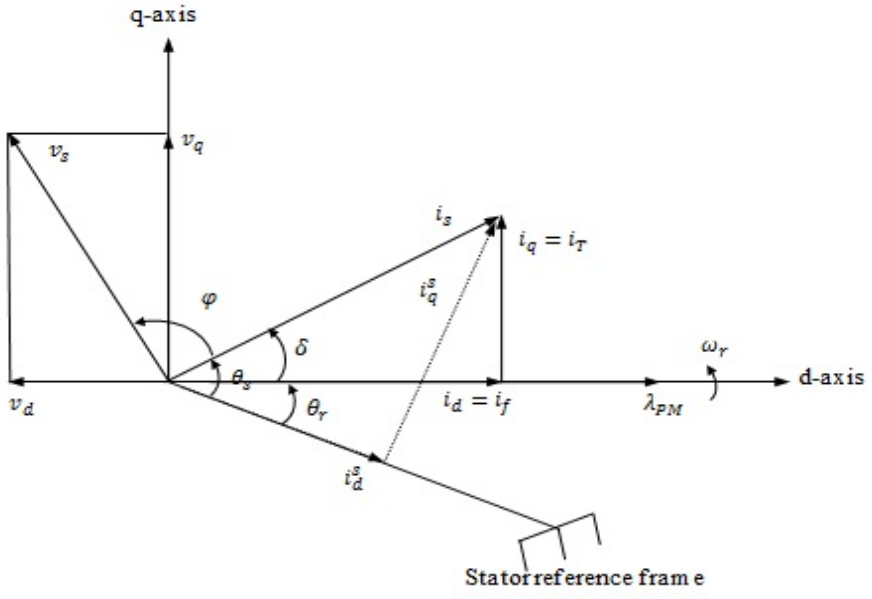

Figure 3.1. Phasor Diagram of the PMSM

Considering the current as input, the three phase currents are:

$$\begin{aligned} i_{as} &= i_s \sin(\omega_r t + \delta) \\ i_{bs} &= i_s \sin\left(\omega_r t + \delta - \frac{2\pi}{3}\right) \\ i_{cs} &= i_s \sin\left(\omega_r t + \delta + \frac{2\pi}{3}\right) \end{aligned} \tag{3-1}$$

where ω_r is the electrical rotor speed, and δ is the angle between the rotor filed and stator current pharos and is known as the torque angle.

In the rotor reference frame, the dq-axes stator currents are obtained by applying Park's transformation as:

$$\begin{bmatrix} i_q \\ i_d \end{bmatrix} = \frac{2}{3} \begin{bmatrix} \cos\omega_r & \cos(\omega_r - \frac{2\pi}{3}) & \cos(\omega_r + \frac{2\pi}{3}) \\ \sin\omega_r & \sin(\omega_r - \frac{2\pi}{3}) & \sin(\omega_r + \frac{2\pi}{3}) \end{bmatrix} \begin{bmatrix} i_{as} \\ i_{bs} \\ i_{cs} \end{bmatrix} \tag{3-2}$$

Then the dq-axes currents in rotor and stator reference frame are obtained as:

$$\begin{bmatrix} i_q \\ i_d \end{bmatrix} = i_s \begin{bmatrix} \sin\delta \\ \cos\delta \end{bmatrix} = \begin{bmatrix} i_T \\ i_f \end{bmatrix}$$

$$\begin{bmatrix} {i_q}^s \\ {i_d}^s \end{bmatrix} = i_s \begin{bmatrix} \sin(\omega_r t + \delta) \\ \cos(\omega_r t + \delta) \end{bmatrix} \tag{3-2}$$

where i_T and i_f are the torque producing current and the flux producing current respectively. It should be noted that the dq-axes currents are constants in rotor reference frames, and the torque angle δ is a constant for a given load torque. Substitute the above dq-axes stator current in rotor reference frame into torque expression, the torque is expressed in terms of the stator current magnitude and torque angles as:

$$T_e = \frac{3}{2}\frac{P}{2} \left[\lambda_{PM} i_s \sin\delta + \frac{1}{2}(L_d - L_q) i_s^2 \sin 2\delta \right] \tag{3-3}$$

Obviously, the control variables stator current magnitude and the torque angle determine the electromagnet torque with the machine parameters being assumed as constant. In addition, the mutual flux linkages in the air gap are the result of the rotor flux linkages and the stator flux linkages. It is given as:

$$\lambda_m = \sqrt{(\lambda_{PM} + L_d i_d)^2 + \left(L_q i_q\right)^2} \tag{3-4}$$

So from the perspective of control, by way of controlling the phase angle δ and magnitude of the current phasor i_s from the inverter, which means the dq-axis current in two phase model on rotor reference frame, the torque can be determined and its control is achieved accordingly. The PMSM drive is shown to be analogous to the separately excited dc motor drive. It is achieved by finding the flux and torque producing components of stator current. And the independent control of electromagnetic torque and mutual flux is exercised via the flux and torque producing component current.

3.2 Drive System of PMSM

The general block diagram of vector control drive system is shown as in Figure 3.2.

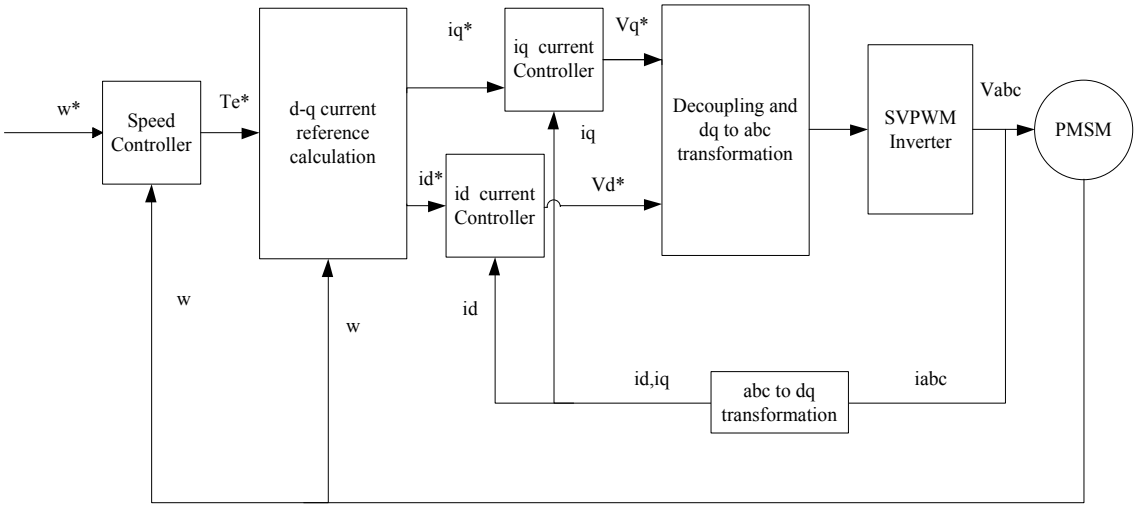

Figure 3.2 Basic Vector Control Block Diagram

There exist two control loops in the drive system. The inner loop is torque loop, and the outer loop is speed loop. Depending on how the torque is controlled, the inner loop can be implemented by indirect torque control mode or direct torque control mode.

Indirect torque control is also called stator current vector control or field oriented current control (FOC) in some literature. The torque equation (3-3) explains the relationship between the stator phase current and the instantaneous torque. Then the torque can be controlled by phase current and torque angle, in other words, the dq-axes current in two phase axes coordinate. For this control mode, the rotor position is needed except the current sensor. The process of deriving the torque component current and flux component current references plays a key role in this control. For the control purpose, different strategies to derive the dq current reference can be applied, for examples, MTPA, MTPV, and LMC.

Direct torque control was first introduced for the induction motor by [15]. It is of great interest to EV/PHEV application, especially for dual motor propulsion system, where the fast torque response is desirable [16]. For PMSMs, direct torque control is also useful. Based on the torque and flux linkage error between the command and estimations, the controller outputs proper voltage vectors command to inverters. This control mode eliminates the current loop and directly controls the torque and flux independently. The torque and flux ripple are the major problems of this control mode. In some research work, these problems are tackled with introducing additional PI-controller, which makes the direct torque control have the same system complexity and the same cost as the indirect torque control.

3.3 Control Strategies for PMSM

Vector control provides the decoupling between torque and flux channel in the PMSM. The control variables include current, voltage, flux, and torque angle. As the application requirements vary, there are different control strategies accordingly.

3.3.1 Constant Torque Angle Control

Constant torque angle control, also called zero d-axis current control, is widely used across the industry. As the phasor diagram in Figure3.3 shows, when torque angle is maintained at 90°, the direct field component of stator current is brought to zero, and all the stator current is used to produce torque.

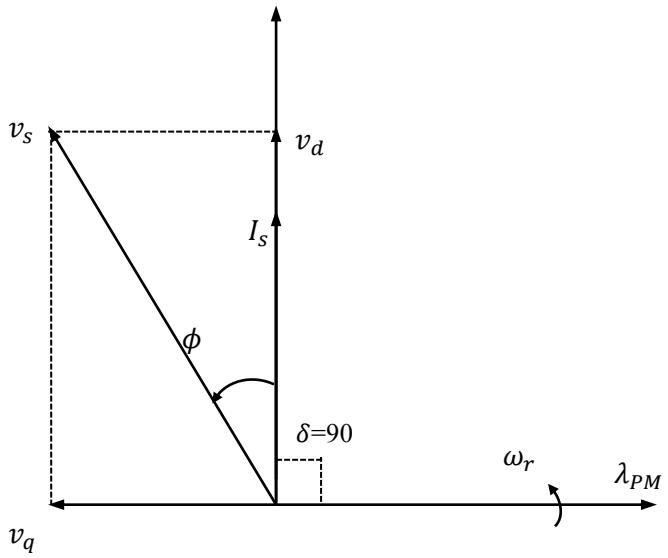

Figure 3.3. Constant torque angle control phasor diagram

The torque control is then the simplified result in the linear relationship between torque and current as

$$T_e = \frac{3}{2}\frac{P}{2}\ \lambda_{PM} i_q = \frac{3}{2}\frac{P}{2}\ \lambda_{PM}\ I_s \tag{3-5}$$

where I_s is the magnitude of the stator current phasor.

Under this mode, the steady state voltage equations in rotor reference frame as

$$v_q = R_s I_s + \omega_r \lambda_{PM}$$
$$v_d = -\omega_r L_q I_s \quad (3\text{-}6)$$

This provides a simple linear torque control, and it is similar to the DC motor control. The flux linkage under this control is

$$\lambda_m = \sqrt{{\lambda_{PM}}^2 + \left(L_q i_q\right)^2} \quad (3\text{-}7)$$

It reveals that a weakening of mutual flux linkages is out of the question. Thus it only works for the speed lower than base speed operating range. Also for IPMSM, the reluctance torque is not utilized.

3.3.2 Unity Power Factor Control (UPF)

UPF control refers to the optimization of the VA rating of the inverter by way of keeping the power factor at UNITY (1.0). This type of control implies the utmost use of the real power input to the PMSM. It is enforced by controlling the torque angle as a function of the motor variables. As shown in Figure 3.1, the angle between the d-axis voltage and q-axis voltage is

$$\tan(\delta + \phi) = \frac{v_q}{v_d} \quad (3\text{-}8)$$

In UPF, the power factor angle has to be zero ($\phi = 0$), which means that the voltage angle equals to the current angle.

Substitute the voltage in terms of current into equation (3-8)

$$\tan\delta = \frac{\sin\delta}{\cos\delta} = \frac{\omega_r L_d i_s \cos\delta + \omega_r \lambda_{PM}}{-\omega_r L_q i_s \sin\delta} \quad (3\text{-}9)$$

From the above equation, the torque angle is solved as

$$\delta = \cos^{-1}\left(\frac{-\lambda_{PM} + \sqrt{{\lambda_{PM}}^2 - 4L_q(L_d - L_q){i_s}^2}}{2i_s(L_d - L_q)}\right) \quad (3\text{-}10)$$

It should be noted that the torque angle needs to exceed 90°. Otherwise, the mutual flux linkages might be enhanced and saturation might be observed in the machine, which is undesirable from the perspective of loss control. In addition, the UPF control strategy has a very low torque per unit current ratio, and its efficiency will be inferior to that of other control strategies due to the increasing copper loss for producing the given torque.

3.3.3 Maximum Torque per Ampere (MTPA) Control

For the IPMSM, the electromagnetic torque is represented as:

$$T_e = \frac{3}{2}\frac{P}{2}[\lambda_{PM}\, I_q + (L_d - L_q) I_d I_q] \tag{3-11}$$

It is composed of two terms. The former corresponds to the excitation torque by rotor permanent magnet, which is also called synchronous torque. The second term corresponds to the reluctance torque, which is the result of the difference in d-q-axis reluctance. Based on this equation, a strategy enabling the full utilization of the torque capacity can be derived, which is called maximum torque per ampere control (MTPA). It provides a maximum electromagnetic torque for a unit stator current via torque angle control and therefore minimizes copper loss for a given torque. By manipulating the torque equation (3-11) with the relationship between d-q-axis current and stator current:

$$\begin{aligned} I_d &= I_s \cos\delta \\ I_q &= I_s \sin\delta \end{aligned} \tag{3-12}$$

Rewrite the equation (3-12) as:

$$T_e = \frac{3}{2}\frac{P}{2}[\lambda_{PM} I_s \sin\delta \; + \frac{1}{2}(L_d - L_q)\, {I_s}^2 \sin 2\delta] \tag{3-13}$$

In order to maximize the torque per unit stator current, take the derivative of the electromagnetic torque with respect to the current angle as:

$$\frac{dT_e}{d\delta} = \frac{3}{2}\frac{P}{2}\left[\lambda_{PM} I_s \cos\delta + \left(L_d - L_q\right) {I_s}^2 \cos 2\delta\right] = 0 \tag{3-14}$$

Equating it to zero, and substituting the d-q-axis current into the above equation, the maximum torque per current unit condition is obtained as

$$I_d = \frac{\lambda_{PM}}{2\left(L_d - L_q\right)} - \sqrt{\frac{{\lambda_{PM}}^2}{4\left(L_d - L_q\right)} - {I_q}^2} \tag{3-15}$$

Due to the current constraint, consider the continuous current rating as:

$$\sqrt{{I_d}^2 + {I_q}^2} = I_{smax} \tag{3-16}$$

The peak torque is produced when

$$I_{dm} = \frac{\lambda_{PM}}{4\left(L_d - L_q\right)} - \sqrt{\frac{{\lambda_{PM}}^2}{16\left(L_d - L_q\right)^2} + \frac{{I_{smax}}^2}{2}}$$

$$I_{qm} = \sqrt{{I_{smax}}^2 - {I_{dm}}^2} \tag{3-17}$$

and this peak torque can accelerate the motor to the speed that allows the voltage to reach its limit. The speed under this operating point is defined as the base speed and is given as:

$$\omega_b = \frac{V_{smax}}{\sqrt{(L_d I_{dm} + \lambda_{PM})^2 + (L_q I_{qm})^2}} \tag{3-18}$$

So the MTPA can only be used for the speed range lower than the base speed. The MTPA current trajectory in the d-q-axis current plane is plotted as shown in Figure 3.4. In MTPA control strategy, the saliency ratio significantly influences the torque performance. It is a preferred option for high saliency machine with ratio greater than 2 and operating within the lower speed range. MTPA control strategy does not optimize the whole system for net loss, nevertheless.

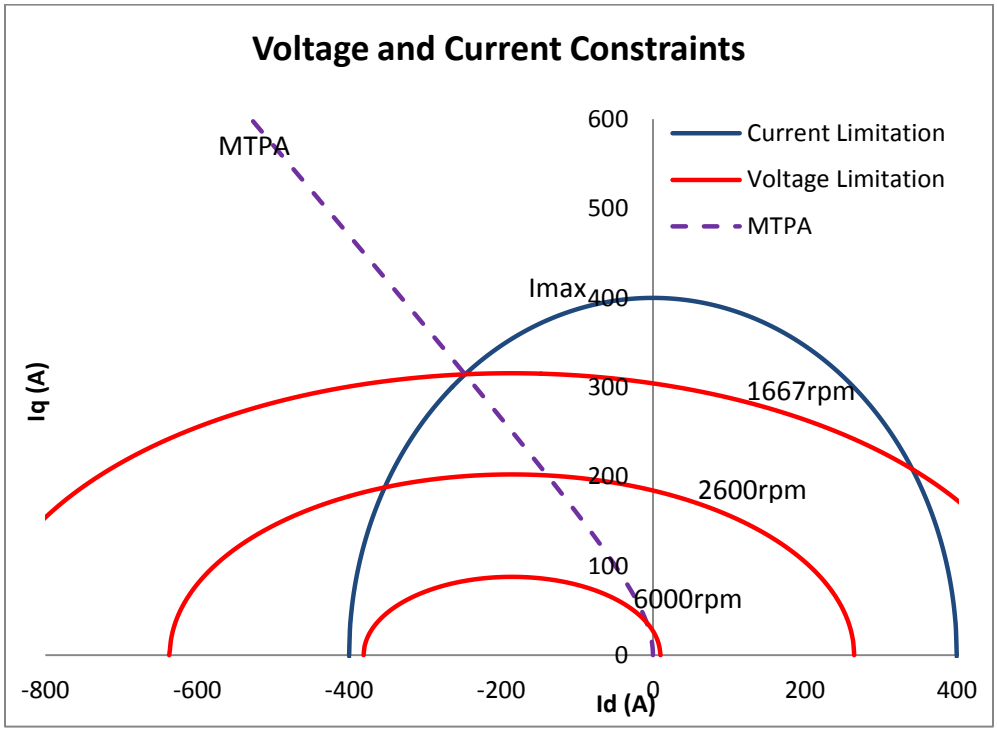

Figure 3.4. MTPA current trajectory

3.3.4 Maximum Torque per Voltage (MTPV) Control

When PMSMs operate within high speed region, the voltage constraint shrinks to its center point. The MTPA cannot be used anymore due to the voltage constraint. In order to utilize the full available voltage to optimize the torque production, the maximum torque per voltage control (MTPV) strategy can be derived. Consider the voltage constraint equation for the PMSM above the based speed as:

$$\left(L_q i_q\right)^2 + (\lambda_{PM} + L_d i_d)^2 = \frac{{V_{smax}}^2}{\omega^2} \tag{3-19}$$

For a given speed, the maximum available torque should be at the point where the voltage constraint curve tangentially intersects with the torque curve in d-q-axis current plane, which is shown in Figure 3.5.

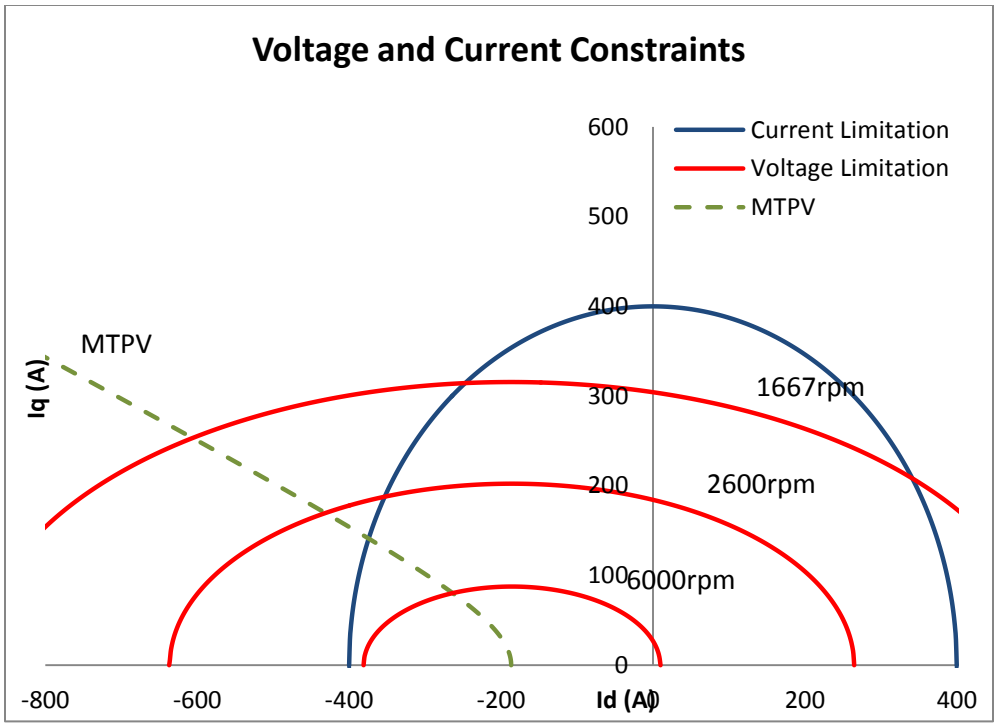

Figure 3.5. MTPV current trajectory

The voltage constraint equation can also be rewritten in terms of d-q flux linkage:

$$\lambda_q{}^2 + \lambda_d{}^2 = \lambda_m{}^2 = \frac{V_{smax}{}^2}{\omega^2} \tag{3-20}$$

where

$$\begin{aligned} \lambda_q &= L_q i_q = \lambda_m \sin\delta \\ \lambda_d &= L_d i_d + \lambda_{PM} = \lambda_m \cos\delta \end{aligned} \tag{3-21}$$

Then rewrite the torque equation with voltage constraint as

$$T_e = \frac{3}{2}\frac{P}{2}\frac{V_{smax}}{\omega}\frac{\sin\delta}{L_q}\left[\frac{L_q}{L_d}\lambda_{PM} + \frac{(L_d - L_q)}{L_d}\frac{V_{smax}}{\omega}\cos\delta\right] \tag{3-22}$$

Taking the differentiation with respect to the angle δ and equating it to zero, the MTPV optimal current trajectory satisfies the relationship as

$$(L_d - L_q)\left[\left(\frac{L_d i_d + \lambda_{PM}}{L_q}\right)^2 - i_q{}^2\right] + \lambda_{PM}\left(\frac{L_d i_d + \lambda_{PM}}{L_q}\right) = 0 \tag{3-23}$$

It is plotted in the dq current plane as shown in Figure 3.5. From the observation, it can be noted that the MTPV curve is independent of a specific speed, and then there is only one MTPV curve depending on machine parameters. The minimum speed for MTPV control strategy is determined by the intersect point between the MTPV curve and the current constraint circle. Below that speed, the intersect point will be outside the current constraint circle. MTPV control strategy makes full utilization of voltage, which means minimizing the core losses of the machine.

3.3.5 Flux Weakening Control

When operating above base speed, the backEMF of PMSMs can be exceeding the available maximum voltage fed by the inverter. In order to enable the speed to exceed the base speed, a negative d-axis current can be applied to reduce the stator flux linkage and then decrease the back EMF. It is generally called flux weakening control. This control strategy allows the machine to work at a speed up to maximum speed, but with a decreasing maximum available torque.

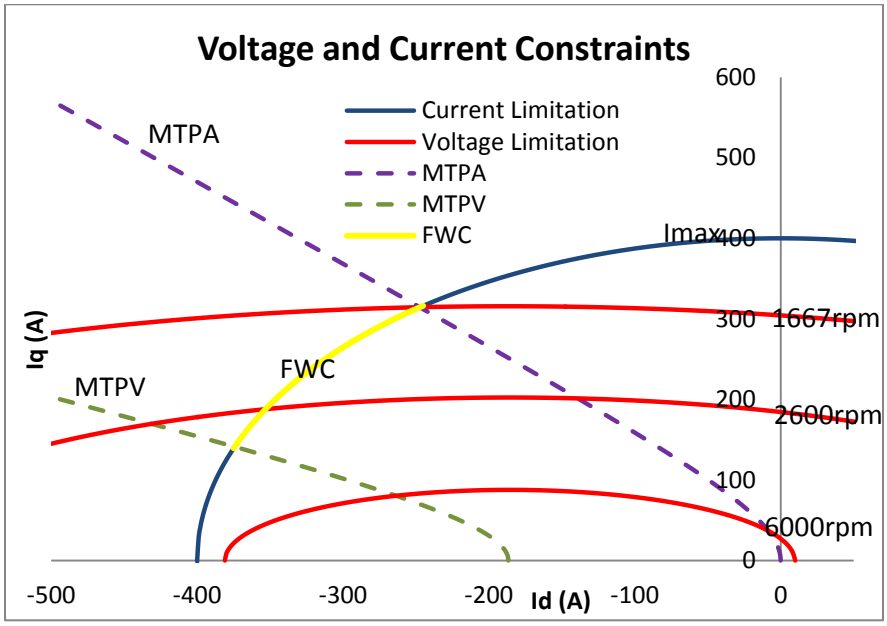

Figure 3.6: Flux weakening region in dq-axis current plane

The flux weakening region is plotted in Figure 3.6, and it is located between the MTPA and MTPV curves. Different flux weakening control strategies are proposed to meet with different objectives of the control. Two examples in this regard are efficiency enhancement flux weakening control [17] and current-voltage constraint maximum power flux weakening control [18].

3.4 Summary

In this chapter, the vector control of PMSMs is described, and different control strategies are discussed. As determined by the constraints of voltage and current, the operation of PMSMs can be divided into three regions with corresponding control strategies. When the machine runs below the base speed, the MTPA can be applied to obtain maximum constant torque, and the copper loss can be minimized. After the speed goes above base speed, the machine enters the flux weakening region. With properly flux weakening control strategy, the speed can be extended to high speed range with constant output power. Once the speed reaches some high value, the MTPV control strategy is used to fully utilize the voltage fed by the inverter, and the core losses will be minimized.

CHAPTER 4 LOSS MINIMIZATION CONTROL

For EV application, the efficiency of the whole drive system is the most concerned issue, especially because of the limited power supply by the battery. In this chapter, the loss minimization control (LMC) will be discussed, and the pertinent control design will be investigated in detail.

4.1 Literature Review of Loss Minimization Control

In the PMSM operation, there are numerous combinations of motor variables such as voltage and current at a given operating point. These combinations result in different total loss, and the one causing minimum loss is chosen. The loss minimization control (LMC) has so far received a lot of attention from research on DC machine, induction machine, and PMSM machine.

Roy S. Colby et al. [19] presented a testing efficiency optimizing controller for non-salient, scalar controller PMSM. In this approach, the output voltage of the inverter was adjusted to minimize the DC link current with the motor speed being maintained constant by independent open loop control of the inverter frequency. The DC link current rather than the input power to the motor drive was reduced. Due to the nature of the open loop, the dynamic performance of this approach was not satisfactory for high performance application.

S. Morimoto et al. [20] established a loss minimization control based on the equivalent circuit including an iron loss model and a copper loss one. By way of taking differentiation of the loss function with respect to d-axis current, the optimal d-axis current was obtained. However, the expression after differentiation is a fourth order

equation, which only can be solved analytically for non-saliency. For rotor saliency, it has to use numerical solution to find optimal value. The machine parameter variation was not taken into account in this research.

C. C. Chan, K. T. Chau et al. [21] proposed a PMSM machine for mini-EV and developed a new PWM algorithm, namely equal-area pulse-width modulation (EAPWM), for the purpose of control. The PWM algorithm can be automatically adjusted for a varying DC link voltage. It has low harmonic content, and allows a real-time calculation of the PWM pattern. By employing the new PWM algorithm, the researchers developed a search algorithm to increase the efficiency of the PMSM. Since the search algorithm was not dependent on the loss model of the machine, it was not sensitive to variations in the motor parameters.

Sadegh Vaez, V. I. John, M. A. Rahman et al. [22] proposed an online adaptive loss minimization controller (ALMC) for interior permanent magnet motor drive. This control minimizes the total input power to the drive system through continuing adjustment of d-axis current until the optimal point was found. Compared to the conventional stepwise change, the ALMC offers advantages such as very smooth performance and fast searching time.

C. Cavallaro et al. [23] developed an online loss minimization algorithm based on the model proposed by S. Morimoto et al. [20]. With the use of a substantial binary search algorithm, the d-axis current was adjusted until the total loss was minimized for a given operating point.

Juggi Lee et al. [24] proposed a loss minimization control law that reflected the effects of saturation and cross decoupling. The optimized current sets were obtained from

experiment and summarized in a table. In another research, Juggi Lee et al. [25] proposed analytic method and used order reduction and linear approximation to identify the loss minimization solution. Two different cases were discussed therein, as the solution lied either within or on the boundary of the voltage constraint. The achieved accuracy was good enough for practical use.

Eleftheria S. Sergaki et al. [26] presented a fuzzy logic efficiency control system incorporated to a standard vector control. By virtue of two fuzzy logic controllers, this system was capable of handling both transient and steady state operation. The search criterion is the minimization of the losses by simultaneously lowering the stator flux and satisfying the demands for speed and load. In another study, the same author et al. [27] proposed a hybrid control strategy which integrated a model based controller with a fuzzy logic search controller. The model based controller was adopted to regulate the transient states based on a simple generalized model with low accuracy, which provided a real time fast gross approximation of the optimal point. The fuzzy logic controller was used after the transient state, which offered a real time refinement of the optimal point during the steady state.

The above literature review attempts to summarize some accomplished research and work on the loss minimization control of PMSM. Basically, the loss minimization control strategies in the literature can be classified to three categories: model based, non-model based, and hybrid control. The model based strategy provides fast response, but it is sensitive to machine parameters. Non-model based control, like search controller, is independent of the machine model and parameters, but its slow convergence time and ripple problem are unfavorable in high dynamic application. The hybrid control strategy

combines both model based strategy and search controller so as to separately deal with transient and steady state conditions. It is relatively complex, however.

4.2 Development of Loss Minimization Control

4.2.1 Losses in PMSM machine

In order to investigate the way of improving the efficiency of the machine, the losses in the machine should be examined carefully at first. The power flow in the AC machine is shown in Figure 4.1.

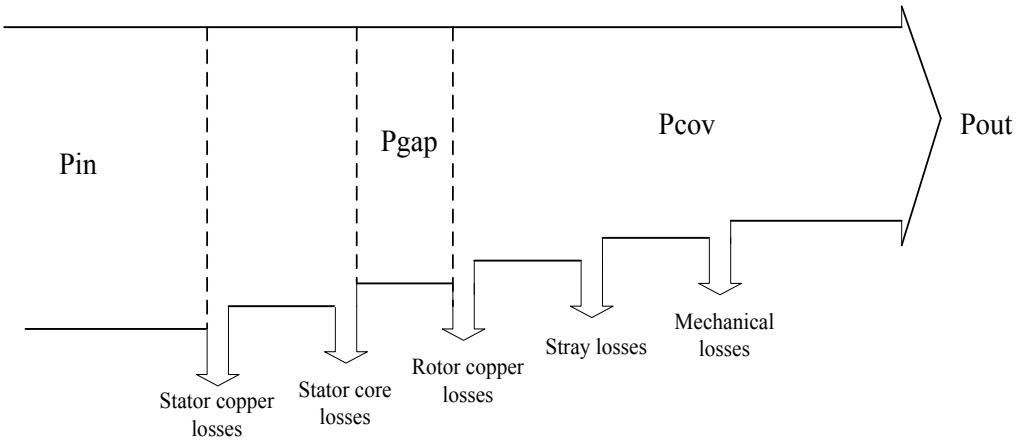

Figure 4.1: Steady-state power losses in an AC machine

For a three-phase machine, the input power is the electrical power flowing into the terminals. Power is then lost due to stator winding and stator core. The remaining power is transferred to the rotor. By deducting the rotor losses, the remaining power is converted into the mechanical power. The output power available to the mechanical load is the one that stray losses and mechanical losses are deducted. Base on the power flow in the machine, the different losses are briefly described as follows:

- **Copper Loss**

The copper loss refers to the joule loss of copper winding due to the coil resistance. Because of the absence of rotor winding in PMSMs, the copper loss of a PMSM is less than that of induction machine.

- **Iron Loss**

The iron loss, also known as core loss, occurs on both the rotor and stator. It involves two components: hysteresis current loss and eddy current loss. The former is caused by energy loss in core material in its B-H loop for each cycle of operation and is directly dependent on the operating frequency and the operating flux density. The latter is the product of the induce emf generating a current in the core. It is proportional to the induced emf and therefore proportional to the flux density and frequency, also. The eddy current loss is inferior to hysteresis loss under the base frequency but becomes dominant in the high frequency range.

- **Stray Loss**

Stray loss accounts for the higher winding harmonics and slot harmonics loss, whose accuracy is difficult to calculate.

- **Mechanical Loss**

Mechanical loss consists of friction and windage loss, which will not be addressed in this research since it is not directly related to the motor current or flux.

In reality, core losses and stray losses are usually electrical losses distributed throughout the motor. They must be taken off after the mechanical power is converted as there is no way to include them in the electrical model. In some cases, to simplify matters, stray, core and mechanical losses are grouped as "rotational losses" and all deducted after calculating the power converted to the mechanical system.

In this thesis, by employing a core loss model for control purpose, the core losses can be separated from the rotational losses. And the loss minimization control strategy will be developed to deal with copper loss and core loss in the machine.

4.2.2 Equivalent Circuit Model with Core Losses

For control purposes, the core loss is modeled as a resistance, known as core loss resistance, in the equivalent circuit, as shown in Figure 4.2.

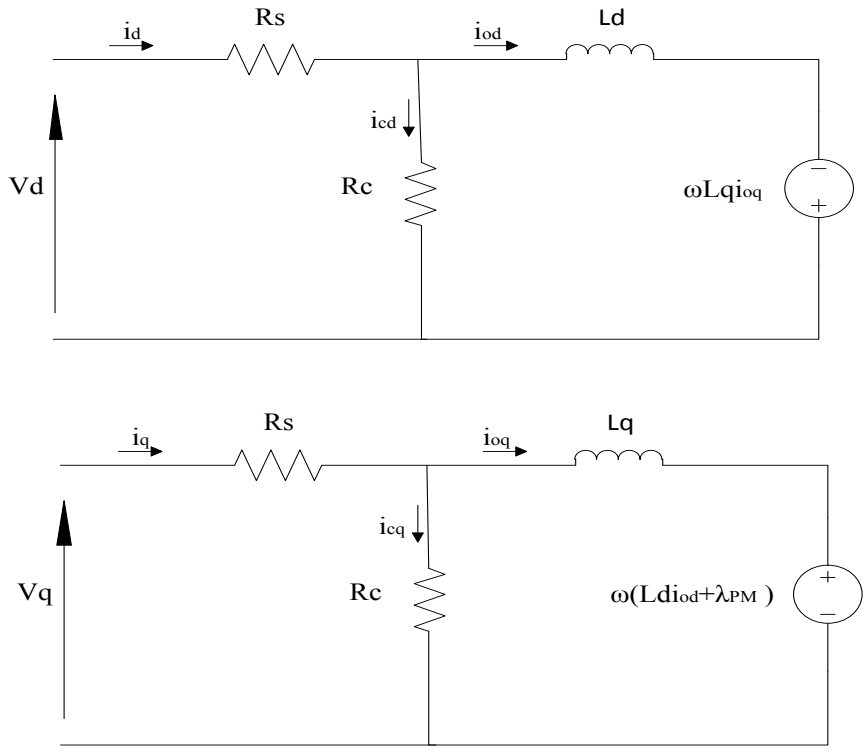

Figure 4.2 : Equivalent circuit of PMSM incorporating core losses

The input stator currents and voltages are derived as:

$$\begin{bmatrix} v_q \\ v_d \end{bmatrix} = \begin{bmatrix} R_s & \omega_r L_d (1 + \frac{R_s}{R_c}) \\ -\omega_r L_q (1 + \frac{R_s}{R_c}) & R_s \end{bmatrix} \begin{bmatrix} i_{oq} \\ i_{od} \end{bmatrix} + \begin{bmatrix} \omega_r \lambda_{PM} (1 + \frac{R_s}{R_c}) \\ 0 \end{bmatrix} + \begin{bmatrix} L_q & 0 \\ 0 & L_d \end{bmatrix} \begin{bmatrix} pi_{oq} \\ pi_{od} \end{bmatrix} \quad (4\text{-}1)$$

$$i_d = i_{od} + i_{cd}, \qquad i_q = i_{oq} + i_{cq} \tag{4-2}$$

$$i_{cd} = \frac{-\omega_r L_q i_{oq}}{R_c}, \qquad i_{cq} = \frac{\omega_r (L_d i_{od} + \lambda_{PM})}{R_c} \tag{4-3}$$

The torque expression in terms of $i_{oq}$and i_{od} is given below:

$$T_e = \frac{3}{2}\frac{P}{2}[\lambda_{PM} i_{oq} + (L_d - L_q) i_{od} i_{oq}] \tag{4-4}$$

The net core losses P_{iron} is computed as:

$$P_{iron} = \frac{1.5\omega_r^2 (L_q i_{oq})^2}{R_c} + \frac{1.5\omega_r^2 (\lambda_{PM} + L_d i_{od})^2}{R_c} = \frac{1.5}{R_c}\omega_r^2 \lambda_m^2 \tag{4-5}$$

The copper loss P_{cu} is:

$$P_{cu} = 1.5 R_s (i_q^2 + i_d^2) \tag{4-6}$$

The final power losses including both copper loss and core loss can be represented as:

$$P_t = P_{cu} + P_{iron} \tag{4-7}$$

Plot of the total losses in the dq-axis plane is as shown in Figure 4.3.

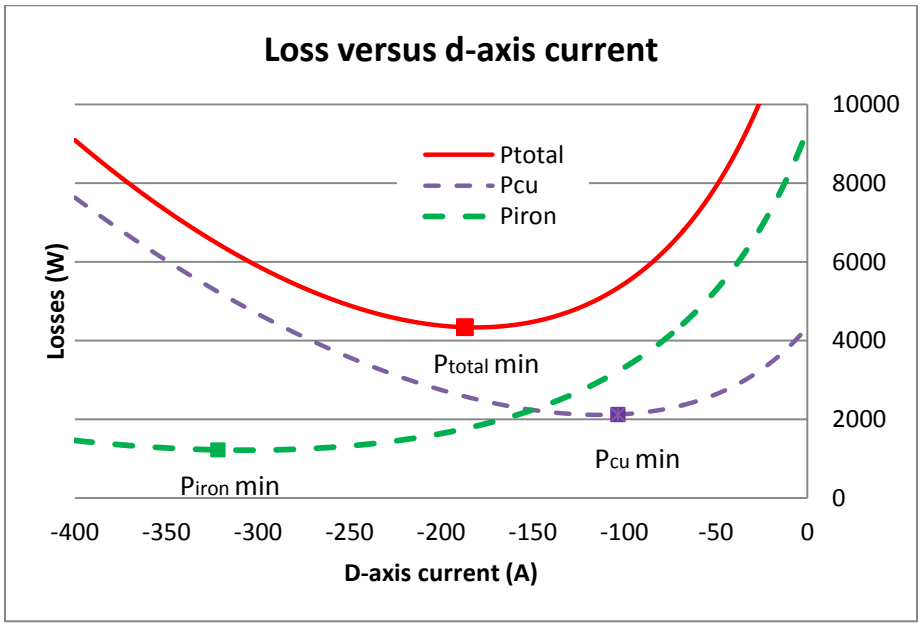

Figure 4.3 : Plot of losses versus d-axis current

It can be seen that the total loss is concave curve with respect to d-axis current, which means that there is certainly a minimum point. Also, it can be noted that for certain operating point, many combinations of dq-axis current can support the operation, but there is only one combination that will give the minimum total loss.

4.2.3 Loss Minimization Control

With the voltage and current constraints, the loss minimization is formulated as a constraint optimization problem for a given torque T_l and speed ω_r as:

Minimize objective function $P_t(i_{od}, i_{oq})$

Subject to

$$\frac{3}{2}\frac{P}{2}[\lambda_{PM} i_{oq} + (L_d - L_q) i_{od} i_{oq}] - T_l = 0 \tag{4-8}$$

$$\omega_r \sqrt{(L_q i_{oq})^2 + (\lambda_{PM} + L_d i_{od})^2} \leq V_{smax} \tag{4-9}$$

$$i_d^2 + i_q^2 \leq I_{smax}^2 \tag{4-10}$$

In order to get the optimal point for the minimized losses, take derivative with respect to i_{od} for the total loss Pt, and make it equal to zero as:

$$\frac{\partial P_t}{\partial i_{od}} = 0 \tag{4-11}$$

It can also be represented as:

$$\frac{\partial P_{iron}}{\partial i_{od}} = -\frac{\partial P_{cu}}{\partial i_{od}} \tag{4-12}$$

It means, the minimum total loss occurs at the point where the core loss changing rate equals to the copper loss changing rate. As Figure 4.3 indicates, the total loss' optimal

point lies on between the minimum point of copper loss and that of iron loss, which is consistent with the aforementioned understanding about (4-12).

Rearrange the equation (4-11) as:

$$i_{od}\left[R_s+\frac{{\omega_r}^2L_d^2}{R_c^2}(R_s+R_c)\right]+\frac{{\omega_r}^2L_d\lambda_{PM}}{R_c^2}(R_s+R_c)+\frac{\omega_r R_s}{R_c}(L_d-L_q)i_{oq}$$
$$+\frac{\omega_r R_s}{R_c}(L_d-L_q)i_{oq}\frac{di_{oq}}{di_{od}}+i_{oq}\left[R_s+\frac{{\omega_r}^2L_d^2}{R_c^2}(R_s+R_c)\right]\frac{di_{oq}}{di_{od}}+\frac{\omega_r R_s\lambda_{PM}}{R_c}\frac{di_{oq}}{di_{od}}=0 \quad (4\text{-}13)$$

Due to the steady state condition, the operating point is unchanged. So, the torque derivative with respect to i_{od} is also zero as:

$$\frac{\partial T_e}{\partial i_{od}}=0 \quad (4\text{-}14)$$

Rearrange the above equations as:

$$\frac{di_{oq}}{di_{od}}=-\frac{i_{oq}(L_d-L_q)}{\lambda_{PM}+(L_d-L_q)i_{od}} \quad (4\text{-}15)$$

Substitute (4-15) into (4-13), the relationship of the optimal point dq current is obtained as:

$$Ai_{od}^2+Bi_{od}+Ci_{oq}^2+D=0 \quad (4\text{-}16)$$

where

$$A=(L_d-L_q)\left[R_s+\frac{\omega^2L_d^2}{R_c^2}(R_s+R_c)\right]$$

$$B=\lambda_{PM}R_s+(2L_d-L_q)\frac{\omega^2L_d\lambda_{PM}}{R_c^2}(R_s+R_c)$$

$$C=-(L_d-L_q)\left[R_s+\frac{\omega^2L_q^2}{R_c^2}(R_s+R_c)\right]$$

$$D=\frac{\omega^2L_d{\lambda_{PM}}^2}{R_c^2}(R_s+R_c)$$

Applying quadratic solution:

$$i_{od} = \frac{-B + \sqrt{B^2 - 4A(Ci_{oq}^2 + D)}}{2A} \tag{4-17}$$

Since the d-axis current generally is negative, this expression will be used to produce the optimal current for minimized losses at given operating point. Compared to other research work on LMC, the relationship (4-16) is a second order expression. Considering the implementation, it can easily get the solution of dq current by numerical iteration. It is noted that the current trajectory of the LMC is dependent on the speed, which means that it is a trajectory family in terms of the speed. Plot of the trajectory in the d-q current plane is as shown in Figure 4.4.

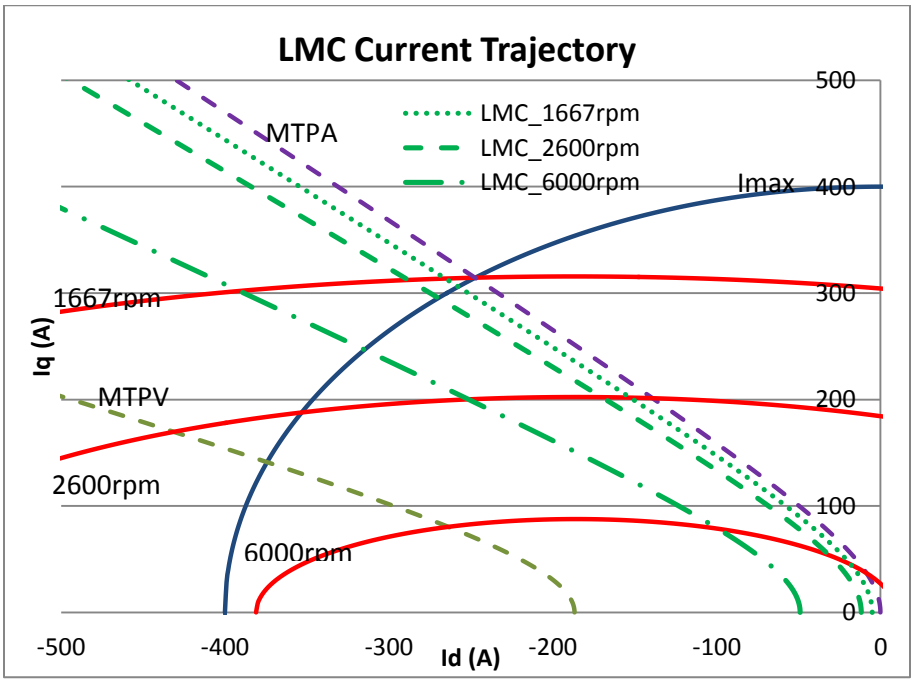

Figure 4.4. LMC current trajectory for varying speeds

Also, the subsequent Figure 4.5 shows an example, by way of plotting, to verify that he LMC current trajectory gives an exact solution for loss minimization. First, the total loss of an example machine operating at 6000rpm with 100 Nm load is calculated

analytically with different dq-axis combinations. Then, the results are plotted in Figure 4.5. The LMC for this speed is also plotted.

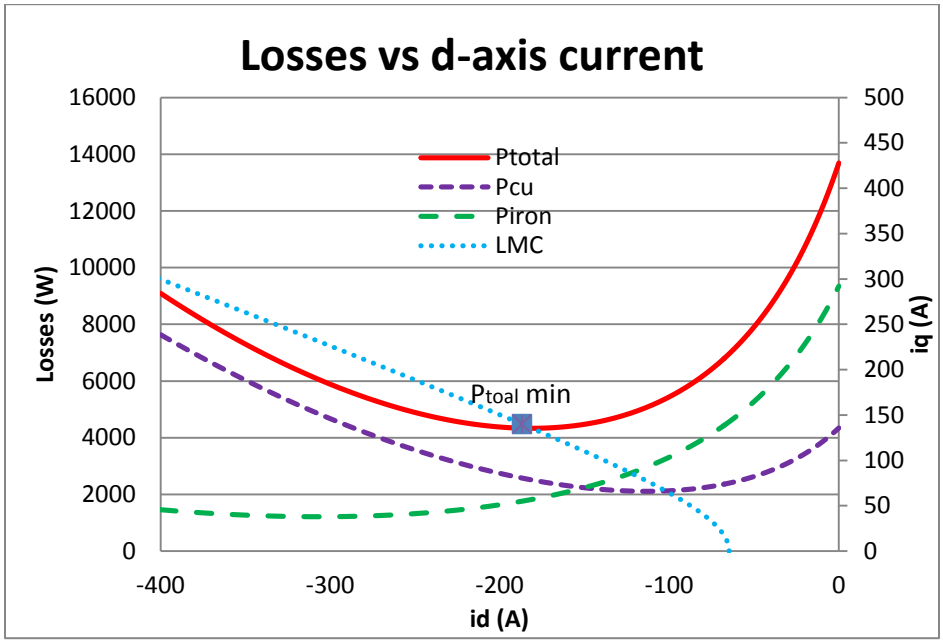

Figure 4.5: Example plot of LMC and total losses

As shown from the plot Figure 4.5, it can be seen that the intersection point between total losses and LMC current trajectory is a minimized point.

4.3 Performance Analysis of LMC

The LMC current trajectory reveals the relationship between d-axis and q-axis currents for optimizing losses operation. The current constraint and voltage constraint are not taken into account in the plot, however. In this section, the performance of the LMC under current and voltage constraints will be investigated.

4.3.1 Current constraint Operation

As for the current constraint, at certain speed, the maximum available torque for the LMC is calculated by setting

$$i_d^2 + i_q^2 = I_{smax}^2 \tag{4-18}$$

And substitute (4-18) into the equation (4-16), it becomes

$$(A - C)i_{od}^2 + Bi_{od} + CI_{smax}^2 + D = 0 \tag{4-19}$$

Solve the equation, the d-q axes currents are

$$i_{odc} = \frac{-B \pm \sqrt{B^2 - 4(A - C)\left(C{I_{smax}}^2 + D\right)}}{2(A - C)} \tag{4-20}$$

$$i_{oqc} = \sqrt{I_{smax}^2 - i_{odc}^2} \tag{4-21}$$

Substitute the d-q-axis currents (4-20) and (4-21) into the torque equation, the maximum torque for the LMC at the certain speed is

$$T_{elmc} = \frac{3}{2}\frac{P}{2}[\lambda_{PM} i_{oqc} + \left(L_d - L_q\right)i_{odc} i_{oqc}] \tag{4-22}$$

Plot of the speed and torque curves are as shown in Figure 4.6.

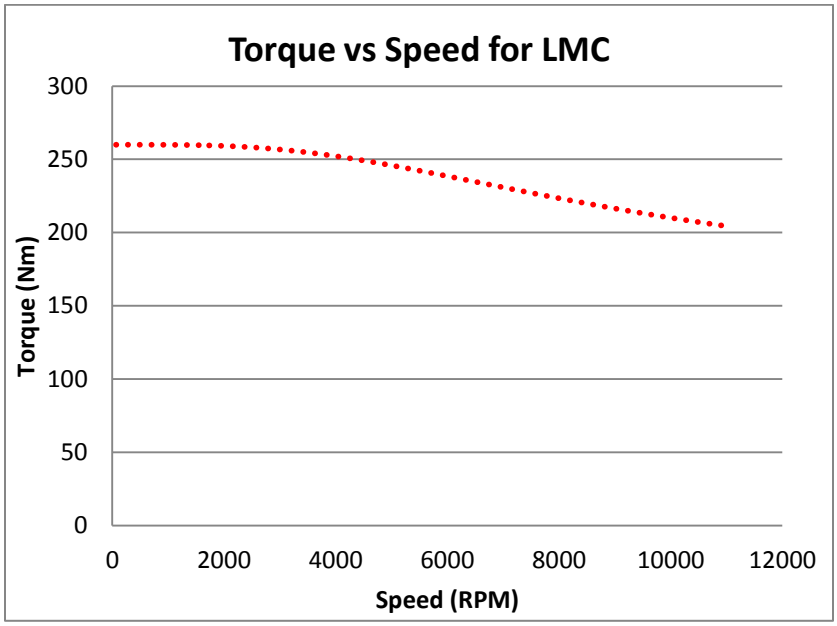

Figure 4.6. Torque-speed characteristic using LMC under current constraint

It should be mentioned that the above torque and speed characteristics do not take into consideration the voltage constraint. Therefore, it is only theoretical analysis with infinite available voltage.

4.3.2 Voltage constraint Operation

When speed increases to a certain value, the voltage constraint is reached. Under this condition, the maximum torque available for the machine is calculate by setting

$$v_d^2 + v_q^2 = V_{smax}^2 \tag{4-23}$$

Or

$$\left(L_q i_{oq}\right)^2 + (\lambda_{PM} + L_d i_{od})^2 = \frac{{V_{smax}}^2}{\omega^2} \tag{4-24}$$

Rearrange the equation as:

$${i_{oq}}^2 = \frac{{V_{smax}}^2}{{L_q}^2 \omega^2} - \frac{(\lambda_{PM} + L_d i_{od})^2}{L_q^2} \tag{4-25}$$

Substitute the above expression into (4-16), and then the follow equation is obtained:

$$A' i_{od}^2 + B' i_{od} + C' = 0 \tag{4-26}$$

where

$$A' = A - \frac{C {L_d}^2}{{L_q}^2}$$

$$B' = B - 2C \frac{L_d \lambda_{PM}}{{L_q}^2}$$

$$C' = D + C\left(\frac{{V_{smax}}^2}{{L_q}^2 \omega^2} - \frac{{\lambda_{PM}}^2}{{L_q}^2}\right)$$

Solve the above equation, and the d-q-axis currents are obtained as:

$$i_{odv} = \frac{-B' \pm \sqrt{B'^2 - 4A'C'}}{2A'} \tag{4-27}$$

$$i_{oqv} = \frac{1}{L_q}\sqrt{\frac{{V_{smax}}^2}{\omega^2} - (\lambda_{PM} + L_d i_{odv})^2} \tag{4-28}$$

Substitute the d-q-axis currents (4-27) and (4-28) into the torque equation, the maximum torque for the LMC at the certain speed is:

$$T_{elmv} = \frac{3}{2}\frac{P}{2}[\lambda_{PM} i_{oqv} + (L_d - L_q) i_{odv} i_{oqv}] \tag{4-29}$$

Plot of the speed and torque curves as shown in Figure 4.7.

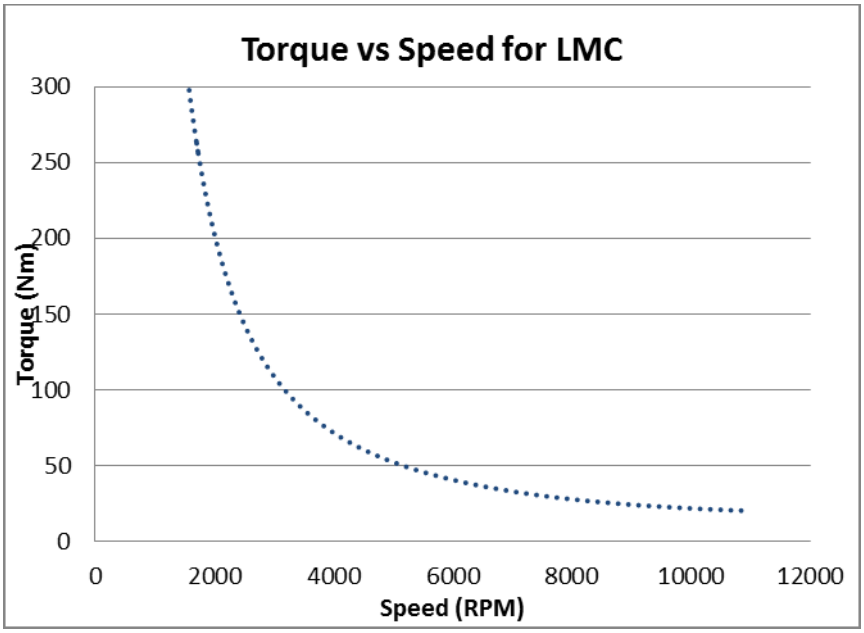

Figure 4.7: Torque-speed characteristic using LMC under voltage constraint

It is noteworthy that the torque-speed characteristics in this case do not take into consideration the current constraint.

4.3.3 LMC Operation Performance Boundary Regions

With both the voltage constraint and the current constraint being taken into consideration, the LMC operation boundary region is obtained in the following plot, which is the overlapped region of the current and voltage constraints.

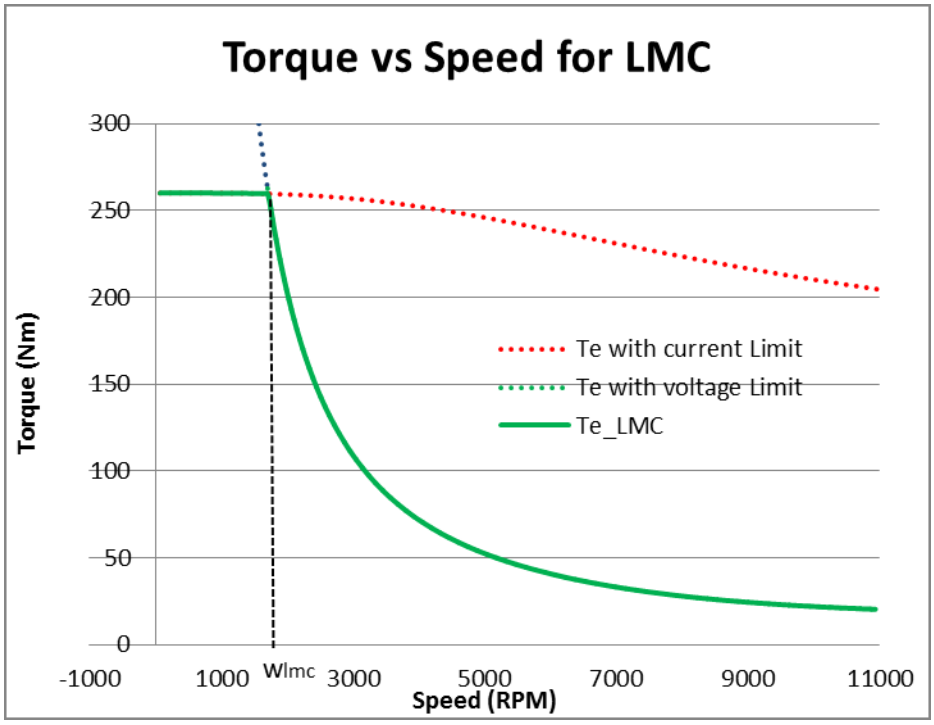

Figure 4.8. LMC operation region considering both voltage and current constraints

The plot shows that, within the low speed range, the voltage constraint is not reached, and the maximum available torque is determined by the current constraint. When motor speed goes up to a certain speed ω_{lmc}, the voltage constraint will be reached, and the maximum available torque is then determined by the voltage constraint. For machine operating within this torque-speed envelop, the LMC can be applied robustly. Here, ω_{lmc} is a critical speed for LMC, which can divide the operation region into current constraint operation region and voltage constraint operation region. It can be calculated from solving the current constraint, voltage constraint, and LMC optimal current trajectory equations.

4.4 Global Solution for Efficiency Improvement

The LMC in the former section is derived from the equivalent circuit with core loss resistance. The optimal current trajectory described by equation (4-16) can be applied in both SPM and IPM. Rewriting equation (4-16) as:

$$Ai_{od}^2 + Bi_{od} + Ci_{oq}^2 + D = 0 \tag{4-30}$$

where

$$A = (L_d - L_q)\left[R_s + \frac{\omega^2 L_d^2}{R_c^2}(R_s + R_c)\right]$$

$$B = \lambda_{PM} R_s + (2L_d - L_q)\frac{\omega^2 L_d \lambda_{PM}}{R_c^2}(R_s + R_c)$$

$$C = -(L_d - L_q)\left[R_s + \frac{\omega^2 L_q^2}{R_c^2}(R_s + R_c)\right]$$

$$D = \frac{\omega^2 L_d {\lambda_{PM}}^2}{R_c^2}(R_s + R_c)$$

For SPM, it can be viewed as a special case with:

$$L_d = L_q$$

Substituting it into equation (4-30), the optimal current trajectory becomes:

$$i_{od} = -\frac{\omega^2 L_d \, \lambda_{PM}(R_s + R_c)}{R_c^2 R_s + \omega^2 {L_d}^2 \lambda_{PM}(R_s + R_c)} \tag{4-31}$$

Equation (4-31) shows that the LMC optimal current for SPM is only related to d-axis current. The torque production of SPM is:

$$T_e = \frac{3}{2}\frac{P}{2}\lambda_{PM} i_{oq} \tag{4-32}$$

The negative d-axis current does not affect the torque production. It just reduces the total flux linkage in the machine and the core loss. Even though the presence of d-axis current will increase the total current and then copper loss, it is still possible to minimize the total loss as discussed in Section 4.2.3.

4.4.1 MTPA Derivation

The MTPA can minimize the copper loss and can also be derived from the LMC current trajectory (4-16). Taking the core loss resistance R_c as infinite, or zero speed, which means to ignore the core losses, it can be seen that coefficients of the equation (4-16) become:

$$A = (L_d - L_q)R_s$$

$$B = \lambda_{PM}R_s$$

$$C = -(L_d - L_q)R_s$$

$$D = 0$$

And (4-16) becomes:

$$\left(L_d - L_q\right)i_{od}^2 + \lambda_{PM}i_{od} - \left(L_d - L_q\right)i_{oq}^2 = 0 \tag{4-33}$$

From (4-33),

$$i_{od} = -\frac{\lambda_{PM}}{2\left(L_d - L_q\right)} + \sqrt{\frac{{\lambda_{PM}}^2}{4\left(L_d - L_q\right)^2} + i_{oq}^2} \tag{4-34}$$

The equations (4-34) and (3-16) are exactly the same. In other words, the MTPA also satisfies the LMC current trajectory. LMC is developed to optimize both copper loss and core losses. It makes sense to take the MTPA as a special case of LMC ignoring the core losses component.

4.4.2 MTPV Derivation

When the speed goes to infinite, the core losses become dominant, and the copper loss can be ignored. Use the LMC current trajectory (4-16), and set the speed to infinite, or zero phase resistance R_s. The equation coefficients of (4-16) become:

$$A = (L_d - L_q)\frac{\omega^2 L_d^2}{R_c}$$

$$B = (2L_d - L_q)\frac{\omega^2 L_d \lambda_{PM}}{R_c}$$

$$C = -(L_d - L_q)\frac{\omega^2 L_q^2}{R_c}$$

$$D = \frac{\omega^2 L_d {\lambda_{PM}}^2}{R_c}$$

And (4-16) becomes:

$$(L_d - L_q)L_d^2 i_{od}^2 + (2L_d - L_q)\lambda_{PM} L_d i_{od} - (L_d - L_q)L_q^2 i_{oq}^2 + L_d {\lambda_{PM}}^2 = 0 \qquad (4\text{-}35)$$

Rearrange the equation (4-35) as:

$$(L_d - L_q)\left[\left(\frac{L_d i_{od} + \lambda_{PM}}{L_q}\right)^2 - {i_{oq}}^2\right] + \lambda_{PM}\left(\frac{L_d i_{od} + \lambda_{PM}}{L_q}\right) = 0 \qquad (4\text{-}36)$$

The equations (4-36) and (3-34) are identified as the same. In this way, the MTPV also satisfies the LMC current trajectory. The MTPV can be taken as a special case of LMC, which focuses on minimizing the core losses instead of the copper loss in MTPA.

4.4.3 Global Solution

The LMC optimal current trajectory (4-16) gives a relationship between dq-axis currents for loss minimization. It is derived based on the equivalent circuit with modeling the core loss as a resistance. MTPA and MTPV are two special case of LMC, which assure the minimized copper loss and the minimized core loss respectively and also satisfy the relationship of (4-16).

In addition, the synchronous machines have similar equivalent circuits with core loss models. The LMC might be applicable to those machines such as synchronous reluctance machine (SRM). To a certain extent, SRM can be viewed as a special case of

IPM, which has no permanent magnet exciting on rotor. The equivalent circuit of SRM is almost the same as IPMs except PM flux λ_{PM}. There is no doubt that the LMC derived from IPM can be applied to SRM with λ_{PM} being set to zero in the optimal current relationship.

The above discussion leads up to the conclusion that the LMC optimal current trajectory (4-16) can be taken as a global solution for the efficiency enhancement control strategy of all the synchronous machines.

4.5 LMC Strategy over Entire Speed Range

The efficiency enhancement control of PMSMs over full speed range can be developed according to the LMC and its operating boundary.

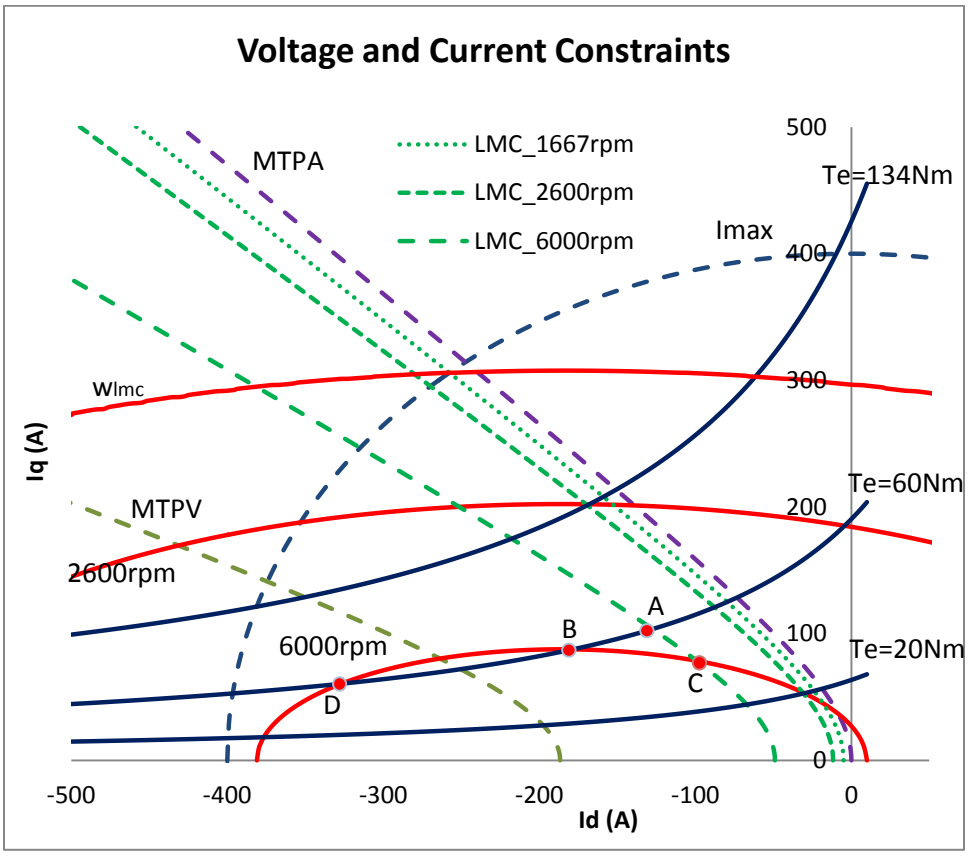

Figure 4.9: LMC current trajectory and constant load

As shown in Figure 4.9, with speed increasing, the LMC current trajectory moves from MTPA to MTPV. The torque capacity decreases with increasing speed due to current and voltage constraints. Based on the operation region and torque speed capacity of LMC, the flow chat of the proposed control strategy is shown in Figure 4.10. The strategy is used to generate dq-axis reference current for the machine operating over the entire speed range.

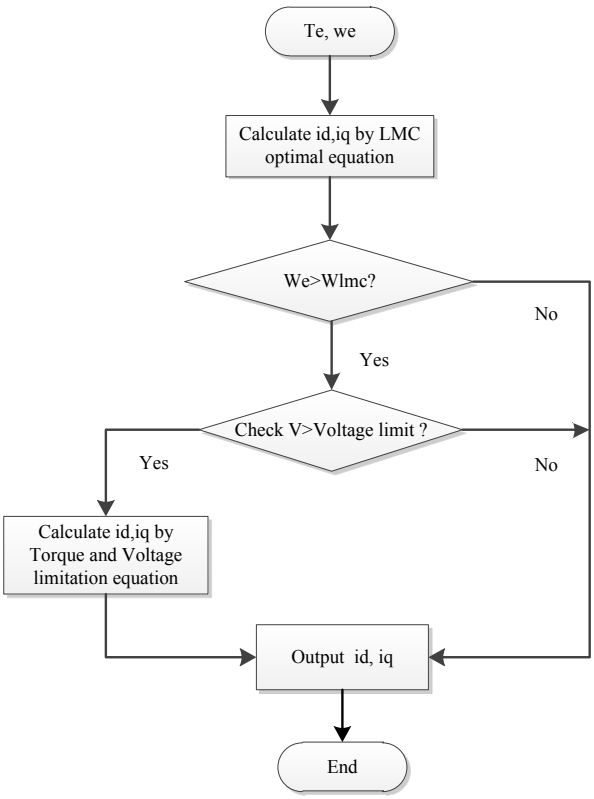

Figure 4.10: Flow chart of efficiency enhancement control strategy

The operation region of LMC can be divided into two regions by the critical speed ω_{lmc} as defined in Section 4.3.3. For speed less than ω_{lmc}, the maximum torque is determined by the current constraint. When the speed goes up to above ω_{lmc}, the maximum torque will be determined by the voltage constraint. Regarding the operation

outside the torque speed envelop, the flux weakening control has to be applied. For example, when a machine runs at the 6000 rpm speed with 60 Nm load, a direct application of LMC at this operating point gives the point A in Figure 4.9. However, the speed in the example is greater than ω_{lmc}, and the machine in question indeed operates in the voltage constraint region. The maximum available torque with LMC for this speed is on the point *C*, which is less than the command load torque. That means point *A* is out of the voltage constraint of 6000 rpm, and the operation point is out of LMC torque speed envelop. Therefore, the LMC optimal current cannot apply to the operating point given in the example. Then the control has to transit to flux weakening, and force the current along the constant torque curve to move to the point *B*, where the voltage constraint can be satisfied. It can be seen that there are still a lot of combinations of dq currents that can afford this operation point between point *B* and *D*. In terms of the efficiency enhancement, the point *B* will be chosen because it is closer to the LMC current trajectory of 6000 rpm, which can still provide a relatively minimized total loss for this operating point under voltage and current constraints. To get the point *B*, it is necessary to solve the constant torque equation with voltage constraint. Since it is a fourth order equation, the approximated solution from [25] is used in this control strategy.

CHAPTER 5 CONTROL SYSTEM SIMULATION MODEL DEVELOPMENT AND RESULTS

In order to analyze and test the control algorithm, the PMSM drive model is built in Matlab/Simulink. This chapter presents the model developed in Simulink. The simulation results of the control strategy are included and analyzed at the end of this chapter. Figure 5.1 shows the block diagram of a basic drive system of PMSM. Table 5.1 lists the parameters of the three machines used in the simulation.

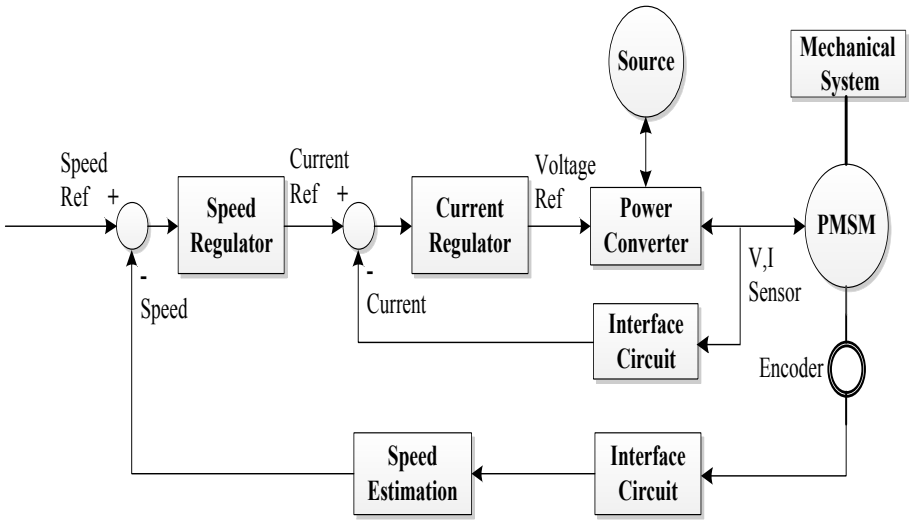

Figure 5.1: Block diagram of a basic drive system

Parameters	Motor A	Motor B
Rs (Ω)	1.93	0.0295
Rc (Ω)	330	47.62*sqrt(wr)
Ld (H)	42.44e-3	3.75e-4
Lq (H)	79.57e-3	8.35e-4
λ_{PM} (V.s)	0.314	0.07
Vdc (V)	300	300
Irate (A)	4.5	268
Pole number	4	6
Rated torque (Nm)	4	133
Rated speed (RPM)	1800	2600

Table 5-1: Parameters of Modeled Machines

5.1 Development of the Simulation Model

5.1.1 PMSM Model with Core Loss

Since the built-in PMSM block in Simulink does not include the core losses, a testing model has to be constructed. According to the equivalent circuit in Figure 4.2, the dynamic equation for the PMSMs is rewritten as:

$$\begin{bmatrix} v_q \\ v_d \end{bmatrix} = \begin{bmatrix} R_s & \omega_r L_d (1 + \frac{R_s}{R_c}) \\ -\omega_r L_q (1 + \frac{R_s}{R_c}) & R_s \end{bmatrix} \begin{bmatrix} i_{oq} \\ i_{od} \end{bmatrix} + \begin{bmatrix} \omega_r \lambda_{PM} (1 + \frac{R_s}{R_c}) \\ 0 \end{bmatrix} + \begin{bmatrix} L_q & 0 \\ 0 & L_d \end{bmatrix} \begin{bmatrix} p i_{oq} \\ p i_{od} \end{bmatrix} \quad (5\text{-}1)$$

In the state form, it is:

$$\begin{aligned} p i_{oq} &= \frac{1}{L_q} [v_q - R_s i_{oq} - \omega_r L_d (1 + \frac{R_s}{R_c}) i_{od} - \omega_r \lambda_{PM} (1 + \frac{R_s}{R_c})] \\ p i_{od} &= \frac{1}{L_d} [v_d - R_s i_{od} + \omega_r L_q i_{oq} (1 + \frac{R_s}{R_c})] \end{aligned} \quad (5\text{-}2)$$

The electromagnetic torque is:

$$T_e = \frac{3}{2} \frac{P}{2} [\lambda_{PM} i_{oq} + (L_d - L_q) i_{od} i_{oq}] \quad (5\text{-}3)$$

The mechanical part dynamic equation is:

$$p\omega_m = \frac{1}{J} (T_e - B\omega_m - T_l), \qquad \omega_r = \frac{P}{2} \omega_m \quad (5\text{-}4)$$

A PMSM model with core loss has been built in Simulink, based on (5-1) and (5-2), for simulation purpose. Figure 5.2 shows the PMSM Simulink model, which includes electrical dynamic subsystem, mechanical dynamic subsystem, and measurements block. The outputs of copper loss and iron loss are calculated by (4-5) and (4-6). The efficiency is calculated by (2-12) and (4-7).

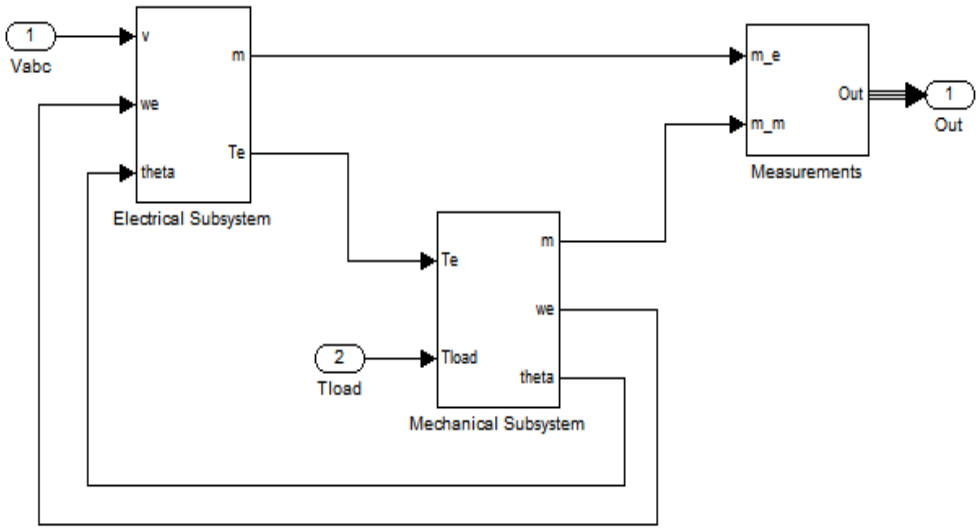

Figure 5.2. PMSM Simulink Model

By way of inserting the model in the Simulink demo to replace the build-in PMSM block, running the simulation and comparing the results, the model is validated.

5.1.2 Current Controller Model

The current controller is used to regulate the machine current so that the latter always tracks the reference command. The output is the voltage reference to the inverter. The current loop is the inner loop of the drive system, and it should have a response faster than that of the outer speed loop. Rewrite the voltage equation (5-1) as:

$$v_q = R_s\, i_{oq} + L_q p i_{oq} + \omega_r L_d \left(1 + \frac{R_s}{R_c}\right) i_{od} + \omega_r \lambda_{PM} (1 + \frac{R_s}{R_c}) \tag{5-5}$$

$$v_d = R_s\, i_{od} + L_d p i_{od} - \omega_r L_q i_{oq} (1 + \frac{R_s}{R_c}) \tag{5-6}$$

Take the backemf component as disturbance, and apply the decoupling feed forward compensation, the voltage equation can be simplified to

$$v_q = R_s\, i_{oq} + L_q p i_{oq} \tag{5-7}$$

$$v_d = R_s\, i_{od} + L_d p i_{od} \tag{5-8}$$

Applying Laplace transformation, the s domain transfer equations are obtained as

$$\frac{I_{oq}}{V_q} = \frac{1}{R_s + L_q s} \tag{5-9}$$

$$\frac{I_{od}}{V_d} = \frac{1}{R_s + L_d s} \tag{5-10}$$

The PI current controller is used in this thesis works, as shown in Figure 5.3.

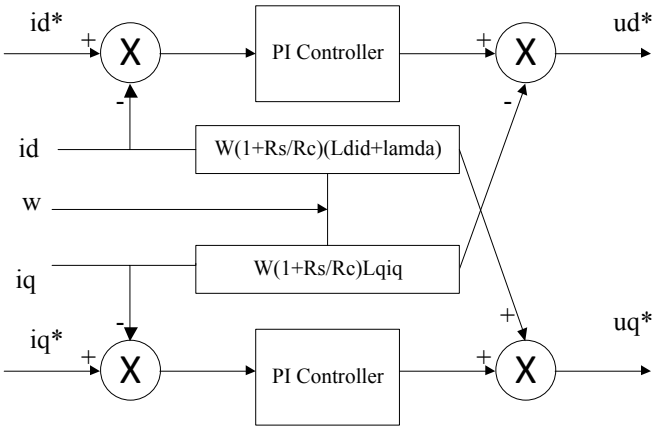

Figure 5.3 : Current Controller

In order to tune the PI-controller, the d-axis current loop in Figure 5.4 is used.

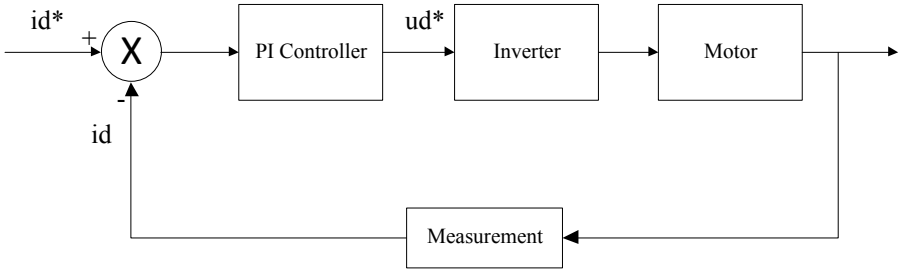

Figure 5.4: d-axis current loop for PI tuning

The transfer functions for PI-controller are represented as:

$$G_{PI}(s) = K_{pi}\frac{(1 + T_{ii}s)}{T_{ii}s} \tag{5-11}$$

The power inverter can be modeled as:

$$G_{inv}(s) = \frac{1}{1 + \tau_{inv}s} \tag{5-12}$$

The motor plant transfer function is:

$$G_m(s) = \frac{1}{R_s}\frac{1}{1+\tau_m s}, \tau_m = \frac{L_d}{R_s} \tag{5-13}$$

For the measurement feedback, it can be modeled as:

$$G_{fd}(s) = \frac{1}{1+\tau_{fd} s} \tag{5-14}$$

By rearranging the current loop, unity feedback can be achieved, as shown in Figure 5.5.

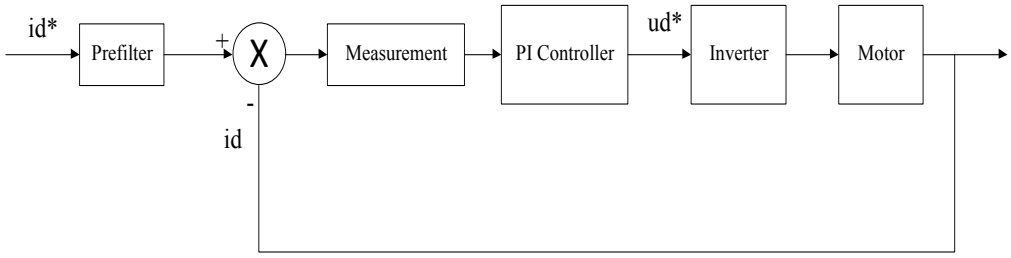

Figure 5.5: Unity feedback current loop

The pre-filter is used with transfer function $G_{prf}(s) = 1 + \tau_{fd} s$

Thus, the open loop transfer function then can be obtained as:

$$G_{ol}(s) = K_{pi}\frac{(1+T_{ii}s)}{T_{ii}s}\left(\frac{1}{1+\tau_{inv}s}\right)\left(\frac{1}{R_s}\frac{1}{1+\tau_m s}\right)\left(\frac{1}{1+\tau_{fd}s}\right) \tag{5-15}$$

Generally, the time constants for inverter τ_{inv} and measurement τ_{fd} are set to 50% of the switching frequency of the inverter, as $0.5\tau_{sw}$. Compared with machine time constant, they are much smaller, and can be approximated as one, first-order transfer function, with time constant equal to the sum of each of them. Also, by applying pole-zero cancellation, the slowest pole of the PMSM can be cancelled by the PI-controller. As a result, equation (5-15) becomes:

$$G_{ol}(s) = \frac{K_p}{R_s T_{ii} s}\left(\frac{1}{1+\tau_{sw}s}\right) \tag{5-16}$$

In order to calculate the PI-controller gains, the Modulus Optimum (MO) criterion by Kessler [28] is applied. Then,

$$K_{pi} = \frac{R_s T_{ii}}{2\tau_{sw}}, T_{ii} = \tau_m \tag{5-17}$$

For the simulated motor A, the bode plot and step response of the current loop are shown in Figure 5.6.

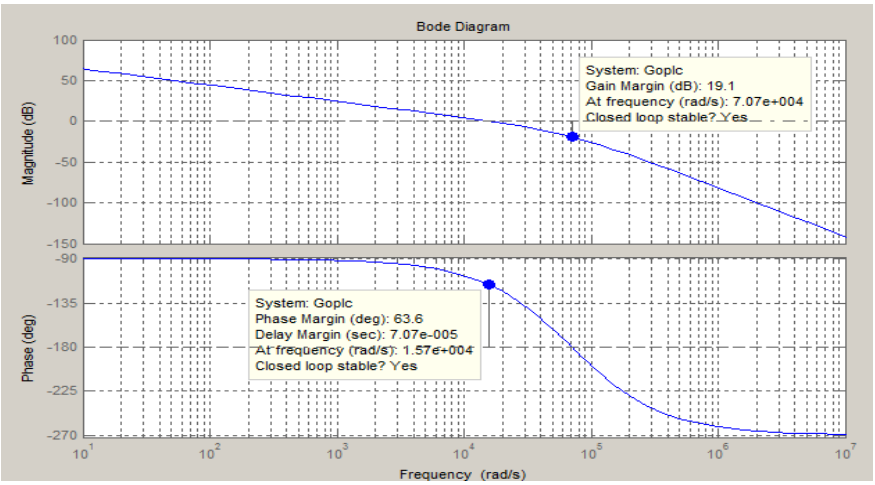

(a)

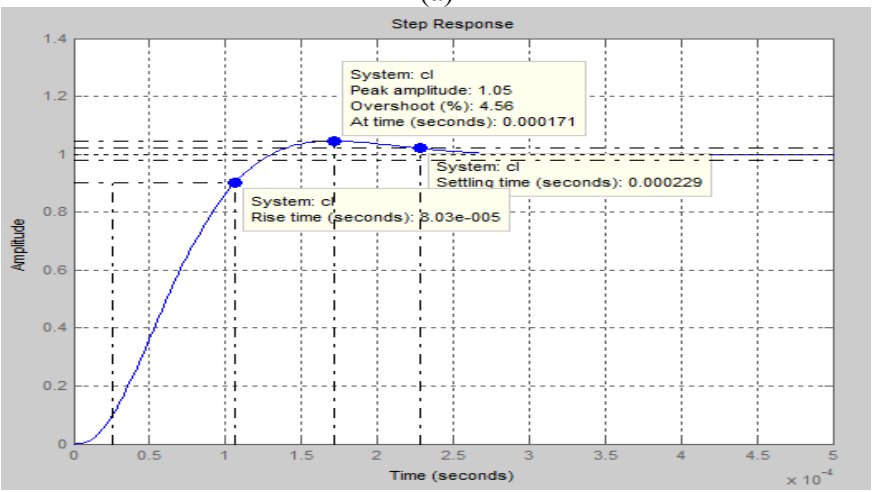

(b)

Figure 5.6: Bode plot and step response of current loop

It shows that the closed loop system is stable with 63.6° phase margin and 19.1dB gain margin. The step response has 0.0303ms rising time, 0.229ms settling time, and

4.56% overshoot. The q-axis current controller can be tuned in the similar way as d-axis current loop.

5.1.3 Speed Controller Model

Compared with the inner current loop, the speed loop is slower. In this thesis, the speed loop is used to produce the torque command to the control strategy block. From mechanical torque speed equation:

$$T_e = Jp\omega_m + B\omega_m + T_l \tag{5-18}$$

Take the load torque T_l as disturbance, and neglect the friction viscous. The transfer function of motor can be represented as:

$$G_m(s) = \frac{K_t}{Js} \tag{5-19}$$

where K_t is torque constant.

The controller design is based on the speed loop shown in Figure 5.7.

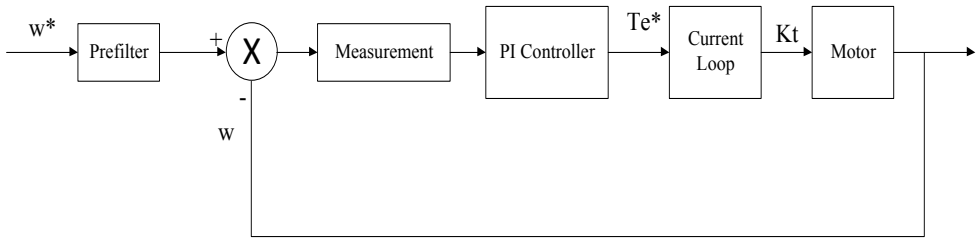

Figure 5.7: Speed loop with unity feedback

Since the current loop is generally 10 times faster than the speed loop, it can be approximated as a first order transfer function

$$G_{cur}(s) = \frac{1}{1 + \tau_{cur}s} \tag{5-20}$$

The measurement transfer function is

$$G_{ms}(s) = \frac{1}{1 + \tau_{ms}s} \tag{5-21}$$

The open loop transfer function then can be obtained as

$$G_{ol}(s) = K_{ps}\frac{(1+T_{is}s)}{T_{is}s}\left(\frac{1}{1+\tau_{ms}s}\right)\left(\frac{1}{1+\tau_{cur}s}\right)\frac{K_t}{Js} \tag{5-22}$$

In order to simplify the transfer function, the delays caused by the current loop and the measurement can be approximated to a first order transfer function with time constant T_d as the sum of the delays. Then the open loop transfer function (5-22) becomes

$$G_{ol}(s) = \frac{K_{ps}K_t(1+T_{is}s)}{JT_{is}s^2(1+T_ds)} \tag{5-23}$$

Applying the Optimum Symmetric Method (OSM) [29], the optimal controller gain can be calculated as

$$K_{ps} = \frac{J}{2K_tT_d}, T_{is} = 4T_d \tag{5-24}$$

For simulation motor A, the bode plot and step response of the speed loop are shown in Figure 5.7.

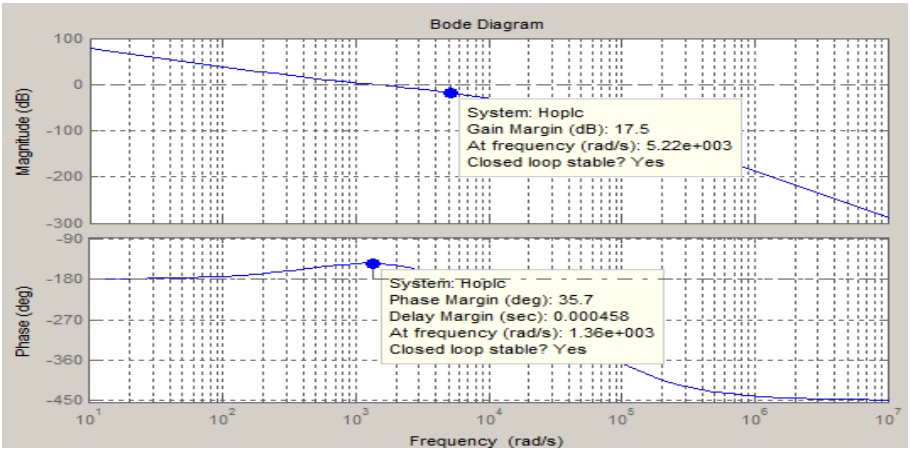

(a)

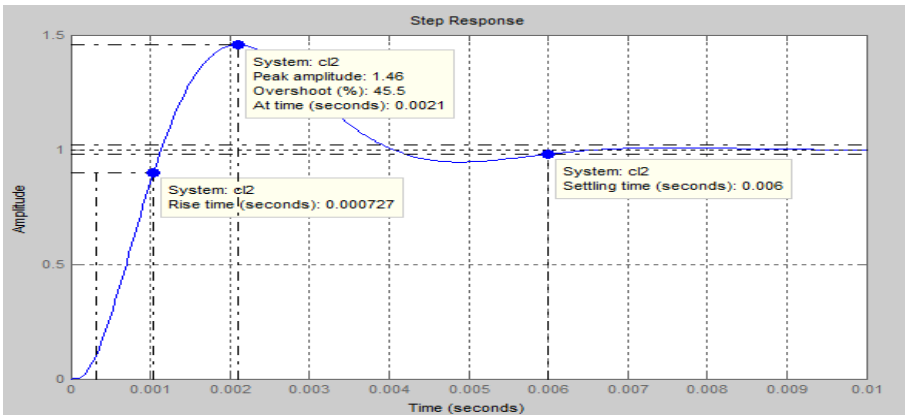

(b)

Figure 5.8: Bode plot and step response of current loop

The results show that the speed loop response is slower than that of the current loop. And it is noted that the step response has a large overshoot. In order to avoid the saturation of the controller output, the anti-windup technique can be used [30].

5.2 Machine Model Validation

A drive system has been built in Simulink using the PMSM model incorporated with core loss. It is shown in Figure 5.9.

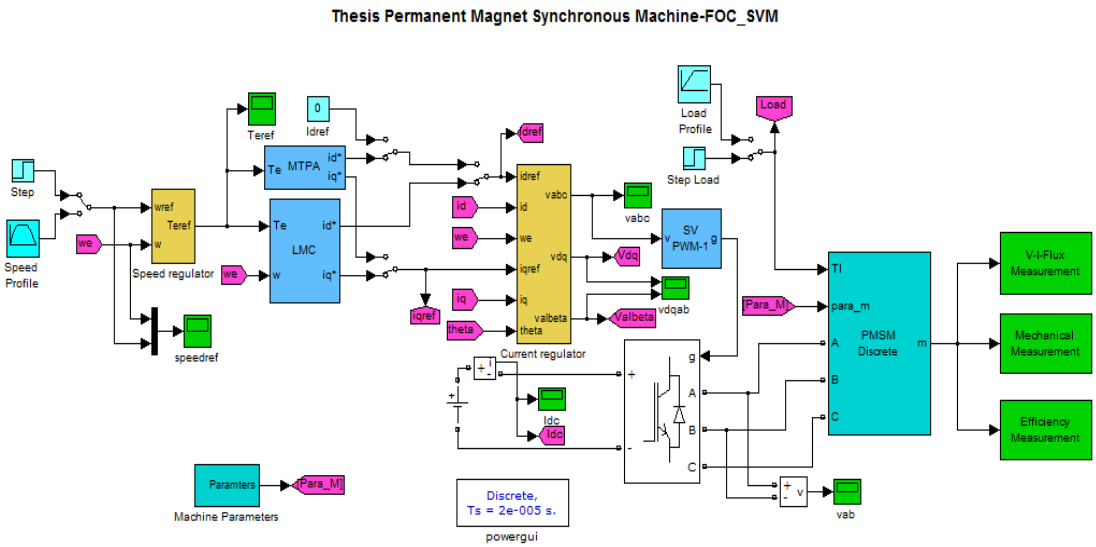

Figure 5.9: PMSM drive system in Simulink

The whole system includes current controller, speed controller and space vector PWM blocks. The LMC and MTPA blocks are used to generate the dq-axis current reference.

To validate the machine model, the simulation is carried out on Motor A first at different operating conditions mentioned in following sections.

5.2.1 No-load Test Case Simulation

The speed response is investigated with zero d-axis current, at no load. At $t = 0$, the rated speed command 188 rad/s is applied. And at $t = 2.5$s, the speed decreases to 120rad/s. The results are presented in Figure 5.10.

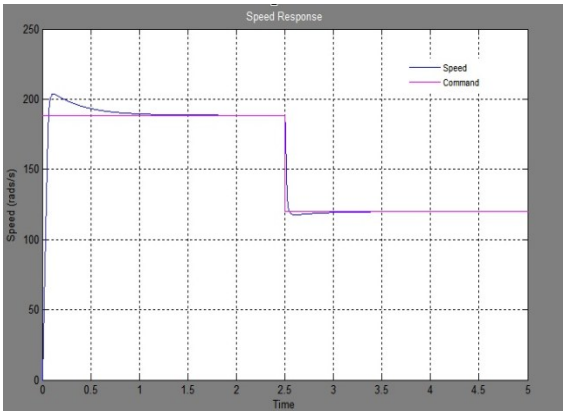

(a) speed response

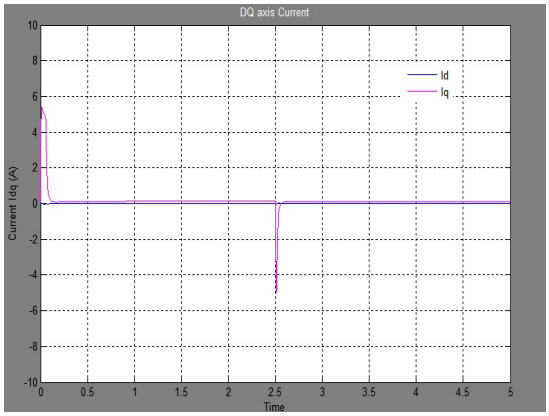

(b) d-q-axis current

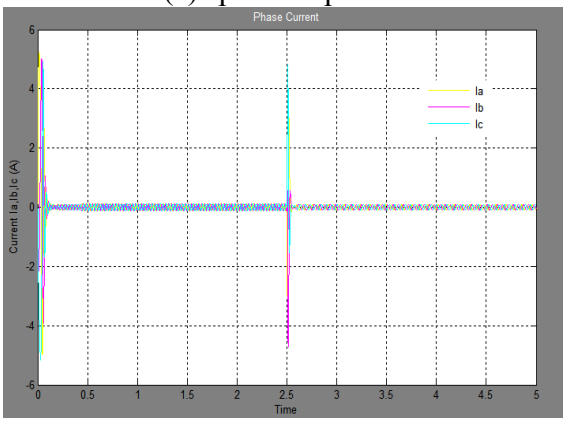

(c) phase current

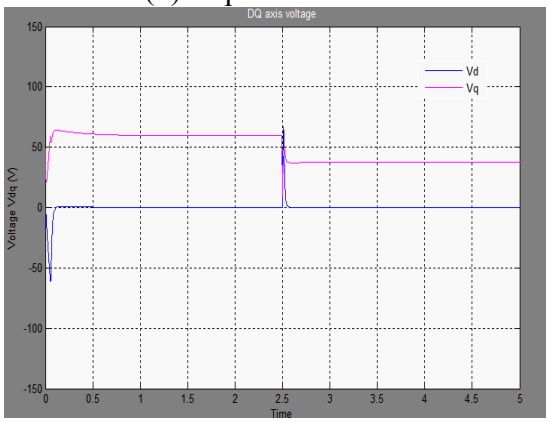

(d) d-q-axis voltage

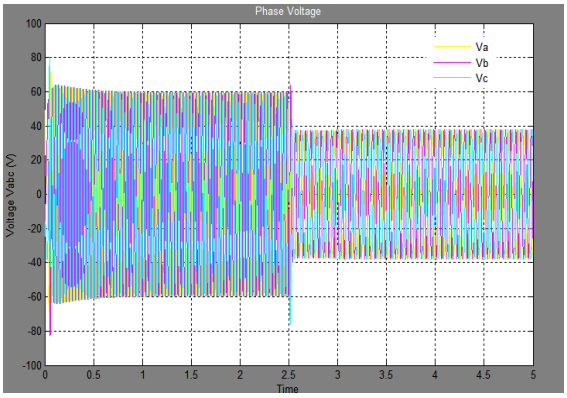

(e) phase voltage

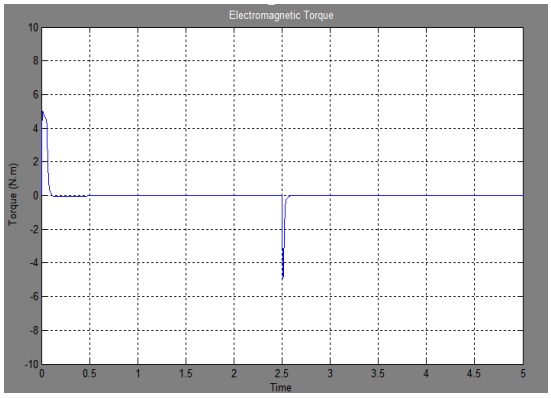

(f) torque response

Figure 5.10: No-load speed response simulation results

The results indicate that the drives have fast response corresponding to a rapid speed transient.

5.2.2 Load Disturbance Test Case Simulation

Subsequently, the load disturbance test is performed. The motor runs at rated speed, and a rated load is applied at t = 1.5s and removed at t = 3s. The results are shown in Figure 5.11.

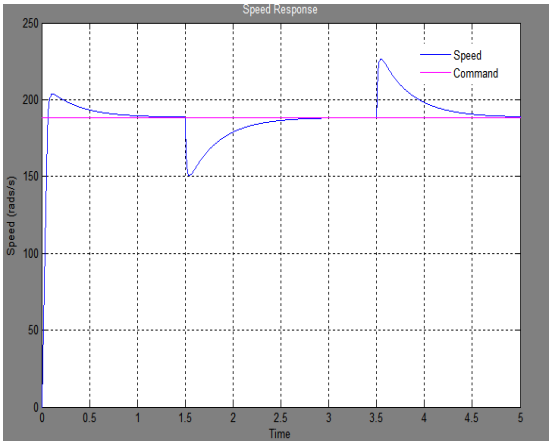

(a) speed response

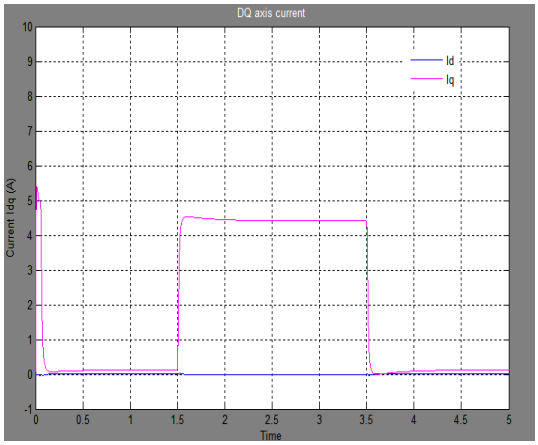

(b) d-q-axis current

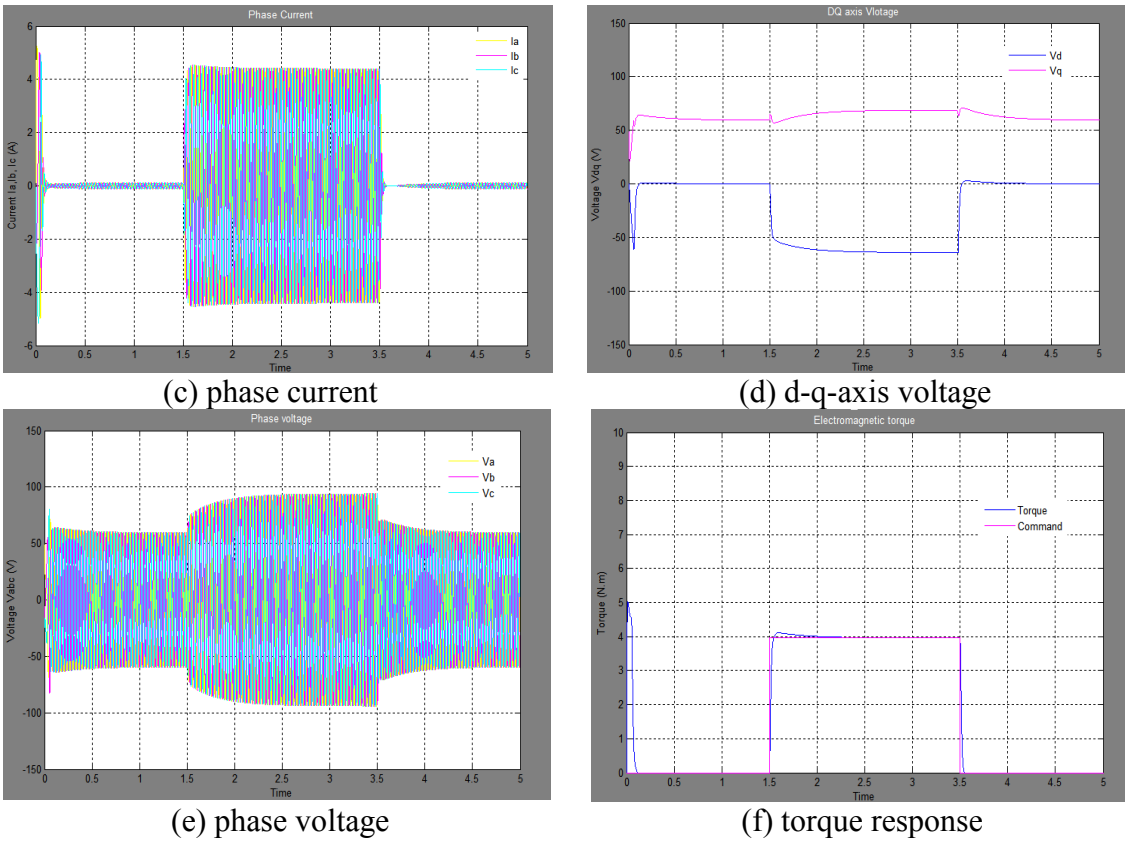

(c) phase current (d) d-q-axis voltage

(e) phase voltage (f) torque response

Figure 5.11: Load disturbance response simulation results

As the results indicate, the torque increases quickly to a high value when the load is applied. It can also be seen that the q-axis current respond quickly to the rated current, which can support the rated speed and load condition. Also, the phase voltage has the same response as the current. The speed overshoot is a little bit large when the rated load is applied and removed. This can be improved by weakening the integrating gain in the PI speed controller.

5.2.3 Effect of d-axis Current on Loss Simulation

In order to investigate the effect of the d-axis current on the losses, a simulation is conducted by applying a continuously changing d-axis current at the rated speed and the rated load. Here, a ramp block in Simulink is used as d-axis current command. The slope

of the ramp signal is set as negative, and the initial value is set as zero. In other words, the d-axis current is decreased from zero to the negative set value. The simulation results are shown in Figure 5-12.

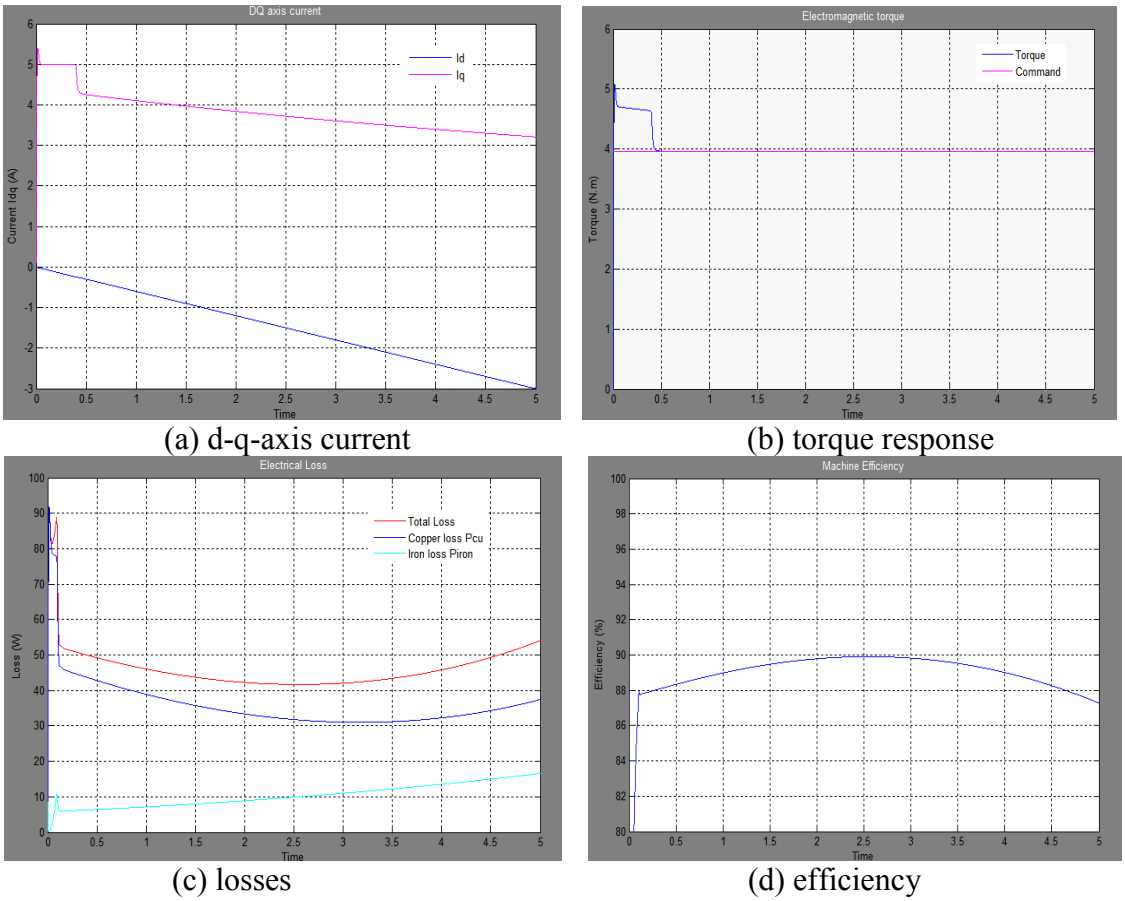

(a) d-q-axis current (b) torque response

(c) losses (d) efficiency

Figure 5.12. Effect of the d-axis current on loss simulation

The simulation results show that total electrical loss is a function of the d-axis current. By injecting different i_d, the drives regulate the q-axis current to ensure the machine running at the command operating point. It can be seen that the varied combinations of i_d and i_q give losses at different levels as well as changing machine efficiency. Based on this observation, the loss minimization control can be achieved by appropriately adjusting the i_d.

5.3 LMC Simulation

In order to test the LMC control strategy, the simulation will be carried out in different cases. First, the steady state operation performance is simulated. And then the transition performance between LMC and FWC is investigated. Last, the drive cycle simulation is undertaken.

5.3.1 Steady State Simulation

The steady state simulation is performed on Motor A. It runs at the rated speed and the rated load. The simulation time is 4 sec with LMC being applied for the first 2 seconds and MTPA for the rest of the time. The results are shown as Figure 5.13.

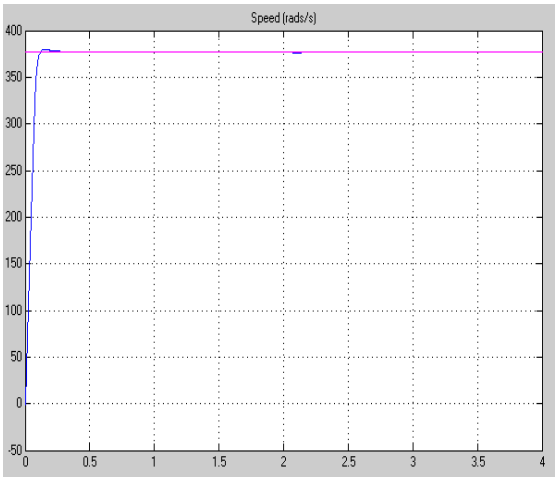

(a) speed response

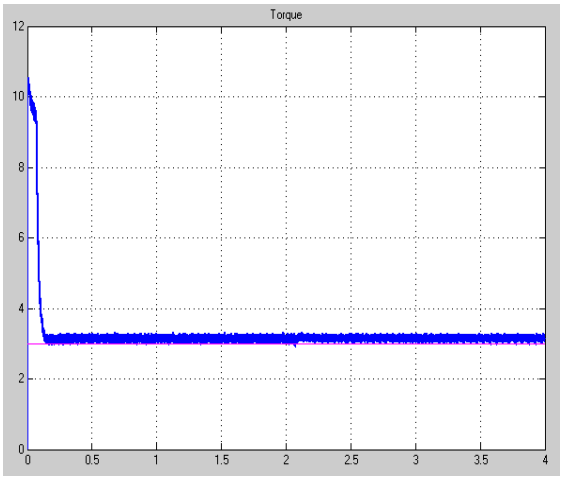

(b) torque response

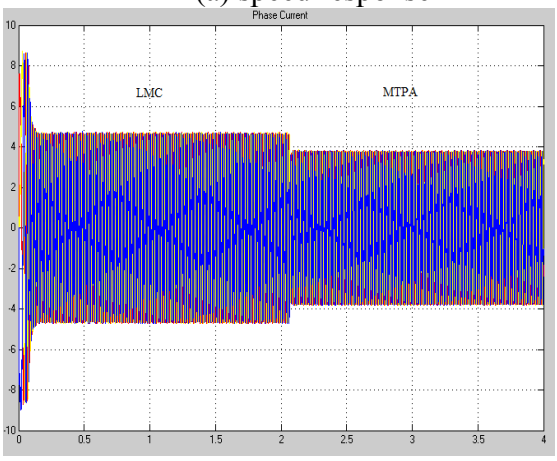

(c) phase current

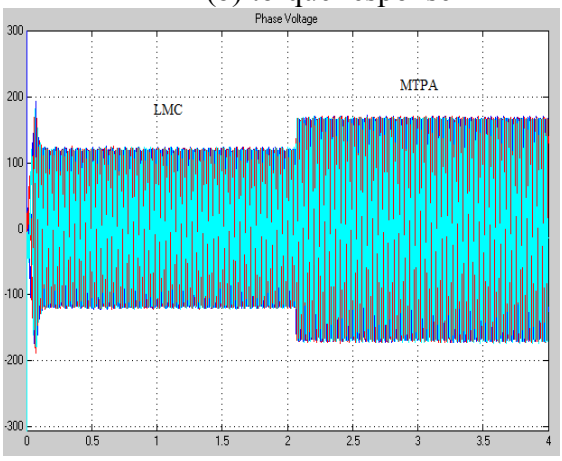

(d) phase voltage

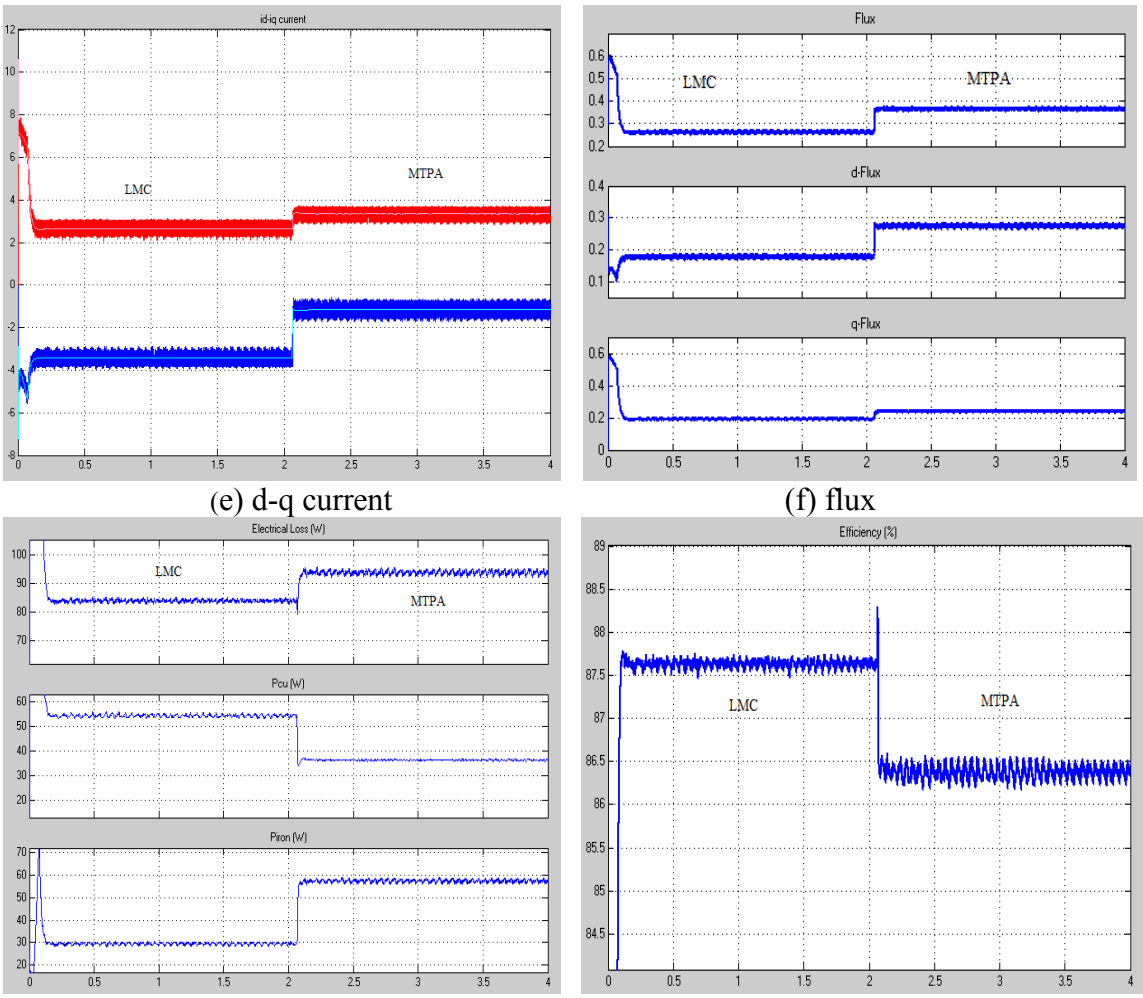

(e) d-q current (f) flux

(g) loss (h) efficiency

Figure 5.13: Steady state simulation for LMC

It can be seen from the simulation results that LMC have fast speed and torque response. When LMC is applied to the motor, id goes to more negative than that of MTPA, and the phase current is larger than MTPA. However, since the id reduces the total machine flux, the phase voltage of LMC becomes lower than MTPA. The loss results also show that the copper loss is larger than MTPA due to larger phase current. The iron loss is inferior to the one of MTPA, however, and their difference is greater than the difference in copper loss. The total loss is found to decrease, and then the efficiency is improved. This steady state simulation validates that the LMC has better performance

than MTPA from the efficiency point of view, while the former maintains the same speed and torque response as the latter.

5.3.2 Simulation for Operating Above Base Speed

When the machine operates at above base speed, the MTPA cannot be applied anymore. The LMC still can be used unless the voltage constraint is reached. As shown in Figure 5.14, the motor B will operate at 6000 rpm with 20 Nm load, and there are many options for this condition between point A to point D along constant torque curve. Generally, flux weakening control will choose point A, LMC will take point B, and MTPV will use point C. In this simulation, the performance of the three controls will be compared.

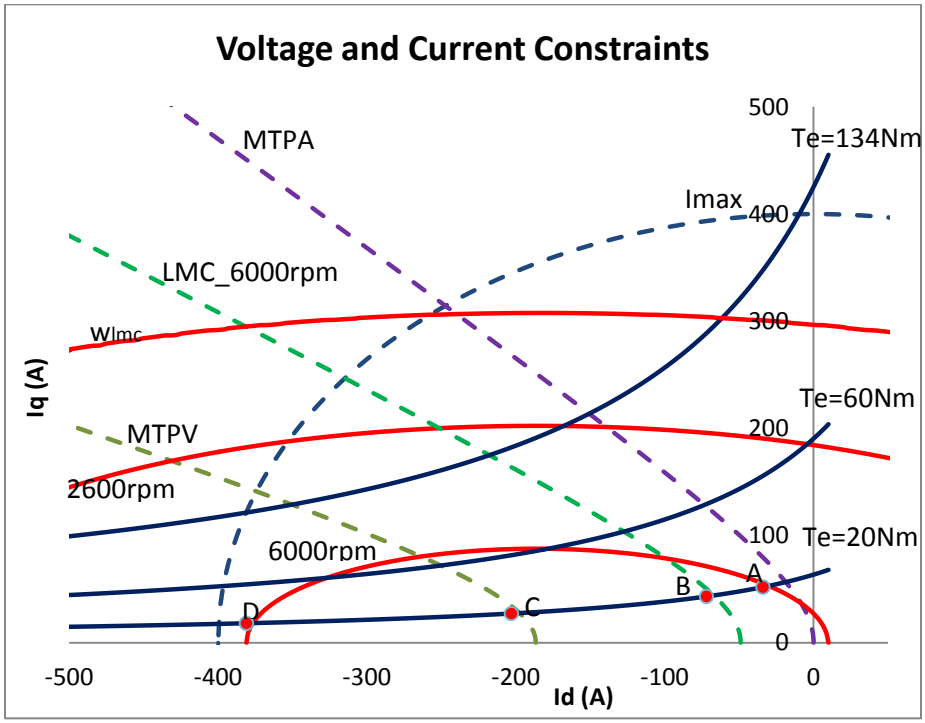

Figure 5.14: Operating point of FWC, LMC, and MTPV

In this simulation, Motor B operates above the base speed, and the performance of LMC is compared with that of FWC and MTPV.

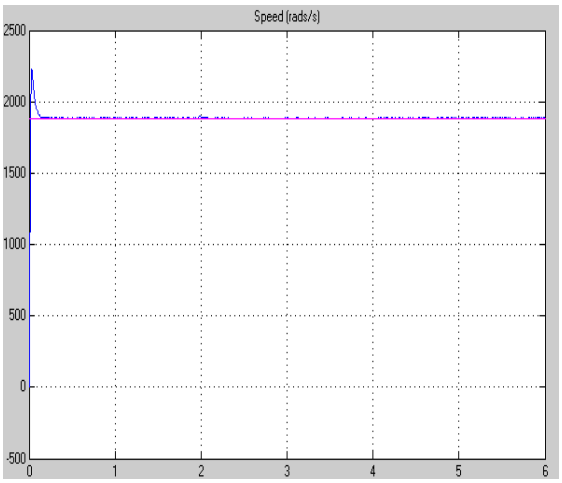

(a) speed response

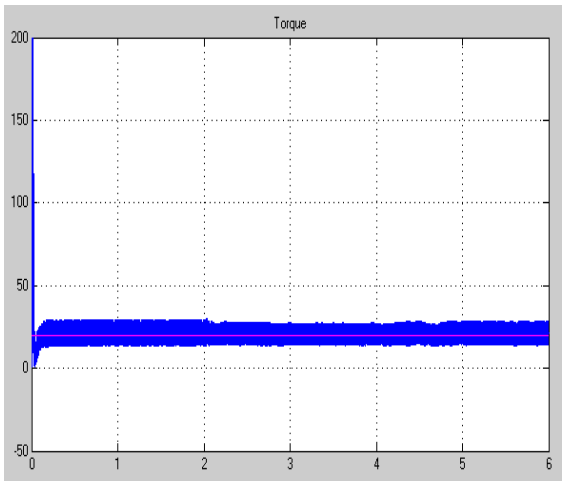

(b) torque response

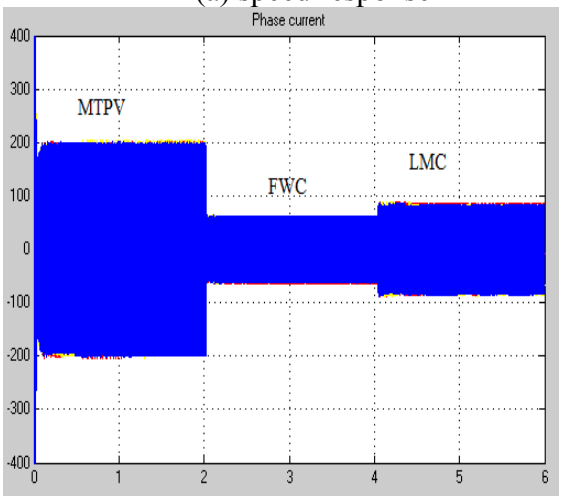

(c) phase current

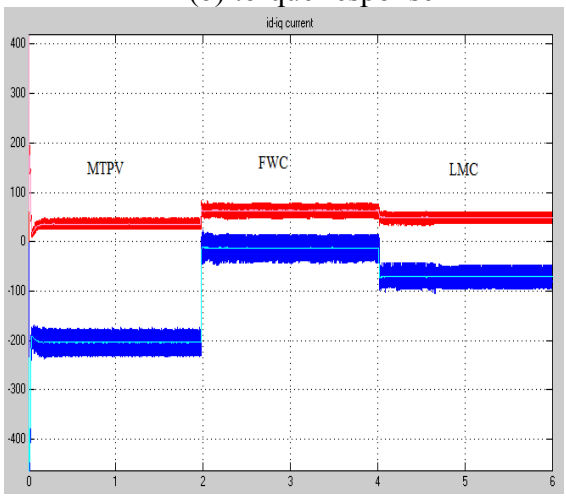

(d) d-q current

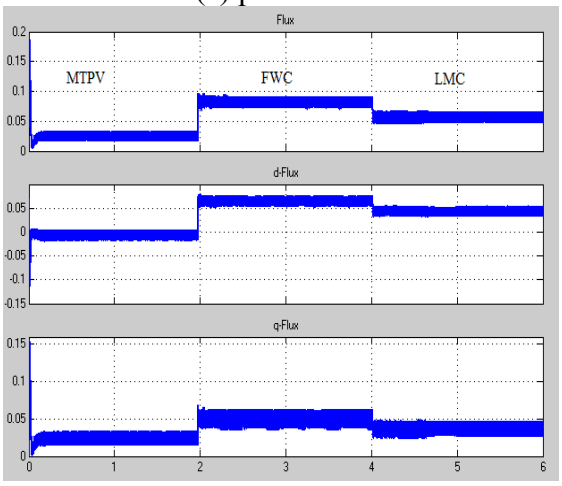

(e) flux

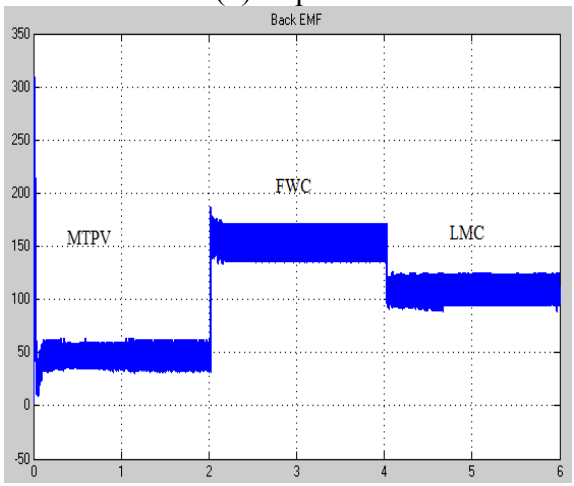

(f) back EMF

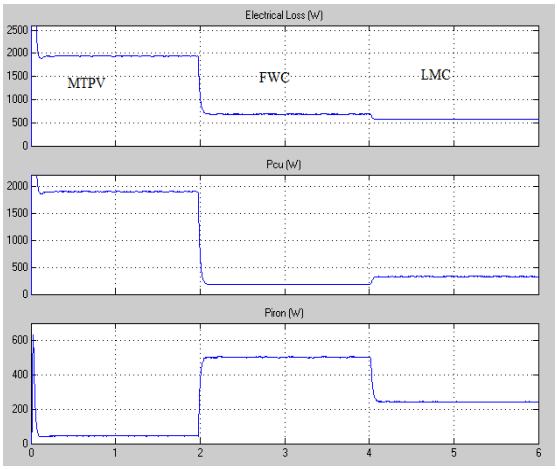

(g) losses

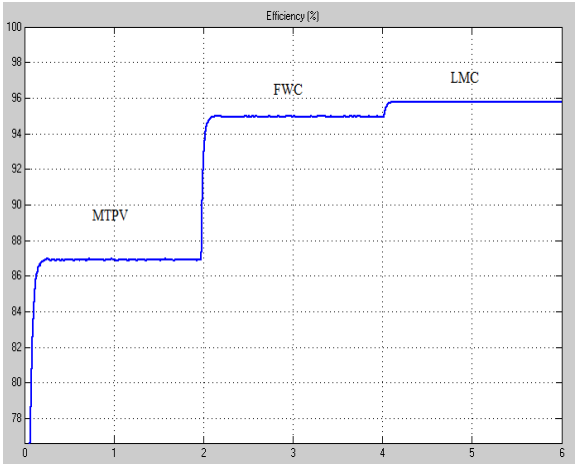

(h) efficiency

Figure 5.15: Simulation comparison of MTPV, FWC, and LMC

The simulation results in Figure 5.15 show that MTPV, FWC and LMC all can support the operating point above base speed. In term of losses, MTPV have minimized core losses. LMC provides highest efficiency. The performance of FWC is between the aforesaid two. It is noteworthy that for MTPV, the d-axis flux becomes a little bit negative. As shown in Figure 5.14, the point C is located on the left side of the voltage constraint center point $(-\frac{\lambda_{PM}}{L_d}, 0)$. Since in the simulation, Motor B has a $\frac{\lambda_{PM}}{L_d}$ inferior to the maximum phase current, it theoretically has an infinite extended speed range. It is thus possible for the the d-axis flux to be negative. In real application, in order to avoid the demagnetization of the permanent magnet, there are certain limiting factors for the allowed maximum demagnetizing current.

5.3.3 Transition Simulation

This simulation is to test the performance of transition between LMC and FWC. The speed is set to 6000 rpm, and the load rises from 0 to 60 Nm. Since the maximum available torque of LMC for 6000 rpm is 38 Nm, the control should transfer from LMC

to FWC after the load toque becomes greater than 38 Nm. The results are shown as Figure 5.16.

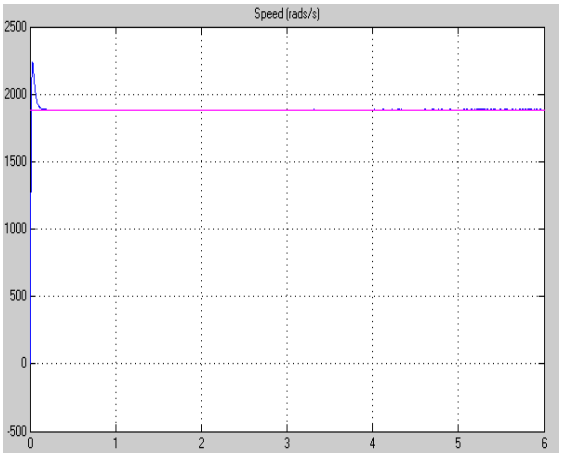

(a) speed response

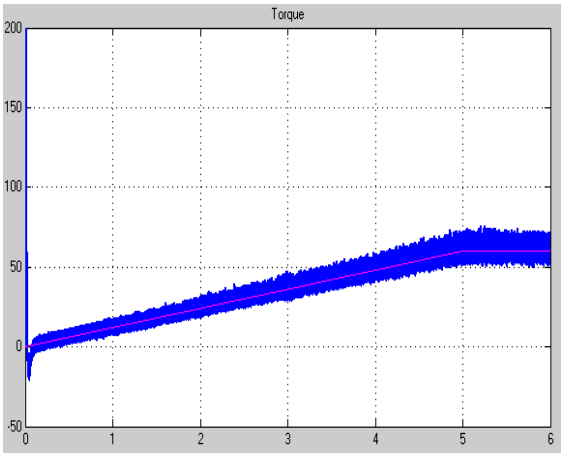

(b) torque response

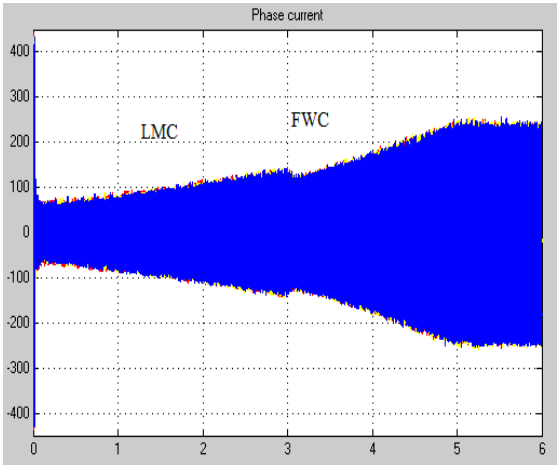

(c) phase current

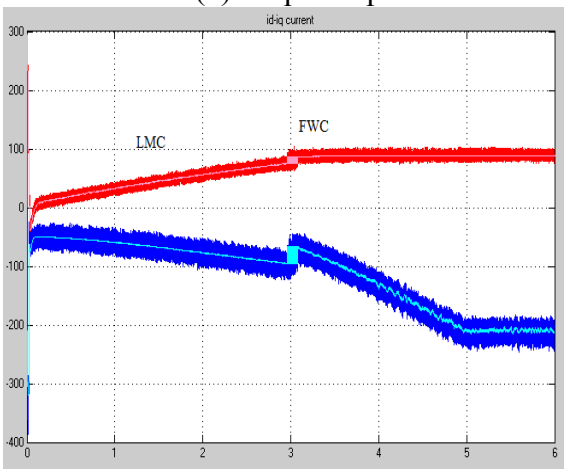

(d) d-q current

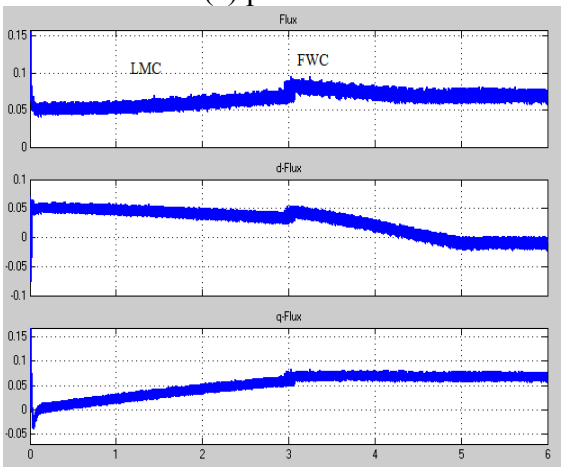

(e) flux

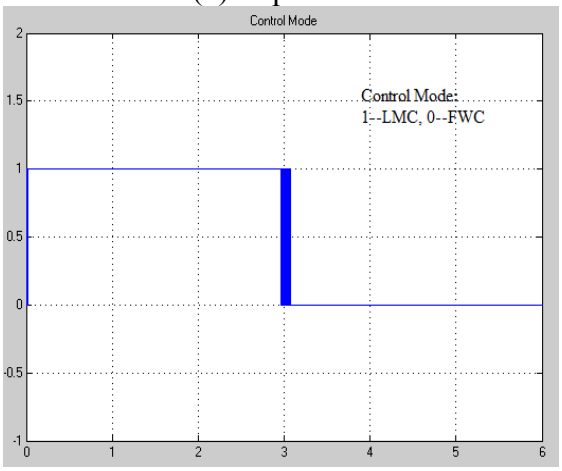

(f) control mode

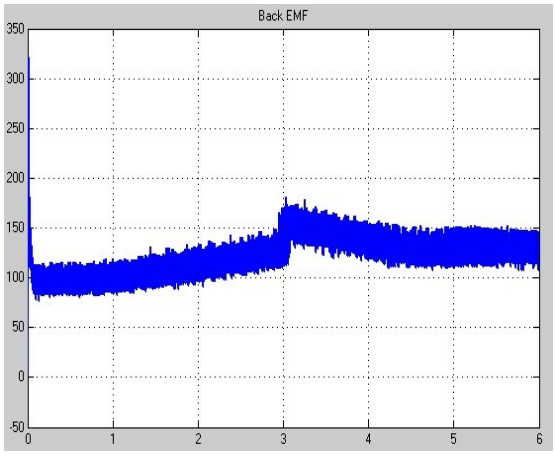

(g) back EMF

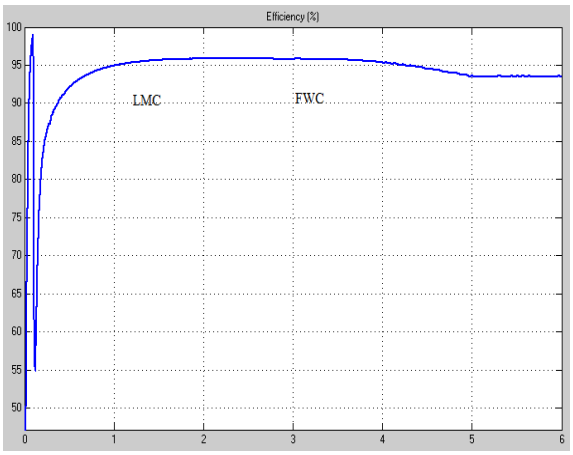

(h) efficiency

Figure 5.16: Transition simulation results

The simulation results in Figure 5.16 show that the speed and the torque have a good tracking of the command. The transition from LMC to FWC happened at 3 second, where the load torque rises to 36 Nm. After that point, the LMC current trajectory goes outside the voltage constraint. So the control has to transfer to FWC. It is shown in back emf result that the voltage goes up to around 173 V, which is the voltage constraint for Motor B. In order to keep the machine working with voltage constraint, FWC forces the current to more negative so as to weaken the flux. The flux result also shows that the total flux decreases after FWC being applied until the machine reaches steady state. The control mode plot is used to show the changes in control mode. It is consistent with the simulation condition. During the transition, there is a short transient period as shown in the dq current results.

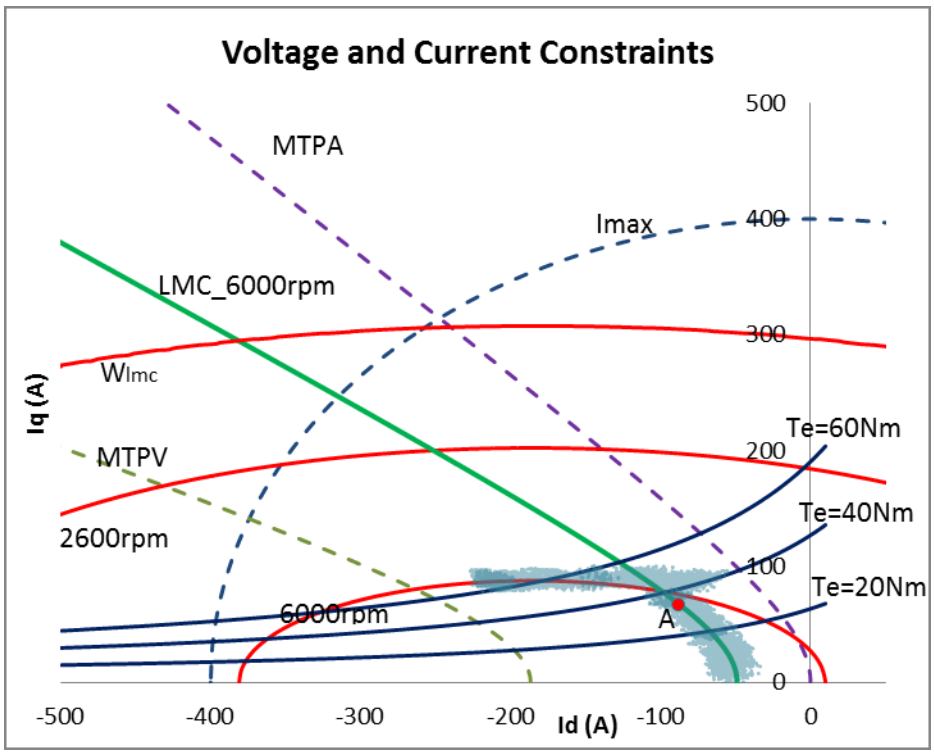

Figure 5.17: Transition simulation current trajectory

By plotting the dq current simulation results in the dq current plane, it is observed that the current exactly follows the LMC curve for 6000 rpm with load torque increasing. After the maximum available torque is reached at the point A, the current trajectory is going to follow the FWC's current trajectory, which includes the intersection points between the torque and voltage constraint curves. In other words, it is on the voltage constraint eclipse.

5.3.4 Vehicle Drive Cycle Test Case Simulation

This test is to simulate one simple operating cycle of motor. The speed profile and load torque profile are shown in Figure 5.18.

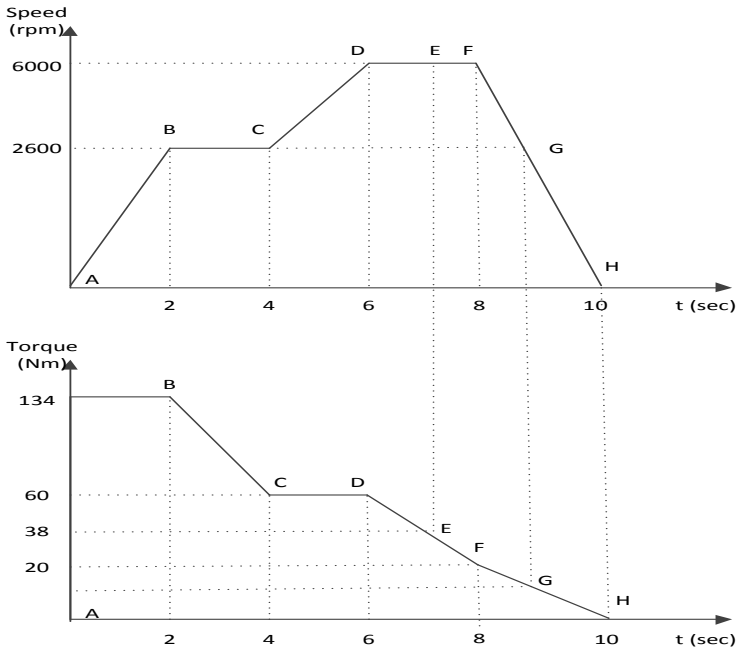

Figure 5.18: Speed and torque profile of drive cycle

The machine starts up with large rated load 134 Nm, and speeds up to the rated speed 2600 rpm. Once the speed is reached at 2 second, the load torque decreases gradually to 60 Nm at 4 seconds. And then the machine speeds up again to 6000 rpm with constant load torques 60 Nm. The machine stays at the 6000 rpm from 6 second, and the load torque begins to reduce. At 8 second, the speed of the machine also decreases to zero with load torque. The simulation results are shown as Figure 5.19.

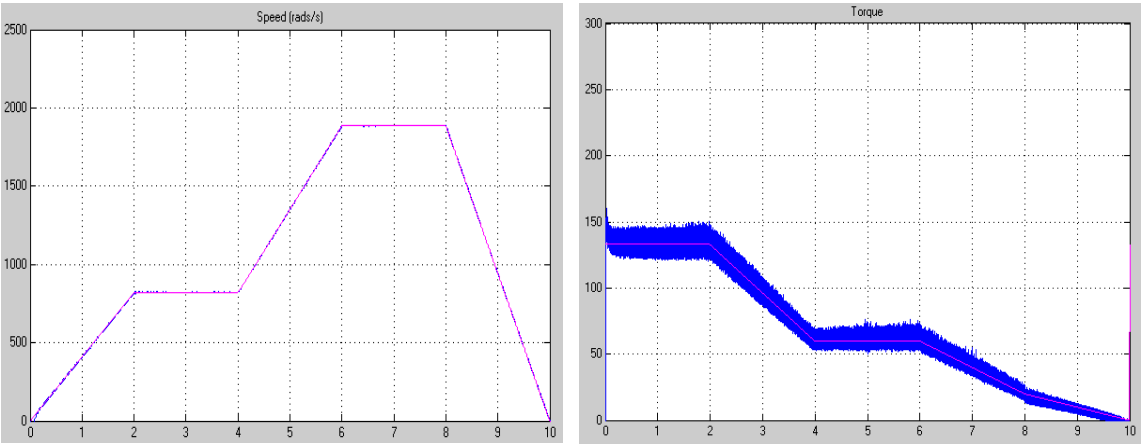

(a) speed response

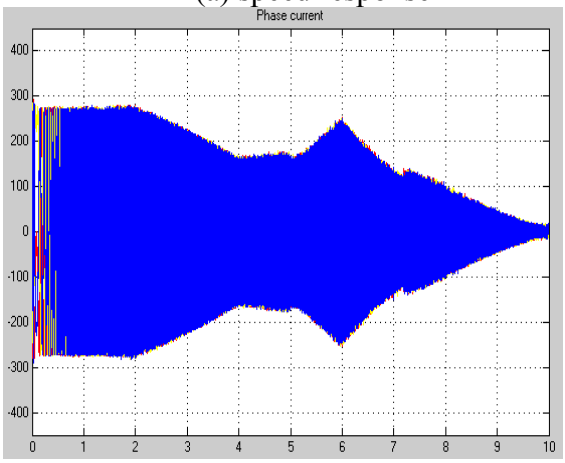

(b) torque response

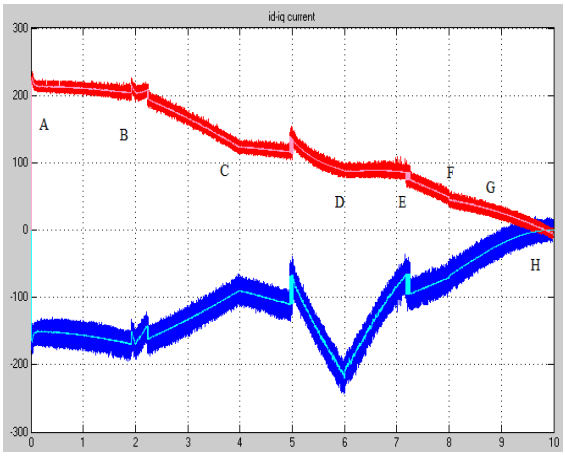

(c) phase current

(d) d-q current

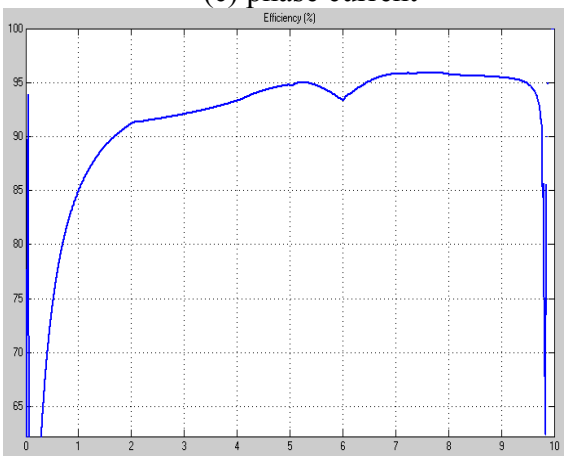

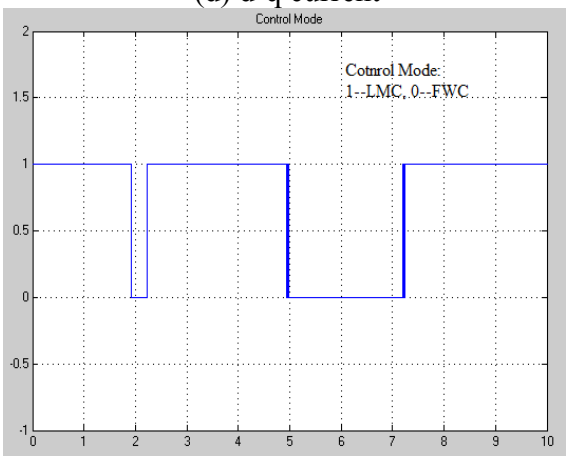

(g) efficiency

(h) control mode

Figure 5.19: Drive cycle simulation results

It is observed that the cycle operation includes the steady state and the transition between FWC and LMC. The speed and torque responses appear to be fast and stable during the whole cycle. The current trajectory in dq current plane is plotted in Figure 5.20.

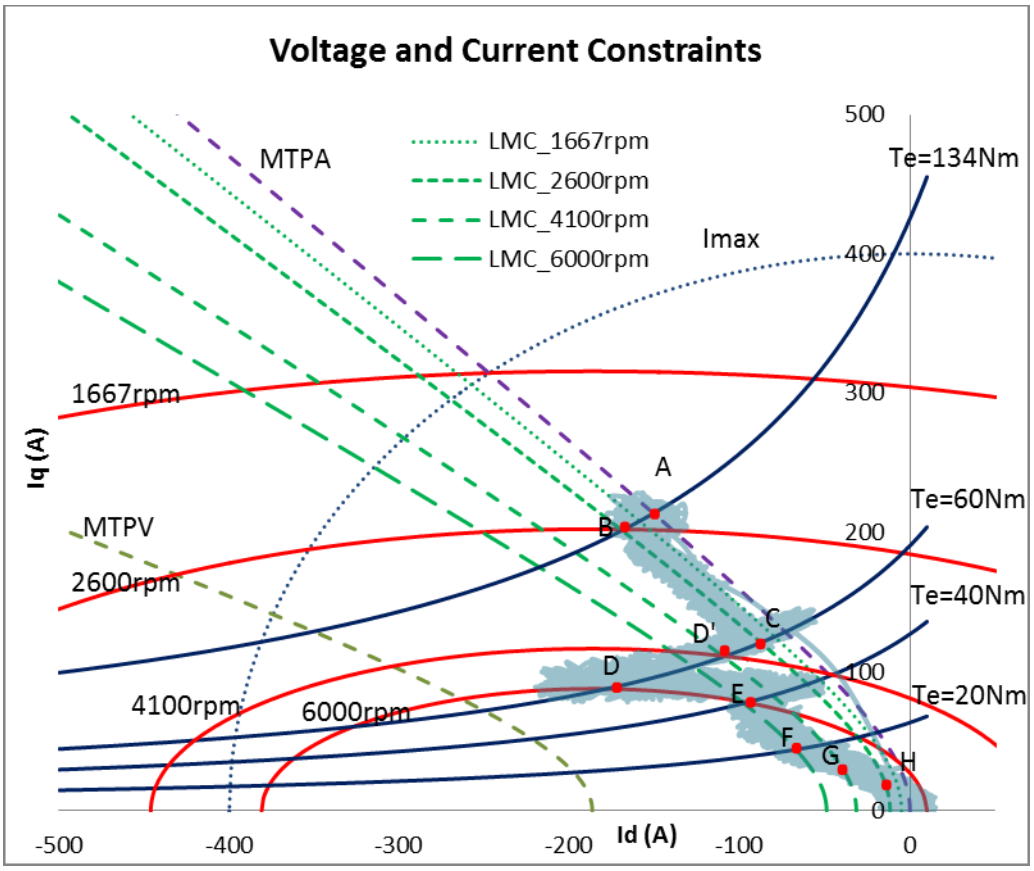

Figure 5.20: Drive cycle simulation current trajectory

When the simulation starts with the load torque 134 Nm, the speed goes up to the rated value within 2 seconds. It is noted that the maximum available torque of LMC for the rated speed is 133Nm. For speed less than the rated value, the LMC torque capacity is higher, which can be seen from the torque speed envelop as described in Section 4.3.3. Therefore, the control gives the command current following the intersect point of LMC and torque curve even when the speed exceeds the critical speed ω_{lmc}. It is corresponding to the region from point A to point B as shown in Figure 5.20. Since the load torque is 1 Nm higher than the rate torque, there is a transition between LMC and FWC around 2 second, which is shown in the simulation dq current and control mode results. After the rated speed is reached, the load torque begins to decrease at 2 second.

Once the load torque goes down to less than the rated value, the control comes back to LMC of the rated speed, and then the current should keep following the trajectory that is the interval from point B to point C. At 4 second, the load torque stays at 60 Nm while the speed goes up to 6000 rpm. During the rise of the speed, the transition occurs again at 5 second. From Figure 5.20, between point C and point D, the D' represents the intersect point of LMC for 4100 rpm with constant torque curve of 60 Nm, which means that the maximum torque capacity for 4100 rpm LMC is 60 Nm. When speed goes over 4100 rpm, LMC cannot support this torque. So the control has to transfer to FWC. This transition is also shown in the dq current and control mode results. At 6 second, the speed stays at 6000 rpm, and the load torque decreases. Similar to the transition simulation in Section 5.3.3, the 6000 rpm LMC can support the maximum 38 Nm torque. Before the load torque decreases to less than 38 Nm, the control mode is still FWC. It is the region from point D to point E. At 7 second, the load torque becomes less than 38 Nm, and the control transfers back to LMC of 6000 rpm, which is region between point E and point F. Finally, the speed and the load torque decrease together at 8 second, and reach zero at 10 second. The current trajectory follows the intersect point between LMC and torque curve, for example, point G and point H at lower load and lower speed.

It can be seen that the simulation dq current result is exactly following the trajectory of the proposed efficiency enhancement control algorithm. The result shows a high average efficiency around 92.6% for the whole cycle operation.

5.4 Summary

In this chapter, the PMSM model with core loss resistance is built within the simulation environment of Matlab/Simulink. With optimal design, the current and speed controllers

are also developed. The whole drive system for PMSM is finally implemented in the Simulink. Two test machines are used to test the control strategies. The steady state simulation is firstly performed with two cases, which include the operation below base speed and that above base speed. The cases are corresponding to the current and voltage constraint regions. The simulation results show that LMC can provide better efficiency if compared with MTPA, MTPV and FWC. Also, the performance of the transition between LMC and optimal FWC is investigated in voltage constraint region. Finally, a simple drive cycle is simulated to test the proposed control strategy in a wide speed range with load variation. Since the proposed control strategy is to generate the optimal current trajectory for loss minimization of the machine, better efficiency can be achieved if the drive system can track them properly. The simulation results suggest satisfactory tracking performance of the drive system, while it still can maintain a good speed and torque response.

CHAPTER 6 EXPERIMENTAL TESTS AND VERIFICATION

In this chapter, a laboratory designed surface mounted PMSM is used to test the proposed algorithm. The simulation of this lab SPM is performed at first. Then the experimental work is conducted by employing the efficiency enhancement control. The experimental results are compared with simulation results and discussed in detail.

6.1 Simulation of SPM

The prototype SPM parameters are shown in Table 6.1.

Parameters	Lab SPM
Rs (ohm)	0.1718
Rc (ohm)	Measured
Ld (H)	3.36e-3
Lq (H)	3.36e-3
λ_{PM} (V.s)	0.591
Vdc (V)	300
Pole number	4
Rated torque (Nm)	27
Power rating (hp)	5

Table 6-1: Prototype SPM Parameters

Before the simulation, the core loss resistance has to be identified. There are different methods can obtained the core loss resistance [31,32]. In this research work, based on the finite element analysis (FEA) results provided by the designer Maged, the core loss resistance is calculated. Table 4 shows the calculation results. The core loss resistance with respect to speed is also plotted in Figure 6.1. Using least square algorithm, the expression of the core losses resistance is approximated as a linear function of speed:

$$R_c = 6.1054\omega_r + 364.58$$

Speed (Rpm)	Stator iron loss (W)	Rotor iron loss (W)	Totoal Iron loss (W)	BackEmf (V)	Rc (ohm)
200	2.133	0.00001361	2.13301361	30.77	443.8785279
400	4.55	0.00005428	4.55005428	61.53	831.8920897
600	7.253	0.0001215	7.2531215	92.3	1174.264645
800	10.24	0.0002146	10.2402146	123.1	1479.844727
1000	13.5	0.0003324	13.5003324	153.8	1750.88379
1200	17.05	0.0004738	17.0504738	184.6	1996.318688
1400	20.87	0.0006372	20.8706372	215.4	2219.959809
1600	24.96	0.0008213	24.9608213	246.1	2422.6084
1800	29.32	0.001024	29.321024	276.9	2609.721239
2000	33.95	0.001245	33.951245	307.7	2782.230091

Table 6-2: FEA results and core losses results

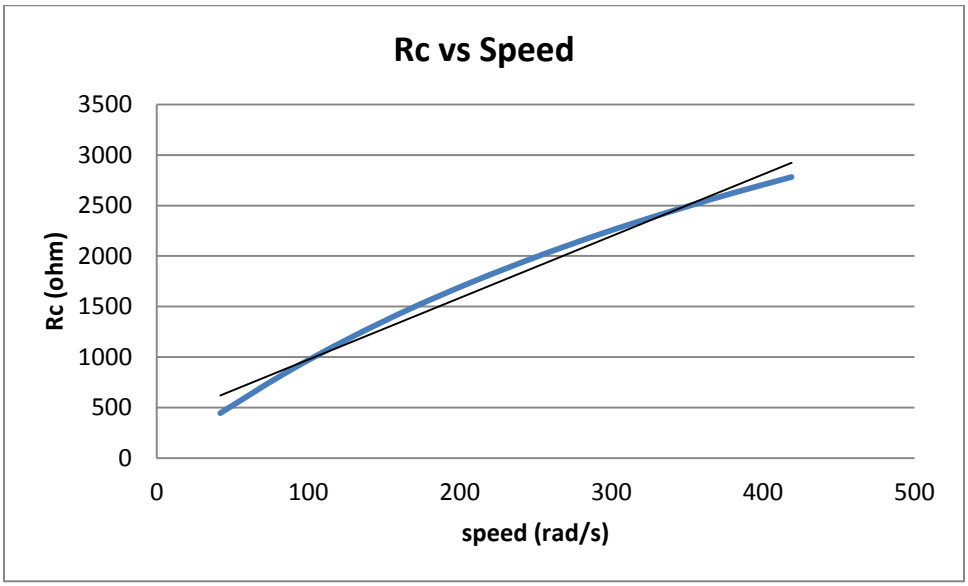

Figure 6.1: Core losses resistance

The simulations are performed on the lab SPM as illustrated in following sections.

6.1.1 No-load Simulation

In this section, the no load simulation is performed by stepping up the speed of the lab machine to1000 rpm. The loss performance of LMC and MTPA is investigated and compared. The results are shown in Figure 6.2.

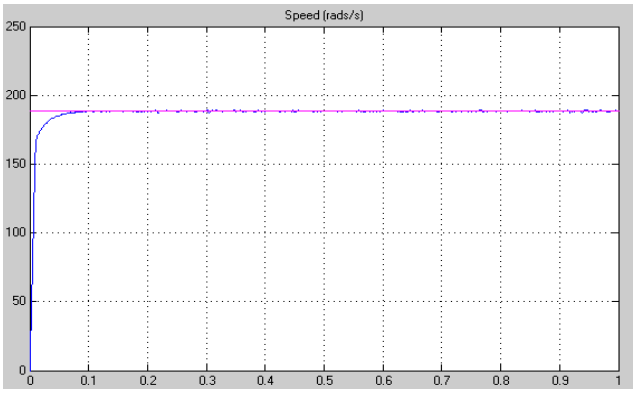

(a) speed response

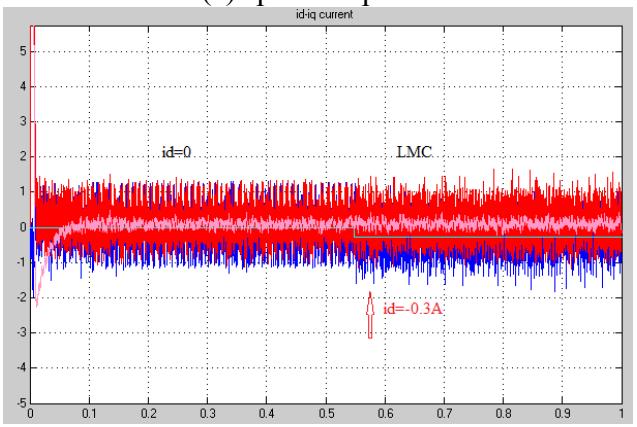

(b) d-q current

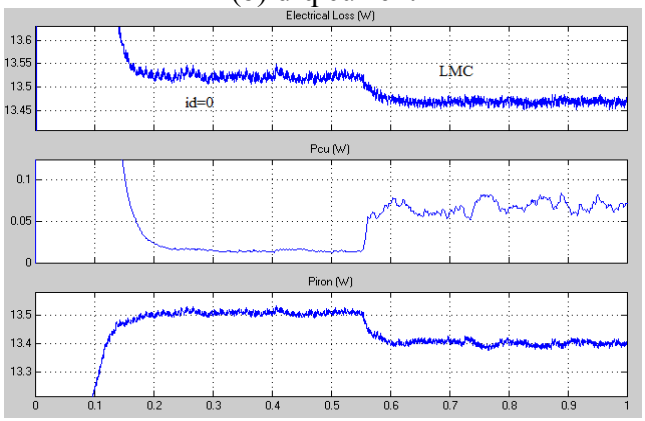

(c) loss

Figure 6.2: No-load simulation of lab SPM

It is observed that MTPA and LMC have same performance in terms of speed and current response. The result shows that LMC has a higher copper loss. However, the core loss in LMC cancels the increasing copper loss and gives a lower total loss in the end. It should be noted that in the simulation, the improvement of core loss is around 0.1W and that of total loss is about 0.05W due to the small core loss design of the lab machine.

6.1.2 Steady-state Simulation

The steady state load simulation is carried out on the lab SPM with 25Nm load and 1000rpm speed. Initially, by applying the MTPA control strategy, which is zero id current control for SPM, the command speed is applied to the machine with the load. At 0.5 second, the control changes from MTPA to LMC. The two control strategies are compared in terms of performance. The simulation results are shown in Figure 6.3.

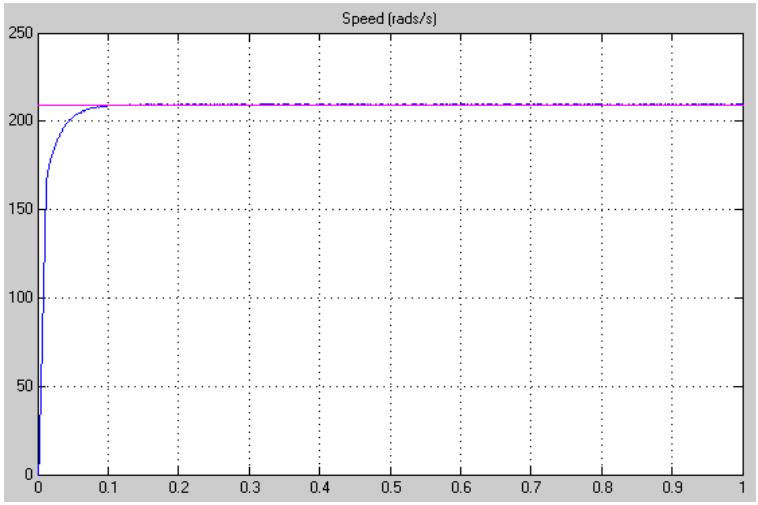

(a) speed response

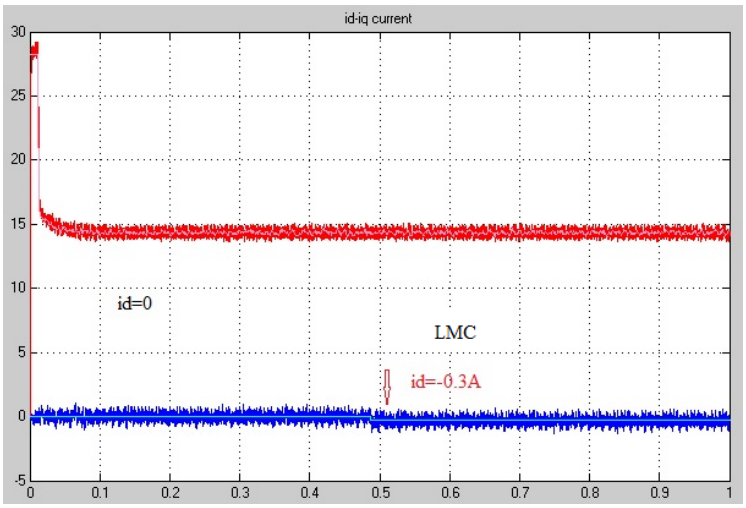

(b) d-q current

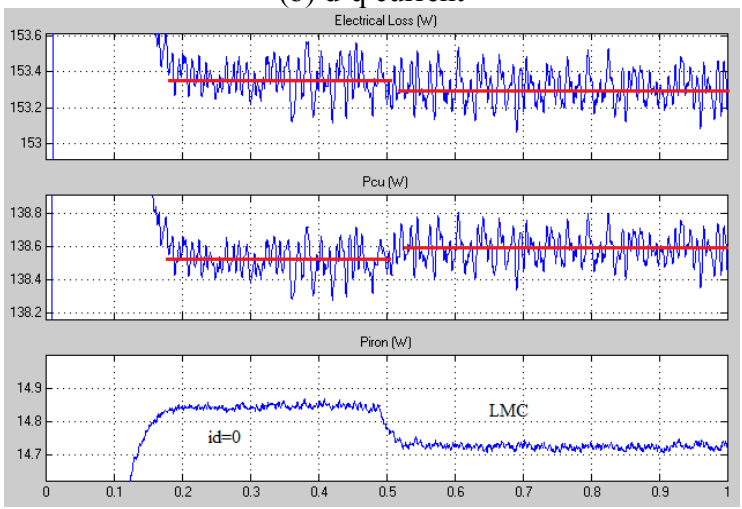

(c) loss

Figure 6.3: 1000RPM with full load simulation of lab SPM

Since the torque of SPM is only related to q-axis current, the id variation does not have any effect on the torque production. The results suggest that the id becomes a little negative during LMC control, but maintains as zero for MTPA. There are no changes on the torque and speed response as shown in the results. The flux becomes lower during LMC due to negative id current, and then the core loss in LMC is lower than that in MTPA. The result shows that MTPA has 153.4 W total loss, 138.51 W copper loss and around 14.85 W core loss. When LMC is applied, the optimal id is around -0.3A. The

core loss decreases to 14.72 W, and copper loss goes up to 138.55 W. However, the core loss in LMC cancels the increasing copper loss and gives a lower total loss in the end. It should be noted that in the simulation, the improvement of core loss is around 0.13W and that of total loss is about 0.1W. Also, it is observed that the optimal current for 1000rpm without load and that with full load is the same. This can be explained by the solution of LMC for SPM as shown in the equation (4-31), which is rewritten here:

$$i_{od} = -\frac{\omega^2 L_d \lambda_{PM}(R_s+R_c)}{R_c^2 R_s+\omega^2 {L_d}^2 \lambda_{PM}(R_s+R_c)}$$

Viewed from the equation, the optimal solution for SPM is not related to the q-axis current. In other words, it is not related to the load.

Figure 6.4 shows 1600rpm and 2000 rpm with full load simulation results.

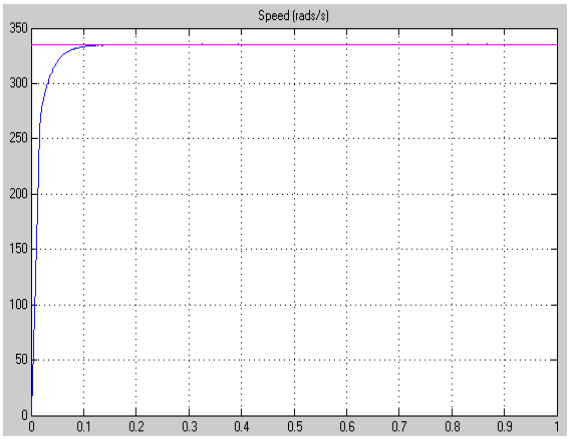

(a) 1600rpm speed response

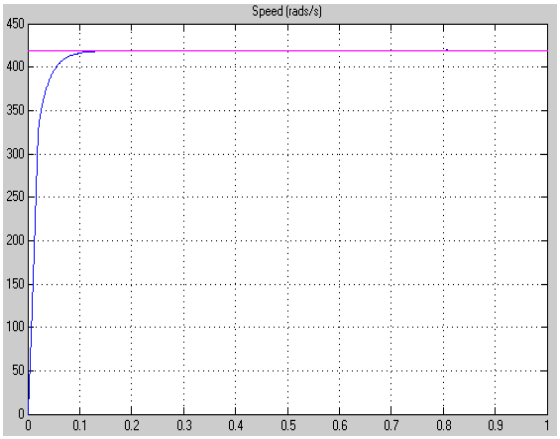

(b) 2000rpm speed response

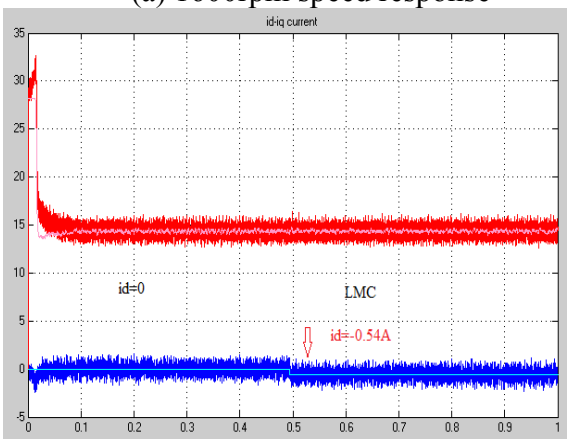

(c) 1600rpm d-q current

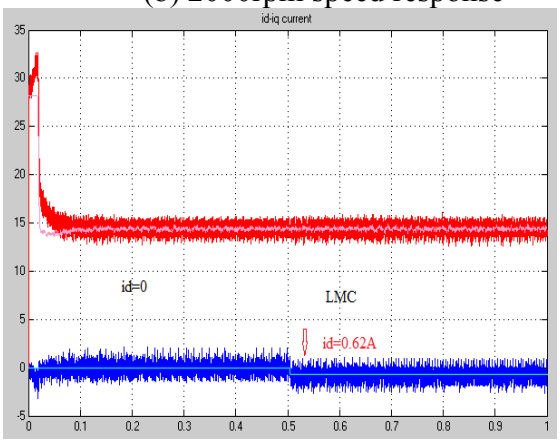

(d) 2000rpm d-q current

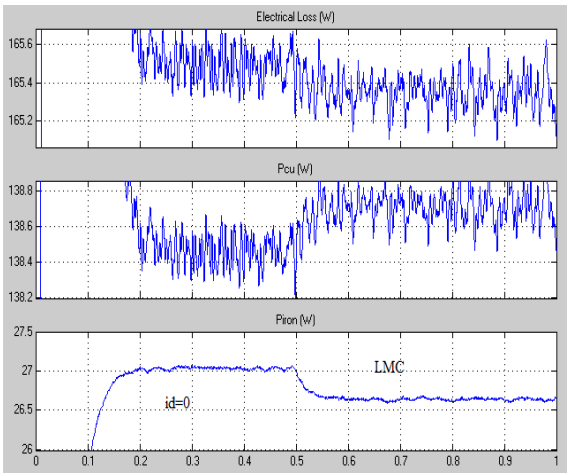

(e) 1600rpm loss

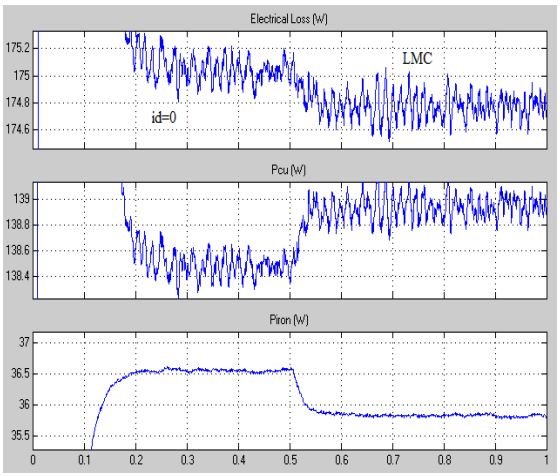

(f) 2000rpm loss

Figure 6.4: 1600RPM and 2000RPM with full load simulation results

As shown in Figure 6.4, the optimal currents for the two high speed cases are -0.54A and -0.62A respectively. It can be seen that the improvement of loss becomes relatively larger than that in the 1000rpm case thanks to high speed with high core loss. However, the improvement in itself is still small due to the small core loss design of the lab machine, which gives around 0.2W and 0.4W loss improvement for 1600rpm and 2000rpm.

6.1.3 FEA Simulation and Verification

In order to validate the algorithm, the FEA experiments are also conducted on the lab SPM with full load at three speeds. With gradually decreasing the d-axis current, the total loss is recorded. The results are shown in Table 4:

Speed	1000RPM		1600RPM		2000RPM	
id (A)	Ptotal (W)	Pcore (W)	Ptotal (W)	Pcore (W)	Ptotal (W)	Pcore (W)
0	153.3404915	14.8404915	165.581215	27.081215	175.091843	36.591843
-0.1	153.3004879	14.8004879	165.511206	27.011206	175.00183	36.50183
-0.15	153.2804862	14.7804862	165.481202	26.981202	174.951823	36.451823
-0.3	153.2204809	14.7204809	165.381189	26.881189	174.821803	36.321803
-0.6	153.7104711	14.6104711	165.383165	26.681165	174.661766	36.061766
-1	154.3604585	14.4604585	166.321134	26.421134	175.111719	35.711719
-1.5	155.8804443	14.2804443	167.691099	26.091099	176.871666	35.271666
-2	158.2004319	14.1004319	169.871068	25.771068	178.94162	34.84162
-2.5	161.2204207	13.9204207	172.75104	25.45104	181.721578	34.421578
-3	164.7304105	13.7304105	176.131015	25.131015	184.99154	33.99154
Improvement of loss compare to id=0						
Loss (W)	0.12		0.2		0.43	

Table 6-3: FEA simulation results

Also, the results are plotted as Figure 6.5:

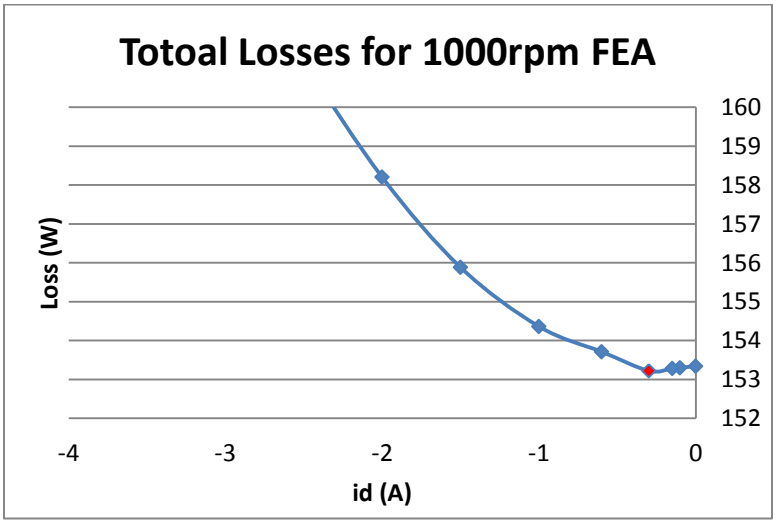

(a) 1000rpm FEA result

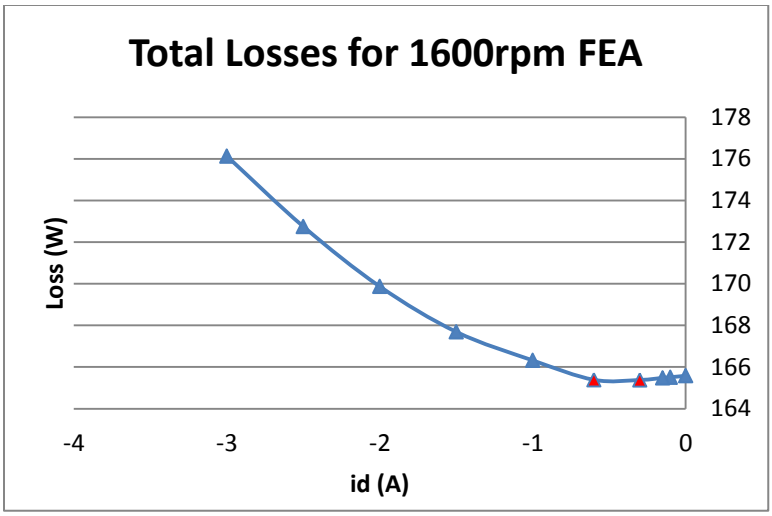

(b) 1600rpm FEA result

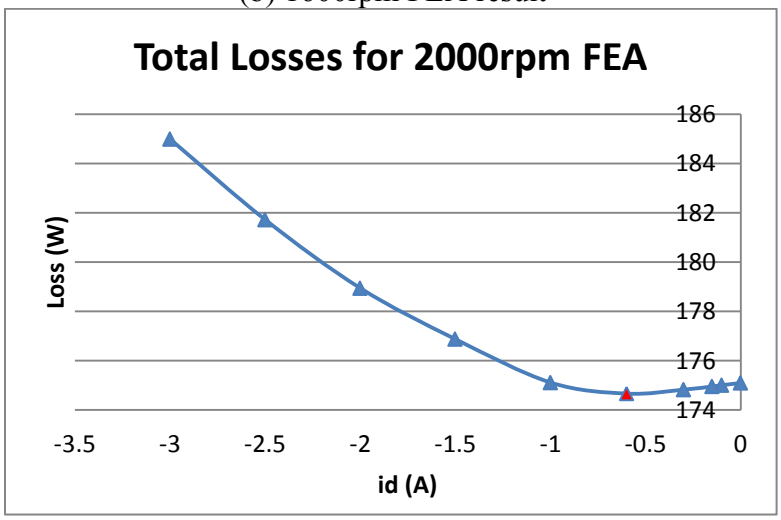

(c) 2000rpm FEA result

Figure 6.5: FEA total loss plot for 1000rpm, 1600rpm, and 2000rpm

The result for 1000rpm shows that the optimal d-axis current happens at around -0.3A, and there is an around 0.12W improvement of loss compared to zero id. For 1600rpm, the optimal id is between -0.5A and -0.6A. For 2000rpm, the optimal id is between -0.6A and -1A. The loss improvement is 0.2W and 0.43W respectively. This result is consistent with the simulation result.

6.2 Experimental Testing and Verification

6.2.1 Experimental Test Set-up

The setup of the experiment is shown in Figure 6.5, which includes power supply, inverter, dSpace control system, lab SPM, and load system.

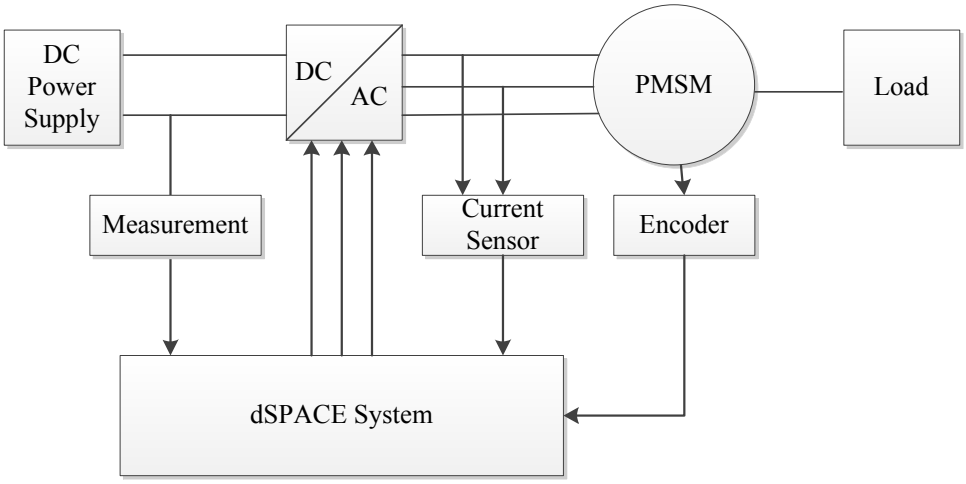

Figure 6.6: Experiment setup block diagram

The dSPACE system provides a convenient environment to support model-based control design and real time hard-in-loop (HIL) simulation. It can use the Matlab/Simulink to develop the controller model, and the output signal will be sent to fire the inverter. The feedback from encoder, current sensor and other measurements is sent via the A/D port to the system. All the calculation and control processes are performed in the Matlab/Simulink. The parameters of the experiment system are listed in Table 5.

Sampling time (sec)	2e-5
Switch frequency (KHz)	5
DC bus voltage (V)	250

Table 6-4: Experiment parameters

6.2.2 No-load Test

As observed from the simulation results, LMC gives the best optimal current in terms of loss even though the improvement of the lab SPM is small. In order to capture the small improvement of the loss, the experiment is at first performed with constant speed 800rpm with no load. The id is swept from 0A to -5A with 0.2A step, and the input power is recorded. Taking the average of the input powers for different ids so as to eliminate the ripple, the results are plotted as Figure 6.9.

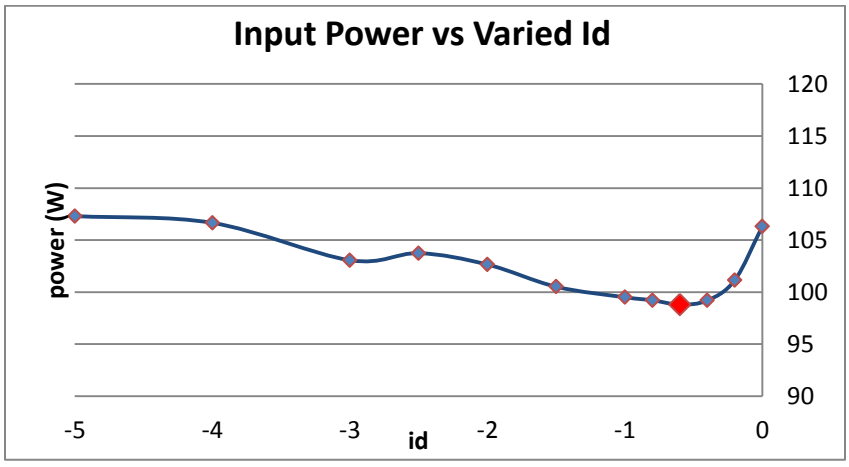

Figure 6.7: Input power result for varied i_d

The input power waveform of ids equal to -0.2A, -0.4A and -0.6A is shown in Figure 6.10.

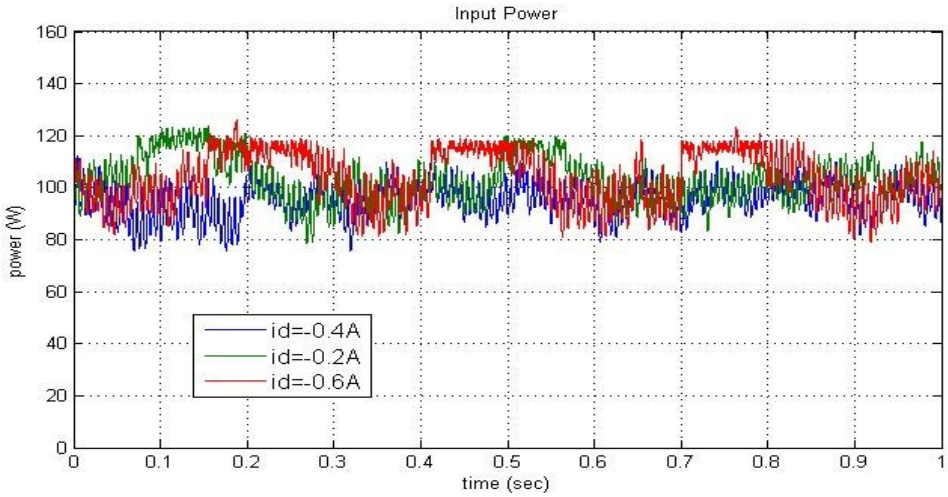

Figure 6.8: Input Power waveform for i_d = -0.2A, -0.4A and -0.6A

The results show that the input power decreases until the id becomes -0.6A. Subsequently, the input power increases. The minimum input power happens between -0.4A and -0.6A. The small improvement of loss can be seen from the power waveform. From the simulation, the 1000rpm optimal current is around -0.3A, and the optimal current is only dependent on the speed for SPM. Therefore, for 800rpm, the optimal current should be larger than -0.3A. The discrepancy in the results is possibly caused by the mismatched parameters. The variation of parameter will be addressed later.

6.2.3 Steady-state Load Test

The steady state load test is conducted by running the machine with light load at 1000rpm. Decrease the d-axis current from zero with step -0.5A, and the phase current and input power waveforms are recorded. The results are shown in Figure 6.11.

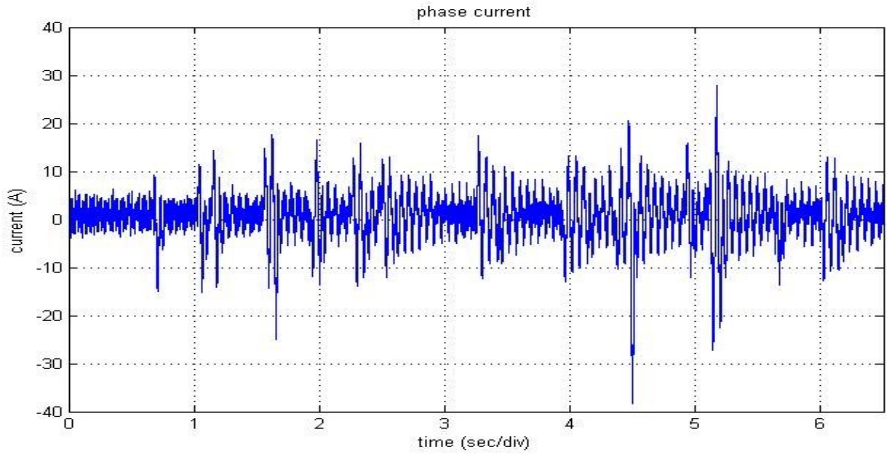

(a) phase current

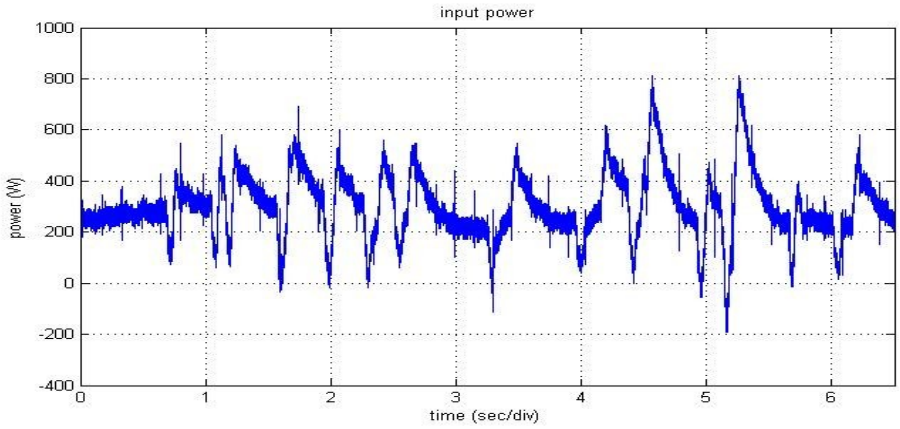

(b) input power

Figure 6.9: Steady-state load test results

The results show that the phase current increases with negative current injection. The input power decreases a little bit when the id is -0.5A and increases at id equal to -1A. The first three-step waveform captures the improvement of the input power even though it is very small. The test suggests that the minimum power occurs at the point around -0.5A. Compared with the simulation result -0.3A, a discrepancy also occurs with same error direction with no load test. Despite that, the test proves that it is possible to improve the total loss performance with certain negative id injection.

6.3 Discussion

The simulation results in Matlab/Simulink and FEA are essentially consistent. But they both suggest that the improvement of the power is small even though LMC gives the best efficiency optimal current. It is hard to capture the small improvement of the power due to the design of the lab SPM. The experiment results do not show a significant improvement of the power, and the optimal current point is not exactly matched with the simulation. The discrepancy regarding the optimal current point is probably caused by measurement errors or parameter mismatches. As a matter for fact, the model based LMC is heavily dependent on the machine parameters. The optimal relationship between d-q currents provides a generalized solution for efficiency enhancement, but it can be seen that the hyperbolic equation's coefficients include the machine parameters. The effect of the parameter variation on LMC is analyzed later.

6.3.1 Effect of Core Loss Resistance

By varying the iron loss resistance from 60% to 140% of the nominal value, the copper loss, iron loss, and total loss are plotted as Figure 6.12.

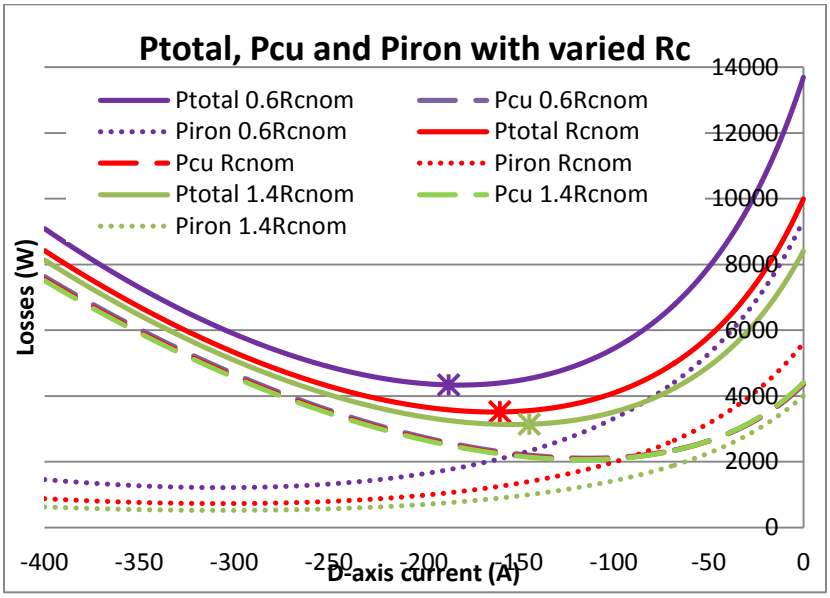

Figure 6.10. Effect of core loss resistance on the total loss

It is observed that the copper loss P_{cu} is not affected much, but the iron loss P_{iron} has significant changes. And the total loss apparently shifts to the bottom right direction. Also, the minimum total loss point as marked (*) in the plot shifts to the right. In other words, the optimal point for the minimization of loss moves to the small negative d-axis current. Plot the LMC in dq current plane as Figure 6.7.

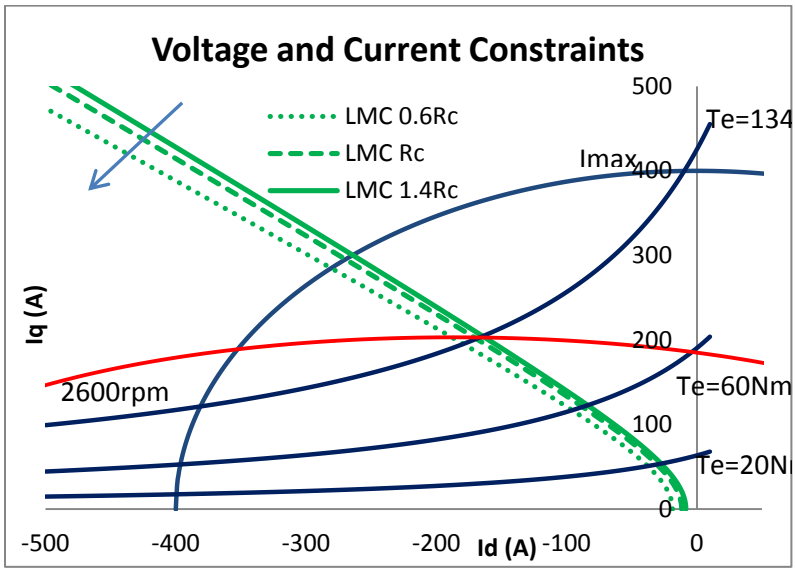

Figure 6.11: LMC with variation of R_c

LMC moves to right with increasing R_c, which is consistent with the former discussion. Also, for the experiment results, the total loss is larger than the simulation and FEA results, which indicate that the real machine has smaller core losses resistance. This probably explains why all the optimal currents are less than the simulation results. In other words, the optimal current shifts to left due to small core loss resistance. The effect of the stator resistance is plotted in Figure 6.14.

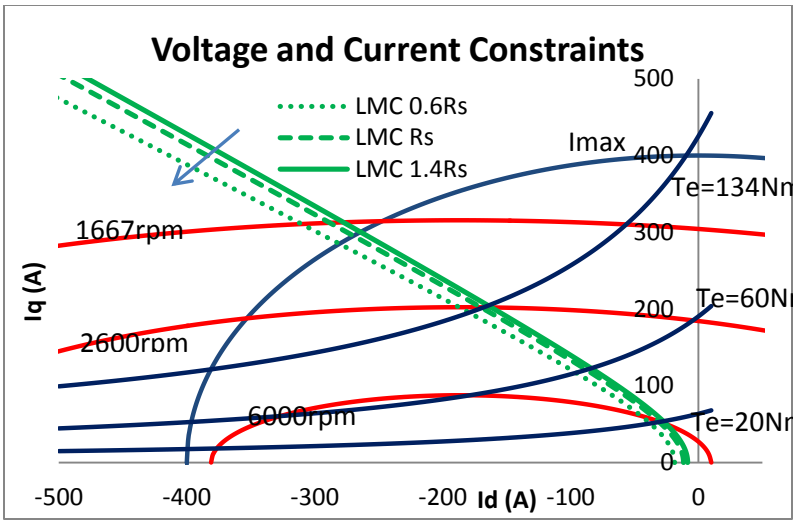

Figure 6.12: LMC with variation of R_s

It shows that the stator resistance has similar effect on LMC as core loss resistance. To be more exact, they both affect the copper loss instead of the core loss. The optimal point of LMC moves to the right side of small negative d-axis current.

6.3.2 Effect of q-axis Inductance

In the PMSM, the inductance is not constant in fact. Instead, it is affected by cross coupling and saturation issues. Especially, the q-axis inductance changes significantly along with saturation. As a result, the variation of q-axis inductance also has impacts on the total loss and the optimal loss points, which is plotted as Figure 6.9.

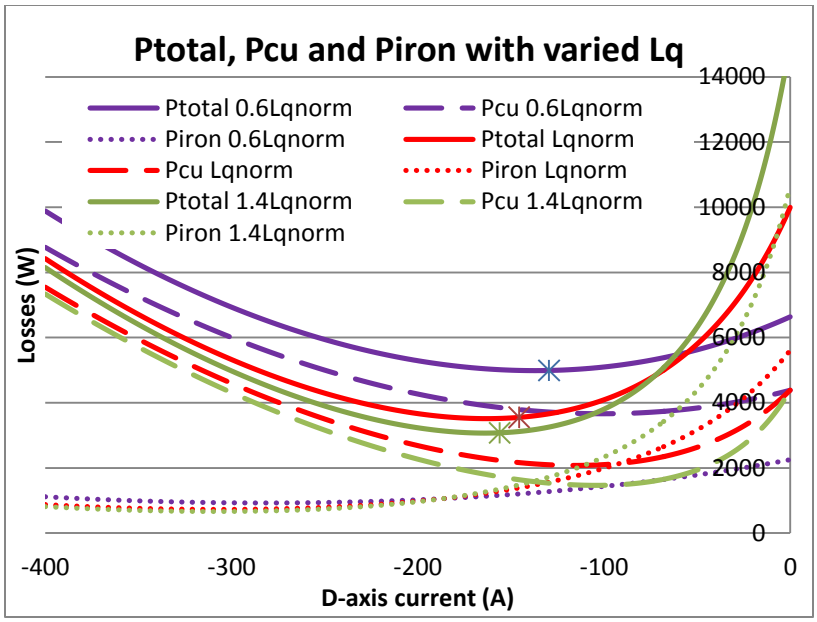

Figure 6.13. Effect of q-axis inductance on the total loss

The plot shows that the decrease of L_q will shift up the total loss curve and shift the optimal loss point to left along the d-axis current, which means that the optimal point for d-axis current will be of larger negative value. When the machine flux becomes saturated, for the same load and the same speed, the current injected to the machine will be larger than that in non-saturation condition. This explains why the copper loss and the total loss have significant changes. Compared with general control strategy, LMC always has negative d-axis current, which reduces the machine's total flux. It helps to decrease the saturation extent and then the variation of L_q.

Changes are observed for LMC trajectory in Figure 6.16, as well. LMC shifts to right significantly when the L_q decreases to 60% of nominal value. For example, the optimal point of 60Nm load with 2600 rpm moves from point A to point B.

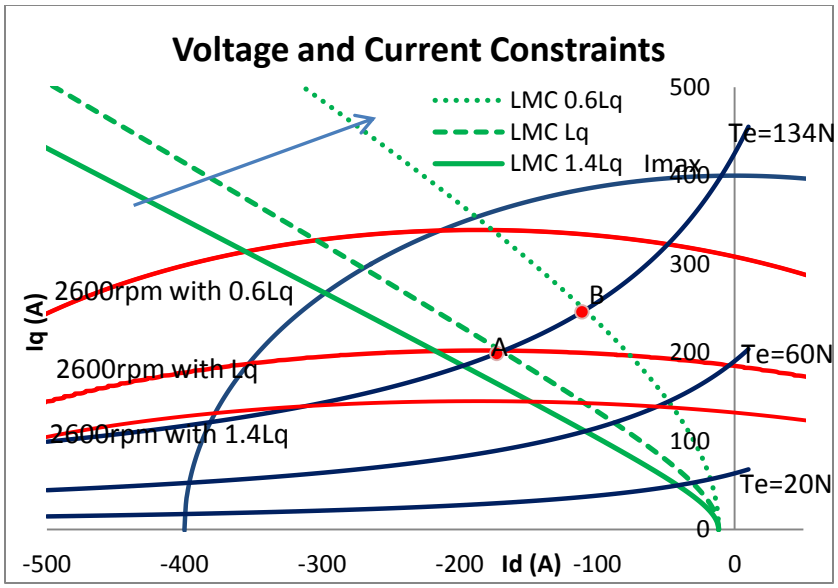

Figure 6.14: LMC with variation of Lq

For the d-axis inductance, it is generally taken as constant in PMSMs when compared to q-axis inductance. Its effect is plotted in Figure 6.17.

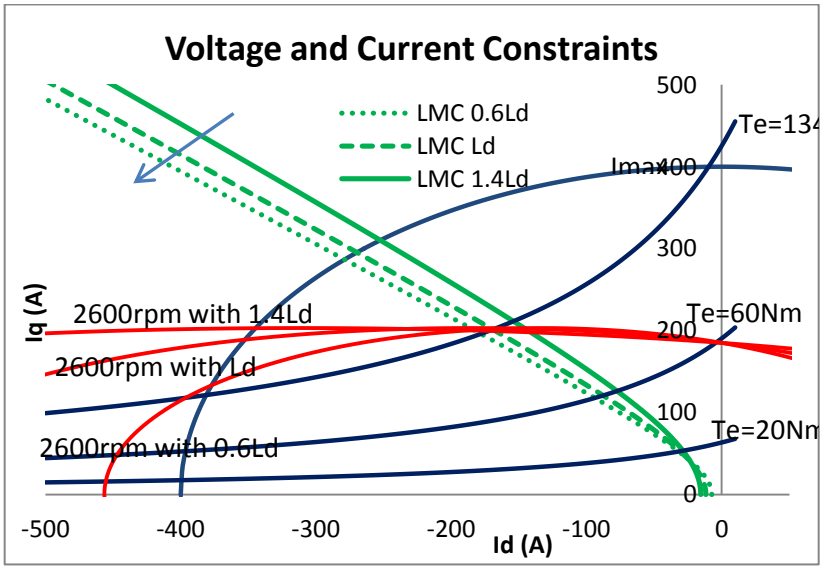

Figure 6.15: LMC with variation of L_d

It can be seen that LMC shifts to bottom left with the L_d decreasing from 140% to 60% of nominal value. The effect of L_d on LMC is not as much as that of L_d, nevertheless.

6.3.3 Effect of Permanent Magnet Flux

The effect of permanent magnet flux linkage on LMC is plotted as Figure 6.18 and found to be similar as that of the resistances. With the permanent magnet flux linkage increasing, the optimal current trajectory shifts to the right side.

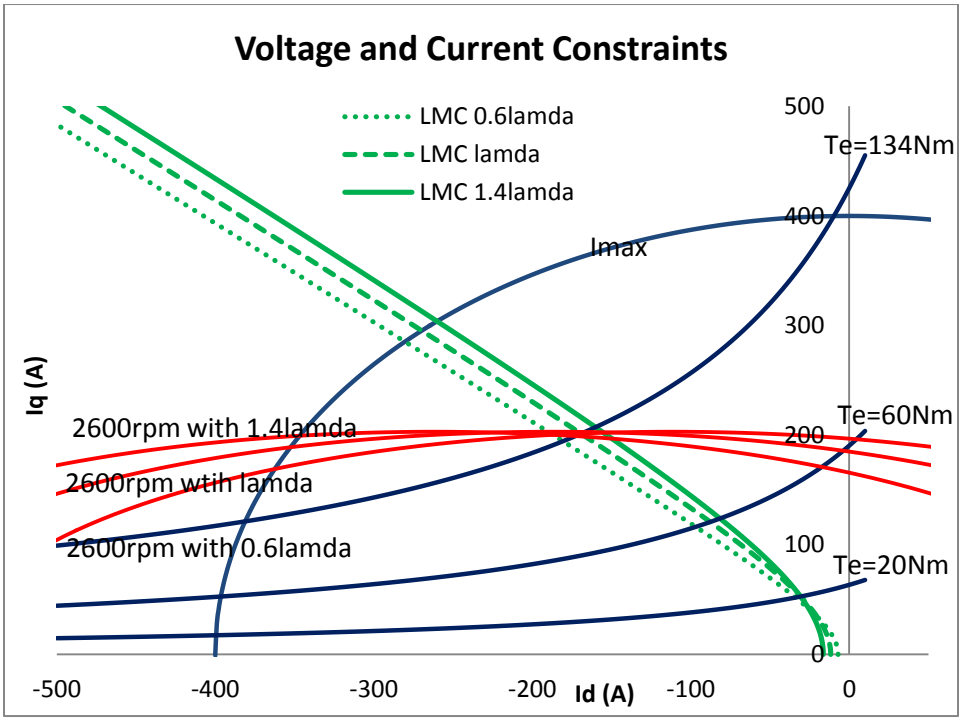

Figure 6.16: LMC with variation of PM flux

In real application, the PM flux linkage is affected mainly by the temperature, which is similar to the resistance. The changes will be slower compared to the inductance. With proper online parameter estimation techniques, the variation of machine parameters can be compensated [33].

CHAPTER 7 CONCLUSIONS AND FUTURE WORK

7.1 Conclusions

As the energy and environmental issues contribute to the ever-growing interest in EV/PHEV application, a lot of research has been conducted on the traction system of EV/PHEV, which mainly includes power source, power electronics, and traction motor. Since the sole power source for EV/PHEV application comes from the battery, the whole system efficiency will be very important when the distance per charge is taken into consideration. A lot of research has been focused on MTPA and MTPV, the two control modes that achieve minimized copper loss and minimized core loss respectively. Also, there have been a few studies considering both copper loss and core loss reduction in this regard.

In this thesis, the working principles of PMSMs are examined closely. For control purpose, the mathematic model of PMSMs is built by Park's transformation, which transfers a three phase model to a fiction two phase coordinate system. The model in the two phase coordinate system is generally called dq model. With the rotor reference frame being chosen, the time dependent variables such as the inductance in the three phase model becomes constant, which significantly facilitates the control design. Based on the dq model of PMSMs, the equivalent circuit is modeled to investigate the dynamic and static performances of PMSMs. According to the power flow in the machine, different losses are identified. As for core loss, it is modeled as a resistance component that is a parallel branch in the equivalent circuit. Based on this equivalent circuit, the total loss is formulated as a function of the d-axis current. The plot of the total loss function indicates that it is a concave curve with respect to the d-axis current. This suggests a

possibility to control the machine with minimum loss. LMC is developed from this consideration. An optimal current relationship is found to satisfy the loss minimization need corresponding to the speed. The operating boundary region for LMC is analyzed with the voltage constraint and the current constraint both being taken into account. For the operation outside the LMC boundary region, an optimal FWC is employed, which can provide a better loss performance. In so doing, the efficiency enhancement control algorithm over full speed range is formed with the combined use of LMC and optimal FWC. Also, the optimal current relationship is proved to be a generalized expression for efficiency improvement algorithm. Control modes such as MTPA and MTPV, which can be considered as special cases of LMC, can be derived from the generalized optimal current trajectory.

A drive system is built in Matlab/Simulink environment for the purpose of validating the control algorithm. Two testing machines with different power ratings are used in the simulation work. The steady state test is performed with the machine operating in both current constraint and voltage constraint regions. The simulation results indicate that the proposed algorithm give better loss performance than MTPA and MTPV without losing speed and toque responses. The transition simulation is also carried out to test the performance of the control mode transition between LMC and optimal FWC. Finally, the drive cycle simulation is conducted with a wide speed range and a load variation profile, whose results show a good optimal current tracking performance. Experimental test is also performed on a lab designed SPM. The experiment results show a discrepancy from the simulation results, which might be caused by measurement errors

and mismatches of the machine parameters. Despite the discrepancy, the experiment proves that with the proposed control algorithm, a reduction of the losses is possible.

7.2 Future Work

The simulation and experiment results prove the utility of the proposed algorithm as well as raises the following questions that have to be tackled with in the future work:

- The algorithm uses a resistance component to model the core loss. Therefore, an accuracy measurement procedure of the core loss resistance should be developed.
- The core loss characteristics have to be investigated in more detail, and there is a need to develop a simple and accurate core loss model for the control purpose.
- Since the algorithm is dependent on the machine parameters, proper estimation techniques have to be developed for online parameters.
- The proposed algorithm can be combined with search-based techniques to avoid parameters dependency, which can provide the initial current reference to the search method to accelerate the convergences.
- The model based control algorithm does not include the inverter losses, which should be added due to the cross effect between the inverter and the motor. For example, LMC injects a negative d-axis current into the machine to improve the efficiency of the machine. However, it increases the phase current, which means that the inverter loss will increase.

REFERENCES

[1] Z.Rahman, M.Ehsani and K.L.Butler, “An investigation of Electric Motor Drive Characteristics for EV and HEV Propulsion Systems”, SAE Technical Paper Series, 2000-01-3062.

[2] Williamson, S.S.; Emadi, A.; Rajashekara, K., "Comprehensive Efficiency Modeling of Electric Traction Motor Drives for Hybrid Electric Vehicle Propulsion Applications," *Vehicular Technology, IEEE Transactions on* , vol.56, no.4, pp.1561,1572, July 2007

[3] M. Olszewski, “Final Report on Assessment of Motor Technologiesfor Traction Drives of Hybrid and Electric Vehicles”, subcontract No. 4000080341, Oak Ridge National Laboratory, March 2011.

[4] Uddin, M.N.; Radwan, T.S.; Azizur Rahman, M., "Performance of interior permanent magnet motor drive over wide speed range," *Energy Conversion, IEEE Transactions on* , vol.17, no.1, pp.79,84, Mar 2002

[5] Inoue, Y.; Morimoto, S.; Sanada, M., "A Novel Control Scheme for Maximum Power Operation of Synchronous Reluctance Motors Including Maximum Torque Per Flux Control," *Industry Applications, IEEE Transactions on* , vol.47, no.1, pp.115,121, Jan.-Feb. 2011

[6] Mademlis, C.; Margaris, N., "Loss minimization in vector-controlled interior permanent-magnet synchronous motor drives," *Industrial Electronics, IEEE Transactions on* , vol.49, no.6, pp.1344,1347, Dec 2002

[7] Bazzi, A.M.; Krein, P.T., "Comparative evaluation of machines for electric and hybrid vehicles based on dynamic operation and loss minimization," *Energy Conversion Congress and Exposition (ECCE), 2010 IEEE* , vol., no., pp.3345,3351, 12-16 Sept. 2010

[8] Fernandez-Bernal, F.; Garcia-Cerrada, A.; Faure, R., "Model-based loss minimization for DC and AC vector-controlled motors including core saturation," *Industry Applications, IEEE Transactions on* , vol.36, no.3, pp.755,763, May/Jun 2000

[9] Krishna, R., "Permanent Magnet Synchronous and Brushless DC Motor Drives," CRC Press, Taylor & Francis Group, LLC, 2010

[10] Krishna, R., Electric Motor Drives, Prentice Hall, Upper Saddle River, NJ, 2001

[11] S.Morimoto, Y.Takeda, T.Hirasa, K. Taniguchi, "Expansion of Operating Limmits for Permanent Magnet Motor by Current Vector Control Considering Inverter Capacity," IEEE Trans, on Ind, Appl., Vol. 26, No. 5, 1990.

[12] W.L. Soong and T.J.E. Miller, "Field-weakening performance of brushless synchronous AC motor drives", IEEE Proc-Electr. Power Appl., Vol. 141, No. 6, November 1994.

[13] F.Blaaske, "The principle of field orientation as applied to the new transvector closed-loop control system for rotating field machine", Siemens Review, Vol.34, pp.217-220,1972

[14] Pillay, P., "Vector control of AC permanent magnet machines," *Electrical Machines and Drives, 1989. Fourth International Conference* , pp.293,297, 13-15 Sep 1989

[15] Takahashi, I.; Noguchi, T., "A New Quick-Response and High-Efficiency Control Strategy of an Induction Motor," *Industry Applications, IEEE Transactions on* , vol.IA-22, no.5, pp.820,827, Sept. 1986

[16]K.T. Chau, C.C. Chan, Chunhua Liu, "Overview of Permanent-Magnet Brushless Drives for Electric and Hybrid Electric Vehicles," *IEEE Trans. on Industrial Electronics,* vol. 55, no. 6, pp. 2246-2257, June 2008.

[17] Ching-Tsai Pan; Shinn-Ming Sue, "A linear maximum torque per ampere control for IPMSM drives over full-speed range," *Energy Conversion, IEEE Transactions on* , vol.20, no.2, pp.359,366, June 2005

[18] Morimoto, S.; Sanada, M.; Takeda, Y., "Wide-speed operation of interior permanent magnet synchronous motors with high-performance current regulator," *Industry Applications, IEEE Transactions on* , vol.30, no.4, pp.920,926, Jul/Aug 1994

[19] Roy S.Colby, Donald W. Novotny, "An efficiency-Optimizing Permanent Magnet Synchronous Motor Drives," IEEE Transaction on Industry Application, Vol. 24, No. 3, pp. 462-469, May, 1988.

[20] S.Morimoto, Y.Tong, Y. Takeda, and T. Hirasa, "Loss minimization control of permanent magnet synchrounou motor drives," IEEE Trans. Ind. Electron.,Vol. 41, no. 5, pp. 511-517, Oct. 1994

[21] C.C.Chan and K.T.Chau, "An advanced permanent magnet motor drive system for battery-powered electric vehicles," IEEE Trans. Veh. Technol.,vol. 45, no. 1, pp.180-188, Feb, 1996.

[22] Sadegh Vaez-Zadeh,V.I. John, M.A.Rahman, "An on-line loss minimization controller for interior permanent magnet motor drives," *IEEE Trans. on Energy Conversion*, Vol. 14, No. 4, pp. 1435-1440, Dec.1999.

[23] C.Cavallaro, A.O.D. Tommaso, R.Miceli, A. Raciti, G.R. Galluzzo, and M.Tranpanese, “Efficiency enhancement of permanent-Magnet Synchronous Motor Drives by Online Loss Minimization Approaches,” IEEE Trans. Ind. Electron.,Vol. 52, no. 4, pp.1153-1160, Aug. 2005

[24] J. G. Lee, K. H. Nam, S. H. Lee, S. H. Choi, and S. W.Kwon, "A lookup table based loss minimizing control for FCEV permanent magnet synchronous motors,"Journal of Electrical Engineering & Technology, Vol. 4, No. 2, pp. 201-210, Jun. 2009.

[25] Junggi Lee, Kwanghee Nam, Seoho Choi, Soonwoo Kwon, “Loss Minimizing Control of PMSM with the Use of Polynomial Approximations,” Industry Applications Society Annual Meeting, 2008. IAS '08. IEEE , pp: 1 – 9, Oct. 2008.

[26] E. S. Sergaki, P. S. Georgilakis, A. G. Kladas, G. S. Stavrakakis, *Fuzzy Logic Based Online Electromagnetic Loss Minimization of Permanent Magnet Synchronous Motor Drives*, Proceedings of the 2008 Int. Conference on Electrical Machines, ICEM 2008, Vilamoura, Portugal, Sep. 2008.

[27] Eleftheria S. Sergaki, Nikolaos M. Afentakis, George S. Stavrakakis, *An Hybrid Loss Minimization Controller incorporated into ACIM speed FOC motor drive, based on a General Loss Model and on a Fuzzy Logic Search Controller, for Transient and Steady States,* Proceedings of The World 2009 Congress on Power and Energy Engineering, (WCPEE’09), Cairo, Egypt, Oct.5-8, 2009.c

[28] Preitl, Z.; Bauer, P.; Bokor, J., "A Simple Control Solution for Traction Motor Used in Hybrid Vehicles," *Applied Computational Intelligence and Informatics, 2007. SACI '07. 4th International Symposium on* , vol., no., pp.157,162, Yearly 17 2007-May 18 2007

[29] Umland, J.W.; Safiuddin, M., "Magnitude and symmetric optimum criterion for the design of linear control systems: what is it and how does it compare with the others?," *Industry Applications, IEEE Transactions on* , vol.26, no.3, pp.489,497, May/Jun 1990

[30] Pillay, P.; Krishnan, R., "Control characteristics and speed controller design for a high performance permanent magnet synchronous motor drive," *Power Electronics, IEEE Transactions on* , vol.5, no.2, pp.151,159, Apr 1990

[31] Urasaki, N.; Senjyu, T.; Uezato, K., "A novel calculation method for iron loss resistance suitable in modeling permanent-magnet synchronous motors," *Energy Conversion, IEEE Transactions on* , vol.18, no.1, pp.41,47, Mar 2003

[32] Yamazaki, K.; Seto, Y., "Iron loss analysis of interior permanent-magnet synchronous motors-variation of main loss factors due to driving condition," *Industry Applications, IEEE Transactions on* , vol.42, no.4, pp.1045,1052, July-Aug. 2006

[33] L. Kan, Q. Zhang, J. Shen, S. Paul, “Comparison of two novel MRAS strategies for identifying parameters in permanent magnet synchronous motors,” International Journal of Automation and Computing, Vol. 3, 2010, pp. 516- 524.